

# Master Thesis



## **Production improvement of hydraulically fractured wells in tight gas plays in Pakistan**

by

PATRICK EMANUEL GROINIG

BSc, University of Leoben, 2016



Chair of Reservoir Engineering

A THESIS

submitted in partial fulfilment of the requirements for the degree

MASTER OF SCIENCE

Department of Petroleum Engineering

Chair of Reservoir Engineering

UNIVERSITY of LEOBEN

Leoben, Austria

2016

Approved by:

Holger OTT, Univ.-Prof. Dipl.-Phys. Dr.rer.nat.





## APPROVAL SHEET

This thesis entitled Production improvement of hydraulically fractured wells in tight gas plays in Pakistan prepared and submitted in partial fulfilment of the requirements for the Degree of Master of Science in Petroleum Engineering has been examined and accepted.

(HOLGER OTT)



## AFFIDAVIT

I hereby declare that the content of this work is my own composition and has not been submitted previously for any higher degree. All extracts have been distinguished using quoted references and all information sources have been acknowledged.

---

GROINIG Patrick Emanuel,

Leoben, Thursday, 01. September 2016

## EIDESSTATTLICHE ERKLÄRUNG

Ich erkläre an Eides statt, dass ich die vorliegende Diplomarbeit selbständig und ohne fremde Hilfe verfasst, andere als die angegebenen Quellen und Hilfsmittel nicht benutzt und die den benutzten Quellen wörtlich und inhaltlich entnommenen Stellen als solche erkenntlich gemacht habe.

---

GROINIG Patrick Emanuel,

Leoben, Donnerstag, 01. September 2016

# Acknowledgement

This is the point where I would like to thank all those who have accompanied me in this thesis. I am quite sure that anyone who has ever been independently working on a thesis project, can very well understand how important to have strong support during that time.

Like a project is divided into phases and sections, I would like to express my gratitude in that frame.

It gives me great pleasure in acknowledging the support and help of Professor Ott, who has enabled me to work on this project and has accompanied me with his professional and personal support.

Furthermore, I owe my deepest gratitude to all the professors and assistants of the University of Leoben, who thought me the knowledge, which is the basis for the implementation of this work.

In addition, I would like to thank my colleagues at the Department reservoir engineering-particularly Mr. PhD. Siroos Azizmohammadi - for the excellent cooperation during this project.

I consider it an honor to work with my colleague Dávid Gönczi together on this project. His permanent suggestions and excellent input as a coworker have significantly contributed that my work has been continuously improved.

I would especially like to thank my amazing parents, Ewald and Maria Groinig who did support me financially, as wells as personally throughout my study and inspired me with wise counsel and encouragement to pursue my goals.

I am very grateful for the support of my siblings Sabrina and Jürgen Groinig in this time. Thanks for supporting me in difficult times and encouraging me to keep working on this thesis. With their help they have made a significant contribution to my studies.

I cannot find words to express my gratitude to the most important person that has accompanied me during this time. In Love, I would like thank my girlfriend Sabrina Moser, who gave me the strength to always keep moving ahead and supported me in both, good but especially in difficult times. Nevertheless she was the one who warned me when I was heading the wrong direction and she also rebuked me when it was necessary. Words cannot describe how grateful I am. This is also true for the fact that our son Jonas was very well taken care of by her, so that I could keep focusing on finishing my work meanwhile.

**THANK YOU!**

# Danksagung

An dieser Stelle möchte ich all jenen danken, die mich im Rahmen dieser Masterarbeit begleitet haben. Jeder, der schon einmal selbständig eine Arbeit verfasst hat, kann bestimmt sehr gut nachvollziehen wie wichtig es ist, Unterstützung in welcher Form auch immer zu genießen.

Ebenso wie ein Projekt in Phasen und Abschnitte gegliedert ist, mochte ich meinen Dank in ebenjenem besagten Rahmen kundtun.

Zuerst möchte ich Herrn Prof. Ott danken, der mir es ermöglicht hat, an diesem Projekt zu arbeiten und mich mit seiner fachlichen und persönlichen Unterstützung begleitet hat.

Des Weiteren ist es mir ein Anliegen, mich bei allen Lehrkörpern der Montanuniversität Leoben zu bedanken, welche mir das Wissen vermittelten, welches Grundlage für die Umsetzung dieser Arbeit ist.

Darüber hinaus möchte ich mich bei meinen Kollegen am Lehrstuhl Reservoir Engineering- besonders sei hier Herr PhD. Siroos Azizmohammadi hervorgehoben- für die hervorragende Zusammenarbeit bedanken

Ein Dank gilt meinem Kommilitonen Dávid Gönczi Seine permanenten Anregungen und seine hervorragende Mitarbeit haben wesentlich dazu beigetragen, dass meine Arbeit kontinuierlich verbessert wurde.

Danken möchte ich hier besonders meinen Eltern, Ewald und Maria Groinig, die mich während meiner gesamten Studienzzeit sowohl finanziell, als auch persönlich mit weisen Ratschlägen und Ermutigungen dazu angespornt haben, meine Ziele kontinuierlich zu verfolgen und in die Tat umzusetzen.

Meinen Geschwistern, Sabina und Jürgen Groinig möchte ich dafür danken, dass sie mich in schwierigen Zeiten aufgebaut und unterstützt haben und damit wesentlich dazu beigetragen haben, dass mein Studium und damit verbunden diese Arbeit zu einem positiven Abschluss kommt.

Es ist mir ein Anliegen am Schluss die wichtigste Person zu erwähnen, die mich während dieser Zeit begleitet hat. In Liebe danke ich meiner Freundin Sabrina Moser, die mir die Kraft gab, immer nach vorne zu sehen und mich sowohl in guten aber besonders in schwierigen Zeiten aufgebaut hat, mich aber gleichwohl auch im rechten Augenblick ermahnt und zurechtgewiesen hat. Worte vermögen hier nicht zu beschreiben wie dankbar ich bin, auch für die Tatsache, dass unser Sohn Jonas bei ihr bestens versorgt war, sodass ich mich auch währenddessen auf die Fertigstellung meiner Arbeit konzentrieren konnte.

**DANKE!**

## Abstract

Tight gas reservoirs contain a significant potential for dry gas production including one big problem: Tight gas reservoirs, having a very low permeability do normally not produce at economic limits. In general tight gas fields are defined as having less than 0.1 millidarcy (mD) matrix permeability and very low porosity (less than ten percent). This special setting is the reason why these fields are normally not economically producible. The common approach to get rid of this is hydraulic fracturing to stimulate the drilled wells.

OMV is currently active in gas fields in Pakistan and holding interest in tight gas production. Several wells which had been drilled are producing dry gas below economic limit. As a typical treatment the wells drilled in the Tight Gas Fields were stimulated via hydraulic fracturing. Contrary to the expectations the wells started to produce water comprising gas instead of pure dry gas, although ~~the fact that~~ the geology indicates no aquifer in this area. Typically tight gas wells are producing dry gas at low rates. This was also the case before the wells were hydraulically fractured. After the fracturing job, the gas rate increased first, but so did the water rate until a point where the amount was so high that the eruptive lifting energy was exceeded and the gas rate went down to zero.

The aim of this thesis is the investigation of the source of water inflow and furthermore the declaration of the amount of the unwanted fluid flowing to each well. First step was to get an insight into the complex structure of the field and get an overview of all the work done in the past. Afterwards the core measurements were conducted and plotted for a better understanding of the reservoir. There I discovered an unusual porosity behaviour for this kind of water wet sandstone reservoir. It shows a bimodal pore size distribution which means that there are two dominant pore sizes present in the reservoir rock- micro pores in the range of 0.02 to 0.1  $\mu\text{m}$  and macro pores with average pore size of one magnitude higher than the small ones.

This was the trigger to start investigating a so called micro pores feeding effect. At a certain pressure drop the water blocked in the small pores gets released and feed into the bigger (gas filled) pores. So instead of gas, water is produced as long as water is available in the small pores. As the measurement showed an average water saturation of around 40% this is quite a lot. In parallel also the possibility of the fracture growth into a water bearing neighbouring layer was observed.

To clarify the water source a simple generic model was built and fed with measured field data.

## Kurzfassung

Tight-Gas-Lagerstätten sind Lagerstätten die einst porös genug waren, sodass Gas migrieren konnte und anschließend mittels Druck von überlagerten Gesteinsschichten zu dichten Gesteinen umgewandelt wurden. Daher haben diese eine sehr geringe Permeabilität und fördern eruptiv im Normalfall nicht wirtschaftliche Mengen an Gas. Im Allgemeinen weisen Tight Gas-Felder weniger als 0,1 Millidarcy (mD) Matrix Permeabilität auf und zudem eine sehr geringe Porosität (weniger als zehn Prozent). Der heute technologisch aktuelle Ansatz um diese Produktionsrate zu steigern, ist die Stimulation mittels Hydraulic Fracturing.

OMV Pakistan hat mehrere Bohrungen mittels stimuliert, doch anstatt der Produktion von trockenem Gas, stieg die Gas-Rate zuerst nur kurz an und mit ihr die Wasser Produktion, bis zu einem Punkt, wo die eruptive Förderenergie nicht mehr ausreichend war die Flüssigkeiten an die Oberfläche zu transportieren und das obwohl Geologen eindeutig belegt haben, dass sich keine wasserführende Gesteinsschicht in unmittelbarer Nähe befindet.

Das Ziel dieser Arbeit ist das Aufspüren der Quelle des Wasserzuflusses und ferner die Quantifizierung der Menge der unerwünschten Flüssigkeit. Ein erster Schritt war das Einlesen in die bereitgestellten Unterlagen, um einen Überblick über die komplexe Struktur des Feldes und die in der Vergangenheit ausgeübten Tätigkeiten zu bekommen. Danach wurden die Kernmessungsanalysen durchgeführt, welche für ein besseres Verständnis des Lagerstättengesteins sorgen sollten. Dort entdeckte ich ein ungewöhnliches Verhalten für diese Art von wassergesättigten Sandsteinlagerstätte in Bezug auf die Porosität. Es zeigt eine bimodulare Porengrößenverteilung, was bedeutet, dass zwei dominierende Porengrößen in der Lagerstätte dominieren. Zum einen sind dies Mikroporen im Bereich von 0,02 bis 0,1  $\mu\text{m}$  und Makroporen mit einer durchschnittlichen Porengröße welche um die der kleinen um einen Faktor zehn überschreiten..

Dies war der Start meiner Untersuchung des sogenannten Micropore- Feeding- Effects. Bei einem bestimmten Druck wird Wasser, welches zuvor in den kleinen Poren gelagert ist, freigesetzt und fließt in die größeren, Gas gefüllten, Poren. Somit wird anstelle von Gas, Wasser so lange produziert, wie Wasser in den kleinen Poren zur Verfügung steht. Da die Messung eine durchschnittliche Wassersättigung von rund 40% aufwies, ist das eine ganze Menge. Zudem wurde zeitgleich untersucht, ob der Wasserfluss eventuell doch daraus resultiert, dass naheliegende Gesteinsschichten stimuliert wurden, welche wasserführend sind. Um dies zu klären, wurde ein generisches Modell erstellt und mit gemessenen Daten komplettiert.



*Das Problem zu erkennen ist wichtiger,  
als die Lösung zu erkennen,  
denn die genaue Darstellung des Problems  
führt zur Lösung.*

*Recognizing a problem is more important  
than resolving it;  
describing the problem accurately  
leads automatically to the right solution.*

**A.Einstein** (\*14. März 1879 †18. April 1955)



## List of Tables

Table 1 rock property summary [1].....	15
Table 2 rock properties .....	17
Table 3 fluid data .....	17
Table 4 simulation scenarios.....	34
Table 5 scenario overview .....	34

## List of Charts

Chart 1 Well 4 .....	24
Chart 2 Well 5 .....	25
Chart 3 Well 6 .....	26
Chart 4 Well 12 .....	27

## List of Equations

Equation 1 pore radius .....	21
Equation 2 Oil-brine capillary pressure.....	22
Equation 3 mean hydraulic radius .....	22
Equation 4 Leverett J function.....	23

## List of Figures

Figure 1 project workflow .....	2
Figure 2 well location map [1].....	3
Figure 3 relative permeability curve.....	5
Figure 4 illustration of the wetting effect [2] .....	6
Figure 5 geological timescale [1].....	7
Figure 6 stratigraphic setting WELL 6 [1].....	8
Figure 7 core box photography [1].....	12
Figure 8 Well structure map .....	13
Figure 9 depositional environment C- Sands [1].....	14
Figure 10 lithotype declaration [1] .....	16
Figure 11 bulk and clay composition [1] .....	16
Figure 12 mercury capillary pressure measurement [3].....	19
Figure 13 pore size distribution .....	23
Figure 14C sands top structure map .....	28
Figure 15 K.h and GIIP map [1].....	28
Figure 16 capillary pressure input curve.....	31
Figure 17 3D model                      Figure 18 cross section slice.....	32
Figure 19 fracture grid refinement .....	32
Figure 20 pressure distribution .....	43
Figure 21 generic model sketch .....	49
Figure 22 cross section n sketch.....	49

Figure 23 gas formation volume factor .....	51
Figure 24 viscosity .....	51
Figure 25 simulated fracture profile .....	52
Figure 26 gas composition .....	52
Figure 27 PVT data .....	53
Figure 28 relative permeability input.....	54
Figure 29relative permeability output .....	54
Figure 30 initial conditions setting .....	55
Figure 31 well perforations.....	55
Figure 32 fracture specification .....	55
Figure 33 auto created fracture design.....	55

## Abbreviations

mD	Millidarcy
M	meter
WGR	Water Gas Ratio
Pa	Pascal
Por	Porosity
Perm	Permeability
MD	Measured depth
STB	Stock tank barrel
MMscf	Million standard cubic feet
lb	Pounds
cp	Centipoise
psi	Pounds per square inch
RB	Reservoir bulk volume
ft <sup>3</sup>	Cubic feet
F	formation resistivity factor
J	J-function
k	permeability
krw	Water relative permeability
kr <sub>g</sub>	gas relative permeability
m	Cementation exponent
n	Saturation exponent
P <sub>ci</sub>	capillary pressure at the inside face of the plug
PV	pore volume
R <sub>w</sub>	resistivity of brine R <sub>0</sub>
RI	resistivity of totally brine-saturated plug
S <sub>g</sub>	gas saturation
S <sub>w</sub>	water saturation
S <sub>wr</sub>	residual water saturation

## Table of content

	<b>Page</b>
<b>1 INTRODUCTION .....</b>	<b>1</b>
<b>2 OVERVIEW .....</b>	<b>2</b>
<b>3 PLAY SUMMARY.....</b>	<b>3</b>
3.1 SOURCE .....	4
3.2 TRAP .....	4
3.3 SEAL .....	4
3.4 RESERVOIR .....	5
3.5 STRATIGRAPHY.....	6
3.5.1 Lower Goru Member.....	9
3.5.1.1 LOWER GORU SHALE INTERVAL.....	9
3.5.1.2 “D” INTERVAL .....	9
3.5.1.3 “C” INTERVAL .....	10
3.5.1.4 “C” SAND.....	13
3.6 Reservoir rock properties .....	15
3.7 Lithology .....	16
3.8 Fluid data.....	17
<b>4 PROBLEM DEFINITION.....</b>	<b>18</b>
4.1 Water source .....	18
<b>5 EFFECT INVESTIGATION .....</b>	<b>19</b>
5.1 Capillary pressure tests .....	19
5.1.1 Mercury injection method.....	19
5.1.2 Mercury Injection tests procedure.....	20
5.1.3 Calculation of mercury injection data .....	21
5.1.3.1 Results .....	23
5.2 Test Interpretation .....	24
<b>6 RESERVOIR MODEL.....</b>	<b>28</b>

<b>7</b>	<b>GENERIC MODEL</b> .....	<b>29</b>
7.1	Model Input.....	29
7.2	Model Setup .....	30
7.3	Simulation Scenarios.....	33
7.3.1	Normal production simulation .....	33
7.3.2	Including hydraulic fracturing .....	33
7.3.3	Comparison normal production- hydraulic fracturing.....	33
<b>8</b>	<b>RESULTS</b> .....	<b>34</b>
8.1	Base case scenario .....	35
8.2	Base case with fracture .....	36
8.3	Comparison base case.....	37
8.4	Capillary pressure scenario .....	38
8.5	Permeability scenario .....	39
8.6	Porosity scenario .....	40
8.7	Water saturation scenario.....	41
8.8	Grid block saturation changes .....	42
<b>9</b>	<b>CONCLUSION/ INTERPRETATION</b> .....	<b>44</b>
<b>10</b>	<b>REFERENCES</b> .....	<b>47</b>
	<b>APPENDICES</b> .....	<b>49</b>
	Model Description .....	49
	Model Input .....	50
	Model Setup.....	53
	Detailed Core Interpretation.....	56
	Geo Mechanical Core Testing Results.....	72
	Special Core Analysis Results .....	73
	Formation Imaging Result.....	74
	Fracture Treatment Sensitivity Analysis.....	76



# 1 INTRODUCTION

In comparison to conventional reservoirs tight gas reservoirs had to be stimulated prior to production to achieve economic flow rates. Reservoirs having a permeability less than 0.1mD are called tight gas reservoirs. Tight gas reservoirs contain a significant potential for dry gas production including one big problem: Tight gas reservoirs, having a very low permeability do normally not produce at economic limits. The setting in the investigated fields in Pakistan shows a widespread distribution of rocks containing tight sandstones with an average permeability of less than 0.03 mD interlayered by others showing a permeability of around 30 mD. The average porosity is around 15 percent.

OMV is currently active in those gas fields and holding interest in tight gas production. Several wells which had been drilled are producing dry gas below economic limit. Contrary to the expectations the wells stimulated from OMV in Pakistan started to produce water comprising gas instead of pure dry gas although the fact that the geology indicates no aquifer in this area. After the hydraulic stimulation job the gas rate increased as proposed, but in the meantime also the water rate increased in parallel which lead to an increase of the Water gas ratio (WGR). As a result of this increased WGR the wells could not lift the liquid anymore without any lifting assistance. OMV is interested in investigating the source and mechanism of water influx since it is of major importance to discover the effect in order find a solution for the already affected wells and for further development. Furthermore OMV wants to know the amount of water they would have to produce to get access to the gas again, if this is possible with the already measured data.

The working procedure arranged with the Department of reservoir engineering is the following:

The first step is the examination of available reservoir data (05/2016- 07/16) after the kick of meeting with one representative of OMV. This step is followed by a general literature research (05/16- 06/16) including tight gas reservoir behaviour investigation as well as already completed studies in tight gas fields. Afterwards data processing (07/16) should be done which means collecting all the data from OMV. Investigation of production behaviour (07/16- 08/16) concludes this phase whereby all the important measurements should be checked and compared. The last part of this thesis deals with the preparation of a numerical model (09/16). A very simple generic model should be developed in order to find the effect which causes water production.

The upfront determined milestones are a Kick off meeting (01.05.2016) as well as weekly reports to supervisor. Midterm presentation and interpretation of screened data set (07/16) followed by a final presentation of the screening process and the determination for further investigations. (09/16)

## 2 OVERVIEW

This thesis is divided into a summary of the basic setting of the petroleum system and to give an overview of conducted tests and measurements and a second part where the results are discussed in detail with the conclusions and the recommendations for the company. The first part is going to be split in the geological setting and the fluid and rock data section.

Rock compressibility tests are going to be discussed in detail, because they are of major importance for the verification or falsification of several proposed effects.

The last section is based on a model. So a model is going to be presented which is created out of the delivered data and based on the results from the outcomes of prior sections. Furthermore, the result of the simulation run with an already existing model is presented and compared to the created generic one. This thesis is accomplished by the conclusion and a recommendation section for the company how to treat the already existing wells in the study area.

***Disclaimer: Most of the data is taken from several reports provided by the company. The sources are therefore not especially marked in this document. If the source differs from the company data source it is written directly below the concerning part.***

The graphic below represents briefly the workflow of this project:

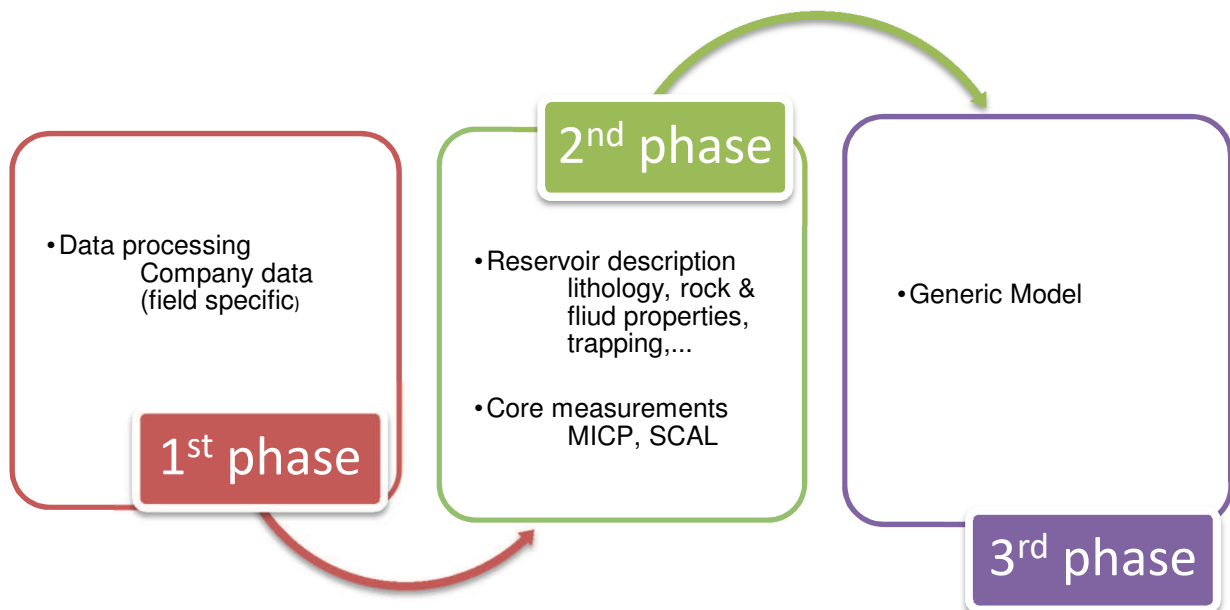


Figure 1 project workflow

### 3 PLAY SUMMARY

The Field is located on the southeast flank of the Khaipur high. The reservoir consists of shallow marine Lower Goru "C" Interval and they are restricted to the NE-SW trending fairway.

The trapping mechanism is only stratigraphic and the hydrocarbon source rocks are the prolific Cretaceous Sembar Formation and the intra-formational shales within Cretaceous Lower Goru Member.

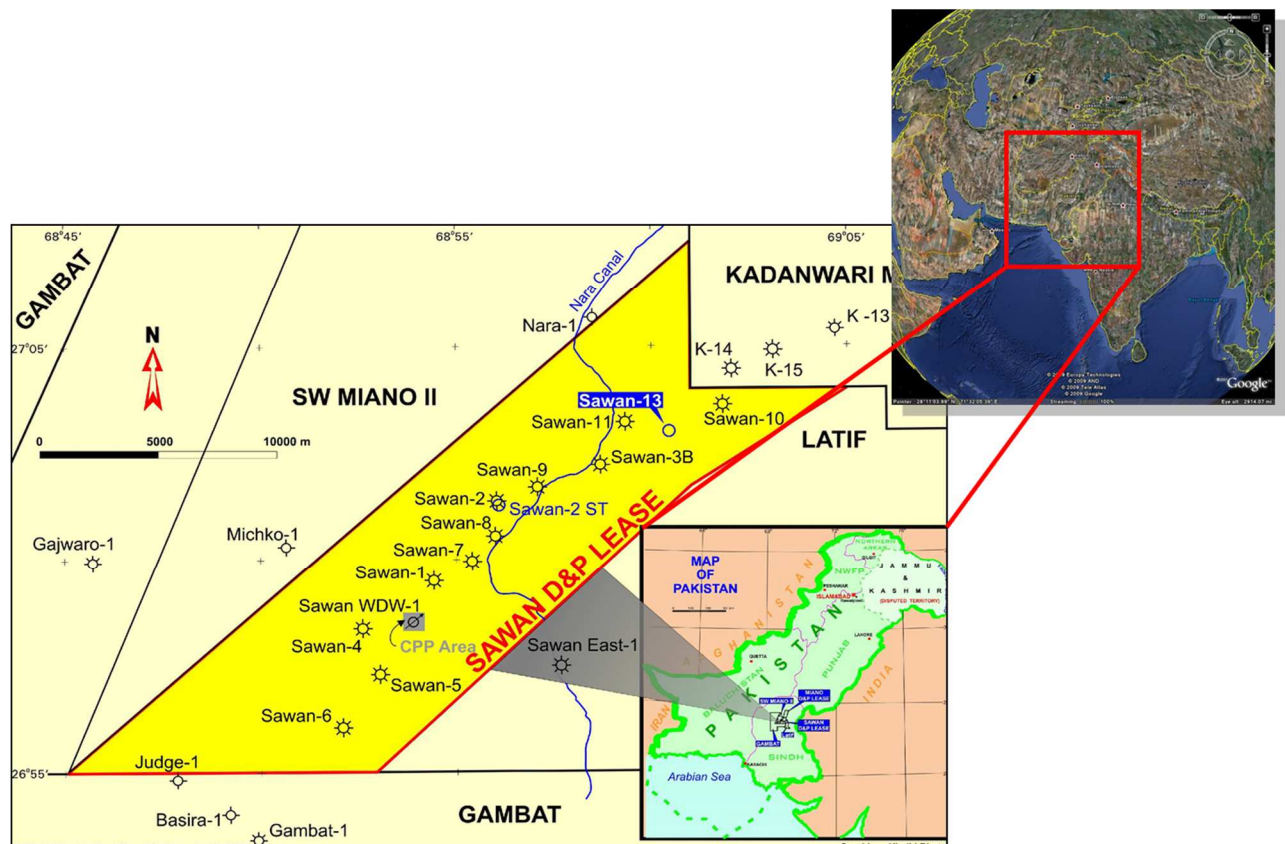


Figure 2 well location map [1]

As shown in the picture above the prior drilled Well 4 and Well 5 are located in the north of Well 6. Based on the success of Well 5, Well 6 drilled the same progradational system further extending in the southwest with a good porosity-permeability range of 15 – 20% and 20 – 40 mD respectively.

### 3.1 SOURCE

The reservoir rocks in the Well area were charged from the older (formed during lower cretaceous) and underlying shelfal marine origin (Sembar Formation) partially proven organic rich shales and also from the organic-rich shales within the Lower Goru Member (this is also the case in nearby gas fields).

The TOC (total amount of carbonate) range of this shales containing terrestrial organic matter is of 0.5 – 1.7%, with Type III kerogen and have been in gas generation phase since Late Cretaceous-Early Tertiary times.

### 3.2 TRAP

The trapping mechanism for the accumulation of hydrocarbons is purely stratigraphic. Last major inversion in the area took place in late Eocene time and therefore, the timing of traps is appropriate relative to the timing of HC generation, expulsion, and migration for optimum reservoir charge and later preservation of the accumulations.

An ENE – WSW isopach thick in the Lower Goru “C” Interval defines the trend of the trapped sand. Local dip is towards the southeast, while towards the north and south trapping is caused by shaling out of the reservoir.

The northern and eastern limits are defined by a facies controlled deterioration in reservoir quality, which creates an “effective zero reservoir” line.

### 3.3 SEAL

More than 15 m thick transgressive shales of the Lower Goru “C” Interval directly overlying the reservoir sands provide an effective top seal, whereas a more than 500m thick shale and marl sequence of the Lower Goru Member is an established regional seal. Shales and tight sands within the “C” Interval also act as lateral and bottom seals.

### 3.4 RESERVOIR

Whereas parts of the reservoir consist of stacked sand bodies of proximal shore face facies comprised of coarse to medium grained sand with a thickness of 40m. The quality of other reservoir parts is low including fine to medium grained sand having a net pay of 17.7 m with porosity averaging 15% and 45% water saturation.

The quality of the reservoir is decreasing to the south which indicates the direction of the channel flowing direction. The reservoir rock is water wet since it is gas bearing, so water is occupying the bigger pores and the walls of the pores and gas is located in between. The behaviour of this kind of rock can be seen in the following Figure 3 relative permeability curve.

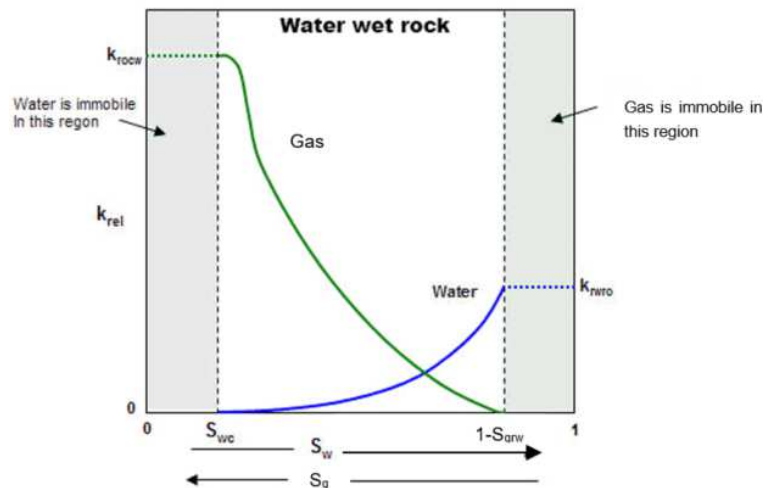


Figure 3 relative permeability curve

The schematic structure of water wet rocks looks like the one in figure above taken from [1] Fekete.com

Water- gas systems are always water wet. The wetting effect can be explained so that water is a polar molecule and is attracted to polar surfaces. Original all rocks have polar surfaces and therefore water wet. The following picture taken from the same reference above [2] is showing the wetting behaviour of water in presence of gas. The grains are represented by the brownish color. Blue is indicating the water in the pore space. The green color is indicating the gas within the pores.

One can see that water forms a film along the grains, this effect is caused by different wettability's of the two fluids (water/ gas). Gas is always the non- wetting phase in this system.

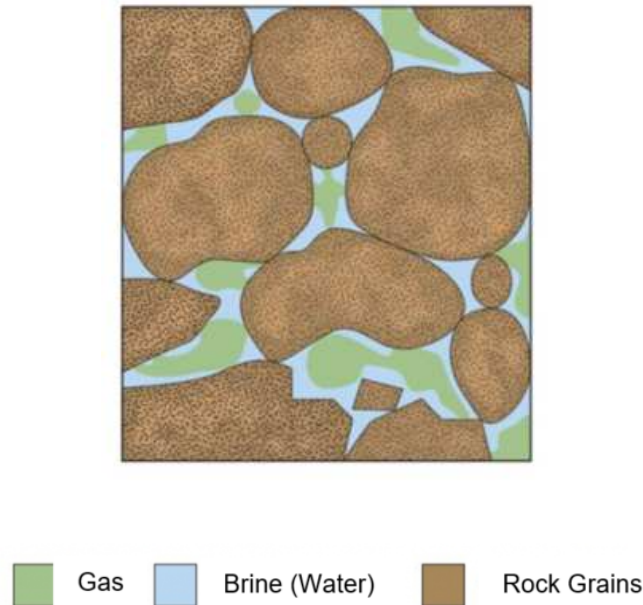


Figure 4 illustration of the wetting effect [2]

No significant reservoir potential could be realized in the finer grained turbidite sandstone facies below the “C” sand reservoir despite thereby relatively in gauged hole across this stratigraphic interval also indicating some permeability streaks.

### 3.5 STRATIGRAPHY

Most of the following data has been evaluated and have been conducted by the company. So all the following data is provided by the company and regarding confidentiality issues the location won't be specified in detail in this thesis.

As briefly explained in the play summary regionally the field is located on the south eastern flank of the Khairpur high. The shallow marine Lower Goru “C” Interval reservoir sands are restricted to the northeast-southwest trending fairway.

The origin of the HC is the underlying Lower Cretaceous regionally proven organic-rich shales of shelfal marine origin (Sembar Formation) and from the organic-rich shales within the Lower Goru Member.

These shales contain terrestrial organic matter, with Type III kerogen a TOC in the range of 0.5 – 1.7%, and have been in gas generation phase since late Cretaceous-early Tertiary times.

The last major impact happened in the late Eocene time and therefore, the timing of traps is appropriate relative to the timing of the HC generation, expulsion, and migration for optimum

reservoir charge and later preservation of the pool. A south-eastward regional tilt and west-and due to the facies change north-westward shale-out away from the shoreline provide stratigraphic entrapment. Lateral seal is provided by the lateral shale-out towards north and south away from the fluvial input. Transgressive lag and about 400m thick shale overlying the Lower Goru “C” sand provide an effective top seal. Shales and tight sands within the “C” Interval act as lateral and bottom seals.

The corresponding time scale in the Figure 5 geological timescale below visualizes this setting.

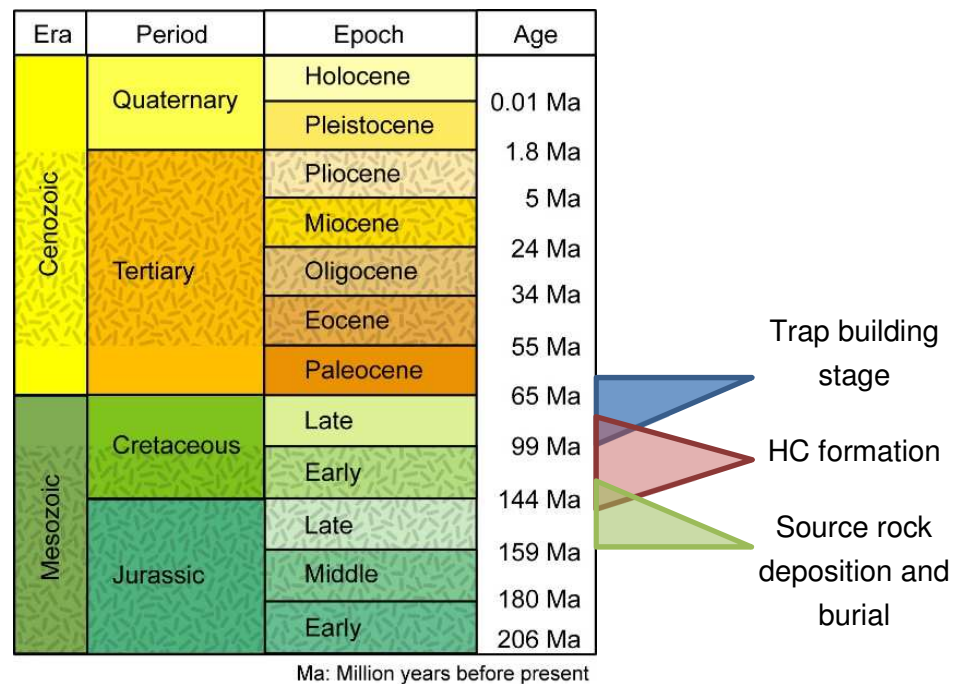


Figure 5 geological timescale [1]

In parts of the reservoir mineral coatings (due to fresh water influx) around the coarse and medium sand grains preserve porosity and permeability during late burial. Due to paleo topography and accommodation space, thicker sedimentary pile was deposited in the northern area, whereas thinner sand sheets were deposited in the south. In the northern area from Well-1 to Well-3, a significant thickness of these stacked sands survived erosion during regression and subsequent transgression. However, in the south only a part is preserved which is why the prediction of the reservoir sand presence is highly uncertain in the southern region. Based on the Jason Inversion the Reservoir Sands at Well-5 location were expected to have a thickness of approximately 25-30m with a porosity ranging between 18 to 20 % and having high net to gross ratio (up to 80% or more). The low AI values of the seismic event represent high porosity and point to the reservoir quality sandstone belt when co-occur with the top set part of the seismic reflection geometry and aligned with the proximal upper shore face belt extrapolated from the north.



The Figure 6 stratigraphic setting WELL 6 shows a typical stratigraphic setting of the wells in the field. The height and the thickness of the layers vary within the reservoir. The stratigraphic interpretation was done from geologist in Vienna. [1]

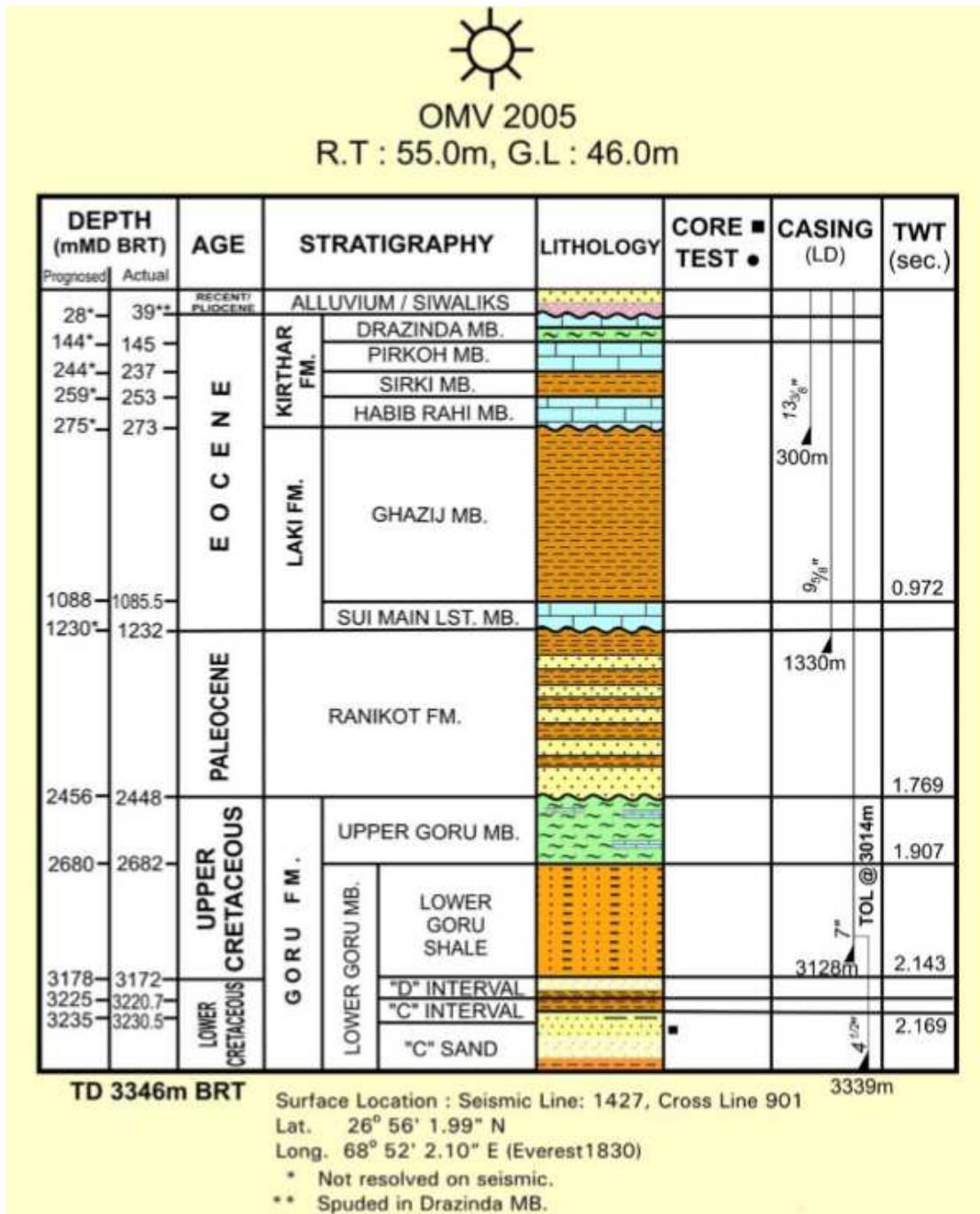


Figure 6 stratigraphic setting WELL 6 [1]



### **3.5.1 Lower Goru Member**

The most important formation from a reservoir engineer point of view is the Lower Goru Member encountered in this well and it can be divided into two distinct intervals, namely Lower Goru Shale Interval, “D” Interval the mainly sandstone Interval “C” and the “C” Sand

#### **3.5.1.1 LOWER GORU SHALE INTERVAL**

With a thickness of about 500 m throughout the whole reservoir this layer is the seal for the reservoir zone. Its age is Lower to Upper Cretaceous and the upper boundary of the Lower Goru Member is marked by a change in lithology from marl & limestone to shales and siltstone.

The shale lithology is Dark grey to dark greenish grey, blackish grey, firm to moderately hard, in parts hard, sub- platy to platy, in parts sub- fissile, slightly to moderately silty, slightly to non- calcareous, carbonaceous, micaceous, traces of disseminated pyrite, occasionally grading to siltstone.

The sandstone is medium to dark grey, grayish black, moderately hard, in parts hard, blocky to sub blocky, in parts sub platy, traces of carbonaceous matter, occasionally micro micaceous, traces of glauconite, traces of disseminated pyrite, traces of very fine grained sandstone.

The lowermost sandstone is off white, light grey, light olive green, fine to medium grained, friable to moderately hard, in parts bit crushed, generally loose quartz grains, sub angular to sub rounded, poorly sorted, weakly calcareous cement, traces of glauconite, occasionally grading to siltstone, no shows.

#### **3.5.1.2 “D” INTERVAL**

Start of “D” INTERVAL formed within the Upper Cretaceous with a thickness of 50 m is marked by the appearance of sandstone following a thick sequence of shale and siltstone.

Lithology of Silty Sandstone is described to be Light grey, light greenish grey, moderately hard, very fine grained, sub rounded, poorly sorted, calcareous cement, slightly to moderately argillaceous, traces of pale green mineral (chlorite), no visible porosity.

In comparison the Siltstone is medium to dark grey, in parts greenish grey, moderately hard, sub blocky, slightly calcareous, carbonaceous, slightly sandy, traces of pale green mineral (Chlorite), traces of pyrite, grades to very fine sandstone.

And the Shale indicating the lowest zone of this formation is medium grey to dark grey, moderately hard, sub platy to sub blocky, slightly calcareous, silty, slight to non-calcareous, carbonaceous, grades to siltstone.

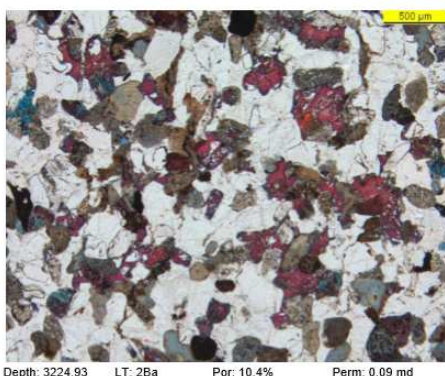
### 3.5.1.3 “C” INTERVAL

Upper Cretaceous is the age when this rock type was formed and its upper boundary is marked by the appearance of sandstone following glauconite/ chlorite rich claystone. The GR log shows low GR value at the top of this interval, below a very high radioactive peak across glauconite/ chlorite rich transgressive marine shale.

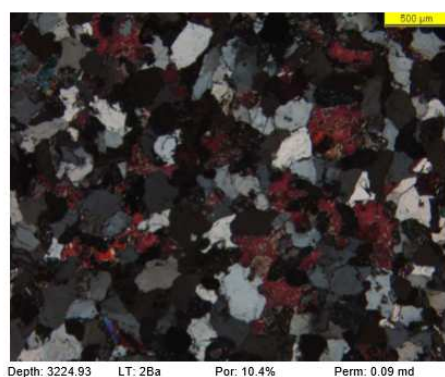
The Lithology description for the Silty Sandstone is Light grey, off white, moderately hard, in parts bit crushed, very fine grained, sub angular, moderately sorted, and common off white lithic grains, traces of pale green mineral (chlorite), no visible porosity.

The next region is a pure Siltstone and defined by medium grey, in parts greenish grey, moderately hard, sub blocky, slightly calcareous, carbonaceous, slightly sandy, traces of pyrite, grades to very fine sandstone.

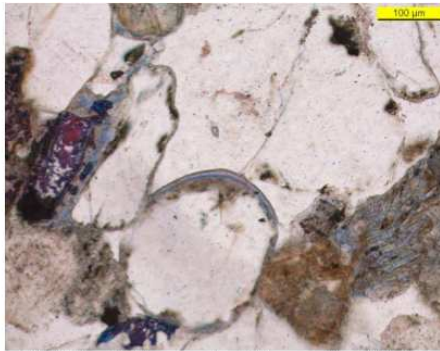
Again the Shale is the lowermost rock and can be described as dark grey, olive black, moderately hard, sub platy to sub blocky, slight to non- calcareous, carbonaceous, silty, traces of pyrite.



Depth: 3224.93 LT: 2Ba Por: 10.4% Perm: 0.09 md Overview of fine-grained, well sorted, quartz-, calcite- and iron chlorite-cemented litharenite (calcite-cement stained red).

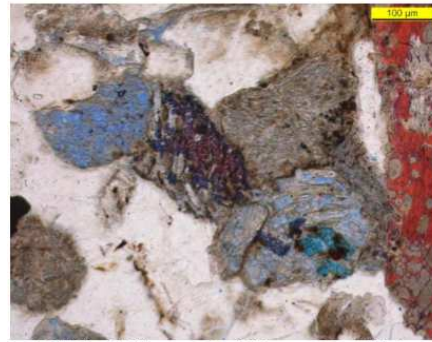


Depth: 3224.93 LT: 2Ba Por: 10.4% Perm: 0.09 md #Pol: Overview of fine-grained, well sorted, quartz-, calcite- and iron chlorite-cemented litharenite.



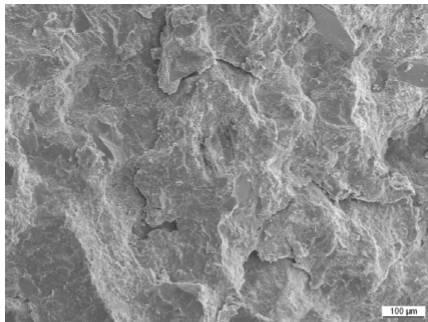
Depth: 3224.93 LT: 2Ba Por: 10.4% Perm: 0.09 md

Depth: 3224.93 LT: 2Ba Por: 10.4% Perm: 0.09 md Detail of quartz grains rimmed by iron chlorite-cement and quartz-cement. The quartz-cement clearly postdates the iron chlorite-cement.



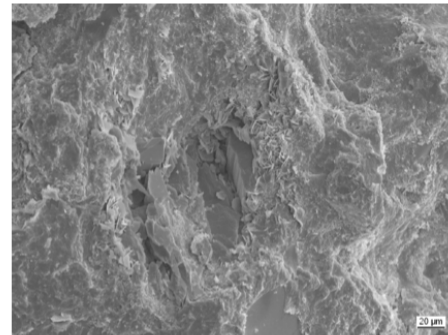
Depth: 3224.93 LT: 2Ba Por: 10.4% Perm: 0.09 md

Depth: 3224.93 LT: 2Ba Por: 10.4% Perm: 0.09 md Detail of quartz grains rimmed by iron chlorite-cement and quartz-cement. The quartz-cement clearly postdates the iron chlorite-cement.



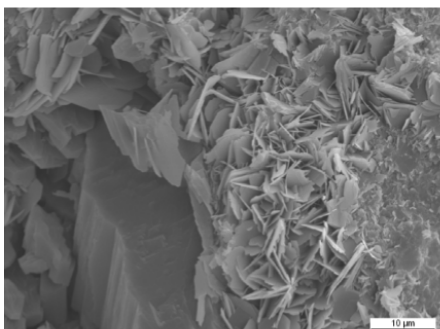
Depth: 3226.14 m LT: 2Ba Por: 10.88% Perm: 0.05 md

Depth: 3226.14 m LT: 2Ba Por: 10.88% Perm: 0.05 md Overview of fine- to medium-grained, iron chlorite- and calcite-cemented litharenite



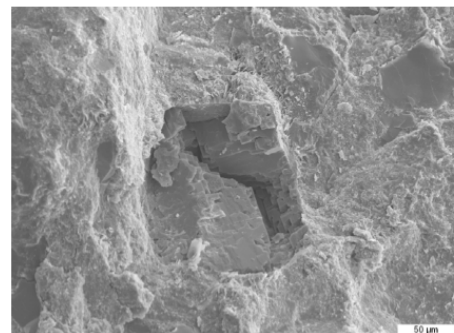
Depth: 3226.14 m LT: 2Ba Por: 10.88% Perm: 0.05 md

Depth: 3226.14 m LT: 2Ba Por: 10.88% Perm: 0.05 md Overview of pore space strongly reduced by iron chlorite- and calcite-cement.



Depth: 3226.14 m LT: 2Ba Por: 10.88% Perm: 0.05 md

Depth: 3226.14 m LT: 2Ba Por: 10.88% Perm: 0.05 md Detail of pore space strongly reduced by iron chlorite- and calcite-cement.



Depth: 3226.14 m LT: 2Ba Por: 10.88% Perm: 0.05 md

Depth: 3226.14 m LT: 2Ba Por: 10.88% Perm: 0.05 md Detail of dissolved potassium feldspar grain.

The photograph is an excerpt of the conducted core experiments from the company in order to evaluate reservoir rock properties.



Figure 7 core box photography [1]

One can see a core box including a complete core section from 3231.1- 3226.1m. The holes within the cores are caused by sample drilling operations in order to conduct core measurements.



### 3.5.1.4 “C” SAND

The deepest and therefore the oldest formation was also formed in Upper Cretaceous and the top boundary is marked by the appearance of sandstone followed by glauconite/ chlorite rich claystone. The GR log shows low GR value at the top of this interval, but a very high radioactive peak across the glauconite/ chlorite rich transgressive marine shale interval below.

#### Lithology description:

**Sandstone:** Light to medium grey, moderately hard to hard, dominantly fine to medium grained, occasionally coarse grained, sub rounded to sub angular, moderately sorted, cemented with calcareous cement, slight to moderately argillaceous, slight to moderately bioturbated with associated argillaceous/ carbonaceous matter, traces of mica, pyrite, and pale green mineral, poor to nil visible porosity .

**Siltstone:** Medium to dark grey, moderately hard, sub blocky, slight to non-calcareous, carbonaceous, sandy, graded to very fine argillaceous sandstone.

**Claystone:** Dark grey to grayish black, moderately hard, sub blocky, slight to non-calcareous, silty, in parts sandy, graded to siltstone.

The C sands are described as shaly sand by available XRD measurements. Chlorite is the dominant clay type and makes up 30 – 40% of the bulk volume. This clay is distributed as both laminated and dispersed clay, where the latter is dominant in the reservoir sands.

The Figure 8 Well structure map on the next page shows the C sands top structure map including the wells.

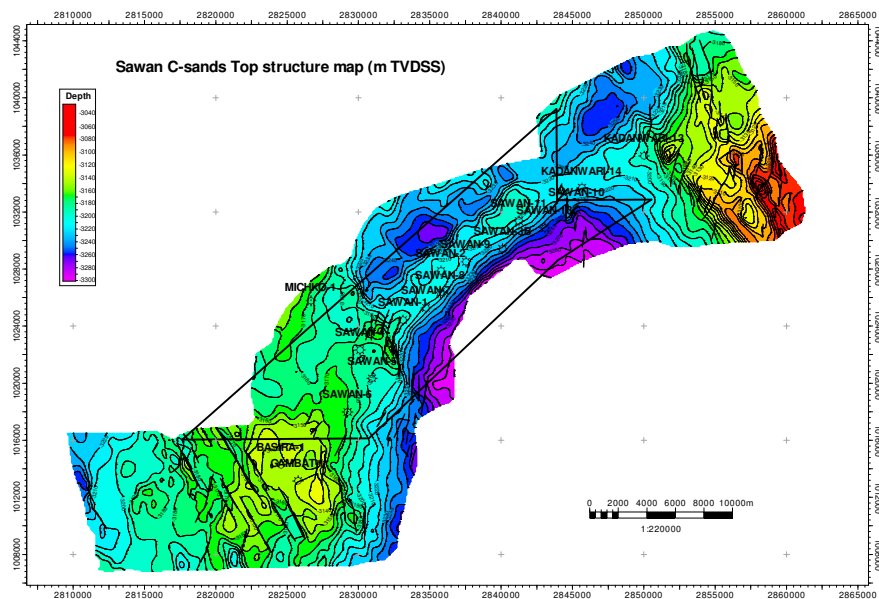


Figure 8 Well structure map

The following picture indicates the depositional environment of C Sands and helps to get a better understanding of the reservoir.

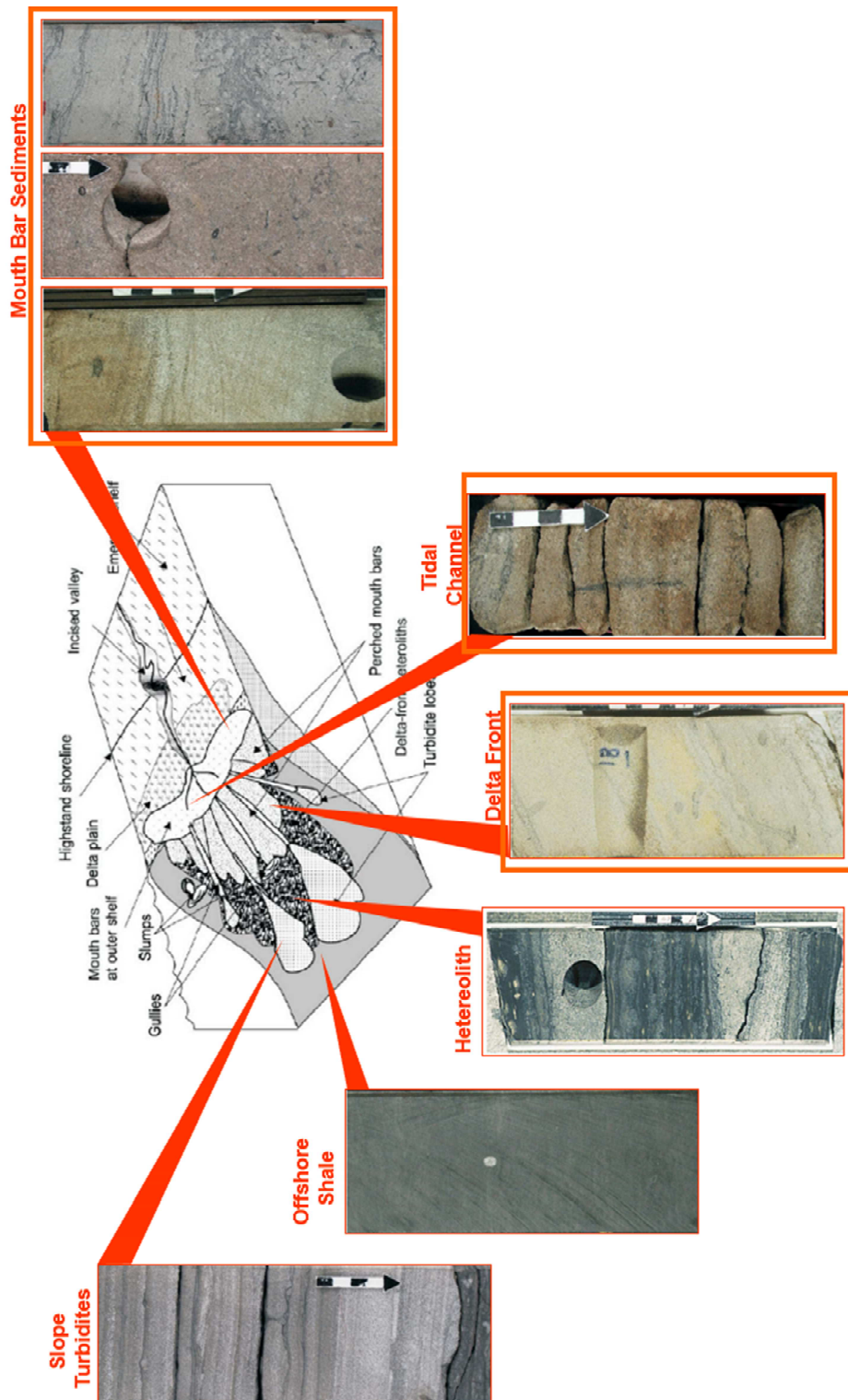


Figure 9 depositional environment C- Sands [1]

### 3.6 Reservoir rock properties

Summation of “C” sand for one representative well is presented in the table below. Hydrocarbon volumes were calculated using the following cut-off values:

Clay Volume <30%	Porosity >6%	Water Saturation <60%
------------------	--------------	-----------------------

FORMATION			GROSS	NET	AVG	AVG	AVG	SUM	SUM	WGHT
C-Interval	FROM	TO	PAY	PAY	VCL	PHIE	SWE	POR.	HC	HC
	M	M		M	%	%	%	M	M	
Zones of interest	3230.5	3235.5	5	2.9	22	11	48	0.32	0.17	0.17
	3235.5	3241.0	5.5	5.5	8	16	42	0.91	0.53	0.53
	3241.0	3243.8	2.8	2.3	13	15	45	0.35	0.19	0.19
	3243.8	3248.7	4.9	4.7	9	16	47	0.75	0.4	0.4
	3248.7	3250.8	2.1	2.1	19	15	44	0.31	0.17	0.17
	3250.8	3259.0	8.2	0.2	29	12	53	0.02	0.01	0.01
	3268.0	3270.0	2	0.2	28	7	59	0.01	0	0
	3272.0	3274.0	2	0.3	25	8	44	0.02	0.01	0.01
Total	3230.5	3274.0	43.5	17.7	13	15	45	2.62	1.44	1.45

Table 1 rock property summary [1]

3220 - 3230.5 mMD The upper part of the C-Interval is influenced by high chamosite/chlorite content. Data from previous wells show that interval consists of low or no permeability zones.

3230.5 - 3235.5 mMD The top of this interval consists of a tight layer (around 3231mMD). Below this layer follows a low porosity interval with higher clay content and indication of heavy minerals.

3235.5 – 3241.0 mMD Good porosity. Low crossover indication from the neutron/density. Low gas indication. This seems to be influenced by chlorite coating of the quartz components.

3241 - 3243.8 mMD This interval consists of higher clay/silt content than the sand layer above. Average porosity is lower than in the layer above, too.

3243.8 – 3248.7 mMD This interval is similar to the interval from 3235.5 - 3241.0 mMD

3248.7 - 3250.8 mMD Porosity is decreasing with increasing clay content. Core shows higher bioturbation than in the sand layers above.

3250.8 – 3259.0 mMD Effective porosity is mainly below the cut off value of about 6%. Clay content is higher than in the intervals above.

3259 – 3268 mMD This interval indicates high shale/silt content with no or marginal effective porosity.

3268 - 3270 mMD A silty sand layer with low porosity and high water saturation. 3272 - 3274 mMD A silty sand layer with slightly higher porosity than the layer above.

### 3.7 Lithology

The following Figure 10 lithotype declaration shows the lithology definition after PETTIJOHN, POTTER & SIEVER, 1972. The dots in green represent samples taken from 3234m-3237m, the red ones are from 3264m- 3294m and the blue ones represent a different type taken from 3264m-3291m. It is obvious that the majority of the samples is defined as Sublith-arenite.

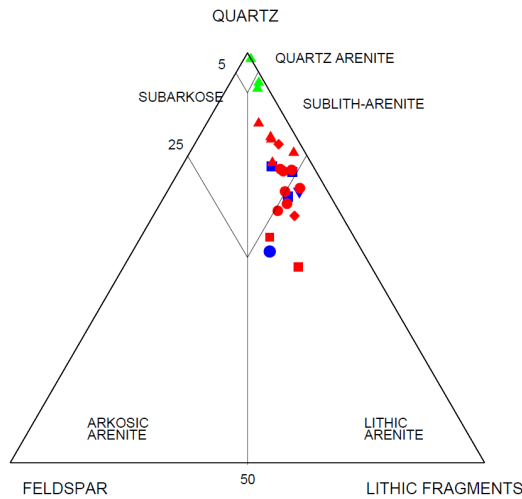


Figure 10 lithotype declaration [1]

To be consistent in describing the lithology the following Figure 11 bulk and clay show the detailed composition of a typical rock sample in the South.

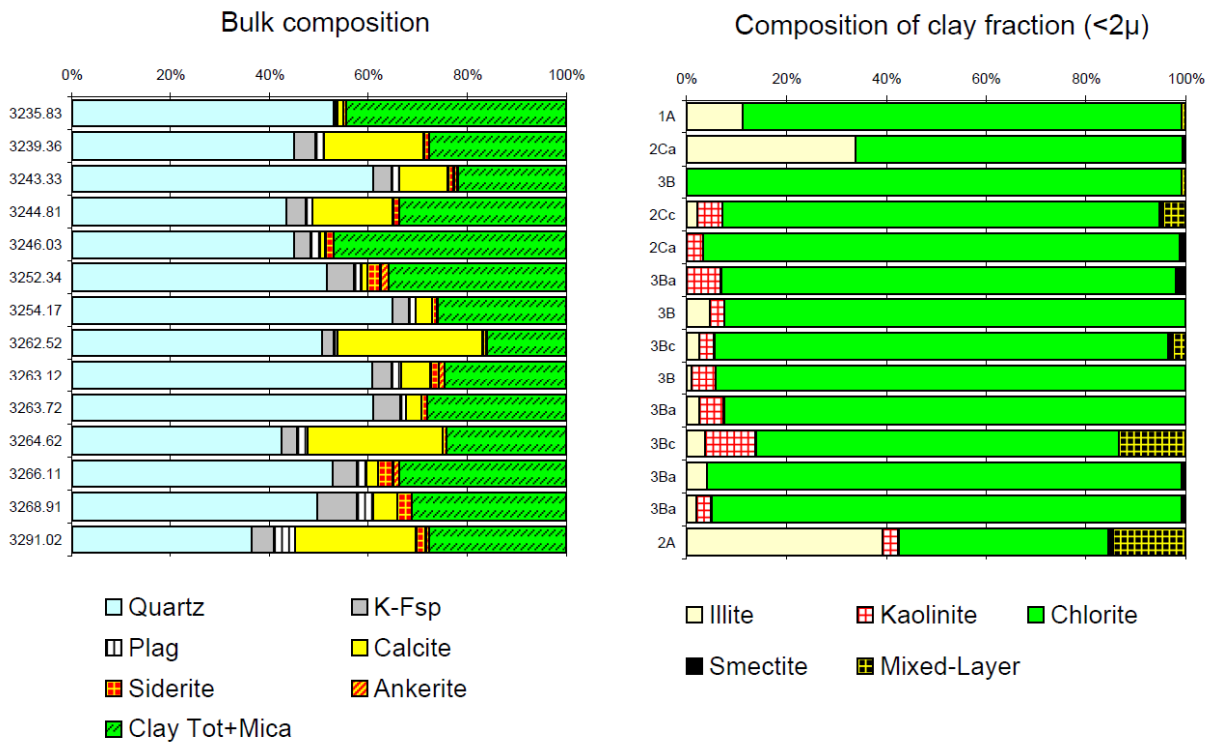


Figure 11 bulk and clay composition [1]



Table 2 rock properties

Formation thickness:	66.6 ft.
Average formation Porosity:	15 %
Water saturation:	45 %
Gas saturation	55%
Total system compressibility	8.0118 e-5 psi-1
Layer pressure (for PVT calculations):	5375 psi
Layer temperature:	346 °F
Well Parameters Data Well radius:	0.25 ft.

### 3.8 Fluid data

The basic input parameters were taken from the log and core data conducted earlier by the company and are as follows:

Fluid Parameters Data as input [1] for simulation can be seen in the table below:

Table 3 fluid data

Gas gravity	0.64
Water-Gas ratio	5 STB/MMscf
Gas viscosity	0.0245 cp
Gas formation volume factor	0.0045 ft <sup>3</sup> /scf
Water density	56.441 lb/ft <sup>3</sup>
Water viscosity:	0.1493 cp
Water formation volume factor	1.1053 RB/STB
Initial Z-factor	1.0797
Gas compressibility	1.3453 e-4 psi-1
Water compressibility	4.4878 e-6 psi-1

## 4 PROBLEM DEFINITION

The wells encountered the southern area are producing dry gas before and little gas with a very high water cut after the hydraulic fracturing so that it is not economically at all to produce anymore. Despite the fact it happens also that after a few days the production is aborted due to too much water influx. This information is given by production history where one can see the huge increase in water production. The reason why the production stops is known and it is very simple: gas is produced because it is very light (low density) and the reservoir pressure is sufficient to lift the gas eruptive to the surface. When water comes into account the density is changing according to the amount of water in the fluid- the fluid mixture gets denser and therefore heavier.

In comparison to that a normal behaviour of a long time produced gas field would be the following: during the production of natural gas the available energy responsible for transporting the fluid to surface declines with time or declining reservoir pressure. This energy of transport eventually becomes so low that the flow rates are very low and the liquid produce together with the gas are no longer transported but stuck and held in the wellbore. So the liquid is accumulating at the bottom of the wellbore hindering new gas to flow into the wellbore and causing additional backpressure. This effect is known as “Liquid Loading” Both above named effects stops the production, but in comparison to the first one this effect is very slow and can be estimated very early with a simple calculation. The second effect is not the production issue of this field → the source of water is unknown and has to be figured out.

### 4.1 Water source

A lot of different studies have been conducted to the field with no satisfying statement where the water is coming from and how avoid water production. This thesis will focus on one effect and clarify whether this effect is prominent or not.

#### 1) Micro pore feeding (Capillary bound water)

Different model scenarios will be used later on to understand this fact, one has to know how the reservoir rock in this area is built up and what minerals the reservoir rock layers consists of. Capillary water is kept in micro pores of the reservoir rock by capillary forces. It is immobile. Capillary bound water behaves immobile during the first stage of production. Core investigation shows a water saturation of more than 40% throughout the whole reservoir.

There is a possibility to release this bound water from these micro pores. When a fracture is created in a reservoir rock, the pressure drops all by sudden.

The statement of investigation is now: Is the pressure drop caused by fractures sufficient to release the bound water from the micro pores?

## 5 EFFECT INVESTIGATION

Task of this section is to explain the steps I did to find out whether this effect is the reason for the water influx or not. The investigation starts with capturing the right data, interpreting them and using them for further simulations.

### 5.1 Capillary pressure tests

In order to get capillary pressure curves of a rock sample, tests have to be conducted. In general three methods are described in literature regarding the measurement of capillary pressure:

- Mercury methods
- Porous-plate methods
- Centrifuge methods

Only the data of the mercury injection experiment were taken as input for the simulation scenario and therefore only this method is described in detail.

#### 5.1.1 Mercury injection method

First, the rock sample is evacuated and the volume of mercury that is entering the sample with increased pressure is measured as shown in Figure 10 mercury capillary pressure measurement below. This method is highly recommended for the investigation of porous structures. Therefore the result of this method is going to be used later on in this thesis. A full test is carried out within an hour or so, but is also dependent on the rock permeability.

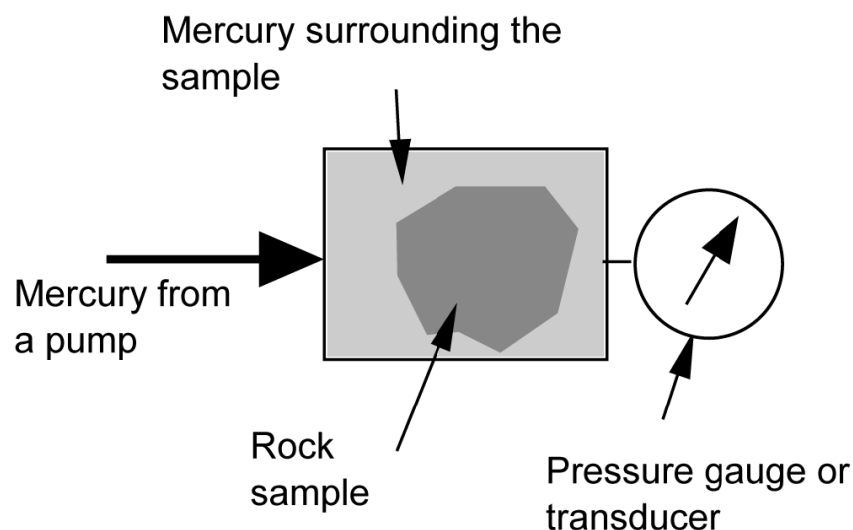


Figure 12 mercury capillary pressure measurement [3]

The first documentation of this method was published in the petroleum literature by Purcell in 1949 [4] There he explained a method for the estimation of permeability from mercury measurements.

### 5.1.2 Mercury Injection tests procedure

The following test procedure was taken from a company report and is displaying how the mercury injection procedure is working.

1. The samples get cleaned and weighted and afterwards placed in the bulb of a penetrometer so that the sample is approximately 80% of the volume of the penetrometer stem.
2. The next step is to weight the penetrometer and sample together.
3. Penetrometer containing the sampled is then loaded into a pressure chamber. In this specific case the chamber of a Micromeritics Autopore 11 9220 porosimeter.
4. After the evacuation of the penetrometer to 50 $\mu$ m of mercury, it is filled with mercury at a pressure of 0.5psi. At this point, the bulk volume of the sample is determined.
5. To increase the saturation of the non- wetting phase (drainage), mercury is injected with increasing incremental pressure form filling pressure of 0.5 psi to 25.0 psi.
6. The equilibrium at each pressure point is identified and monitored over a specified time step. If the pressure remains above 99.5% compared to the injection pressure over this time period, the equilibrium can be assumed and the total intruded volume of mercury can be recorded. If this is not the case and the pressure drops below 99.5%, the pressure is reset and monitored again over the whole time period. This has to happen until the equilibrium is achieved for each pressure step.
7. After the injection procedure, pressure is reduced to atmospheric and the penetrometer is removed and weighted again together with sample and mercury in place.
8. The following step is to load it into a high pressure chamber of the Autopore system.
9. The cumulative volume of mercury injected is increased by increasing pressure. This step is necessary for the later on calculation of the pore size distribution. Pressure is increased up to 60,00psi and the data is recorded for each time step as described in step six above.

### 5.1.3 Calculation of mercury injection data

10. The weight of the pure sample and sample and penetrometer weight with and without mercury are the base for bulk density and grain density calculation.
11. The injected volumes of mercury are also recorded.
12. Due to surface roughness, initial apparent intrusion at low pressures are not representative of the pore structure and have to be removed.  
As a threshold value for mercury injection into pore space is the point where a rapid increase in mercury injection takes place. The cumulative apparent injection up to this threshold pressure is subtracted as surface porosity from measured data before subsequent calculations are made.
13. The minimum radius of pore throat at any mercury displacement pressure that can be penetrated by mercury is given by the following equation pore throat radius.
14. Cumulative volumes of mercury injected are expressed as a fraction of the total pore volume of the sample.

Equation 1 pore radius

$$r = \frac{2\sigma \cdot \cos\theta_1 \cdot C}{Pc} \quad (1)$$

where:

r = pore throat radius,  $\mu\text{m}$

$\sigma$  = interfacial tension between air and mercury, dynes/cm

$\Theta_1$  = contact angle between air and mercury, degrees

Pc = capillary pressure, psi

C = conversion constant

With this relationship, one can construct a graph of fraction of pore volume injected ( $v$ ) versus pore throat radius can be constructed.

The differential of this gives a pore size distribution (PSD) function. Not explained here. The normalized pore size distribution function displayed graphically can be used to identify pore type groupings and the relative volumes of

- Macropores ( $>1.5\mu\text{m}$ ),
- Mesopores ( $1.5$  to  $0.5\mu\text{m}$ ) and
- Micropores ( $<0.5\mu\text{m}$ ).

15. the following conversion is used to obtain Oil-brine capillary pressure (reservoir) data from air-mercury data:

Equation 2 Oil-brine capillary pressure

$$PC_{o-b} = PC_{a-Hg} \cdot \frac{\sigma_2 \cdot \cos\theta_2}{\sigma_1 \cdot \cos\theta_1} \quad (2)$$

Where :

$PC_{o-b}$  = oil-brine capillary pressure (reservoir), psi

$PC_{a-Hg}$  = air mercury capillary pressure, psi

$\sigma_2$  = interfacial tension between oil and brine (reservoir), dynes/cm

$\Theta_2$  = contact angle between oil and brine (reservoir), degrees

$\sigma_1$  = interfacial tension between air and mercury, dynes/cm

$\Theta_1$  = contact angle between air and mercury, degree

16. The mean hydraulic radius (MHR), is the average pore throat size of the sample and is given by the

Equation 3 mean hydraulic radius

$$MHR = \frac{\sum_{i=0}^n (r_i^2 \cdot (S_i - S_{i-1}))}{2 \cdot \sum_{i=0}^n (r_i \cdot (S_i - S_{i-1}))} \quad (3)$$

where:

$S$  = mercury saturation, fraction of pore volume

17. Swanson's parameter is another means of correlating capillary pressure with permeability. [5] The technique involves determining of Swanson's parameter ( $S_b / PC)^A$  (where  $S_b$  = mercury saturation, fraction of bulk volume) which is related to the effective pore space contributing to fluid flow and the corresponding injection pressure. The Swanson parameter is determined by calculating  $(P_c/S_b)$  at all pressures for any sample and taking the minimum of these values, as outlined by Walls and Amaefule [6]. It is recommended that a cross plot of actual measured permeability's against the Swanson parameter be used to better define the correlation coefficients for the formation in question.
18. A method for comparing capillary pressure data from various systems is the use of the Leverett J function. It is a capillary pressure function, is dimensionless and can be expressed as in  
Equation 4 Leverett J function

$$J = \frac{0.2166 * P_c * \sqrt{(k/\phi)}}{\sigma * \cos\theta} \quad (4)$$

where:

J = Leverett capillary pressure function, dimensionless

$P_c$  = Capillary pressure, psi

$\sigma$  = Air-mercury interfacial tension, dynes/cm

$\Theta$  = Air-mercury contact angle, degrees

k = Permeability, md

$\Phi$  = Porosity, fraction

### 5.1.3.1 Results

All of the measured samples show a behaviour of a bimodal pore throat size distribution. The radii range from very small 0.02 to 0.1  $\mu\text{m}$  and a broad maximum around 1  $\mu\text{m}$ , respectively and can be seen in the figure next to this section.

Explanation of the results: [1]

The 1  $\mu\text{m}$  range determined micro-porosity can be explained by an iron-rich chlorite overgrowth layer coating the quartz grains.

Sub porosity of the chlorite crystals is responsible for the peak between 0.02 and 0.1  $\mu\text{m}$ . Additional to that, compressibility under high pressure affects the porosity.

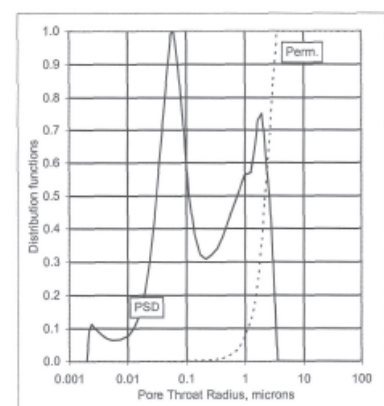


Figure 13 pore size distribution

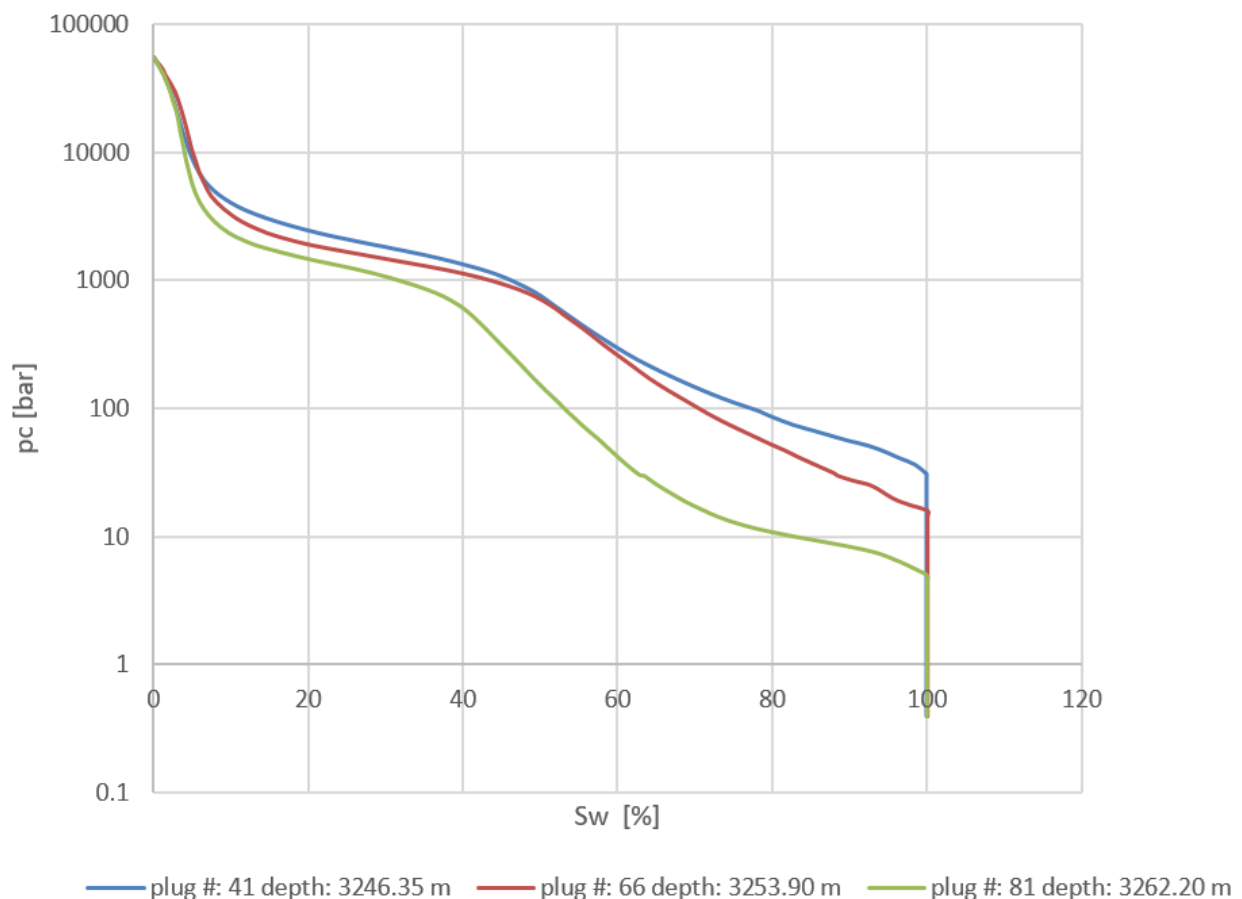
## 5.2 Test Interpretation

In this section the data from the conducted capillary tests (MICP) was used to construct capillary pressure curves. This step is necessary to investigate the behaviour of the reservoir rocks in order to predict eventually water invasion. The following graphs are showing the equivalent water saturation conducted in this tests. During this test the mercury saturation is monitored. The water saturation can afterwards be calculated using the sum of the saturations. The water saturation plus the mercury saturation add up to one.

### WELL 4

In this case only three samples were available for MCIP tests. The result of this test can be seen in Chart 1 Well 4 below.

Chart 1 Well 4



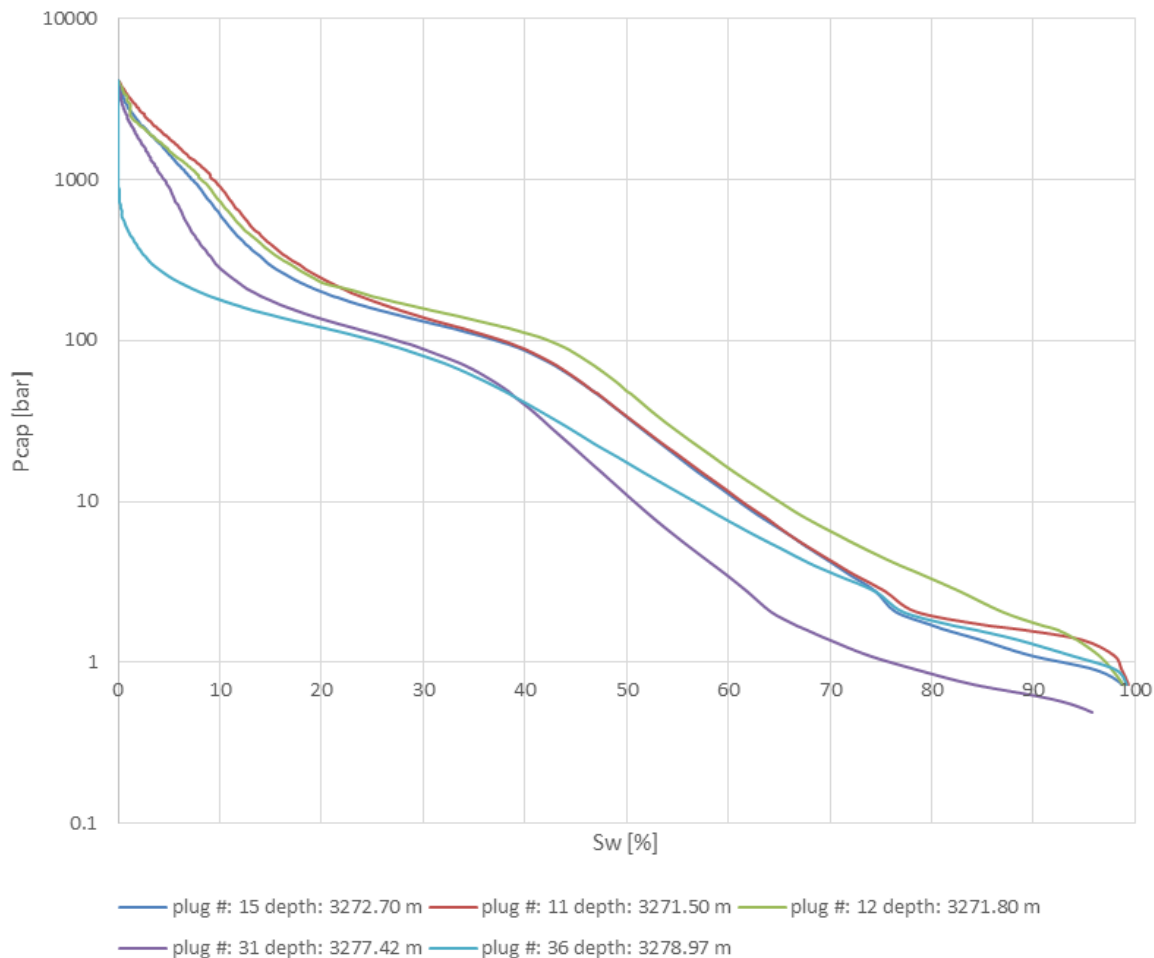
The curves show a bimodal behavior meaning that there are two distinct regions in the reservoir rock regarding the capillary pressure. This behavior is explained as follows. The rock consists of macro pores and micro pores. The meaning of this outcome will be explained in the result section.



## WELL 5

Five different core plugs from depth starting at 3271.5 m down to 3277.42 m were analysed and afterwards plotted. The result is plotted in semi log plot to visualize the behaviour in a better way. The outcome of this measurement can be seen below in Chart 2 Well 5.

Chart 2 Well 5



The core of this well shows not the same behaviour as the one of Well 4. One can see one steep slope from zero to 20 percent water saturation. Afterwards there is a plateau followed again by a steeper slope. The bimodal distribution is not as sharp as in the first well. The production scenario in well number five shows a not very dramatic increase in water production then in well number 4.

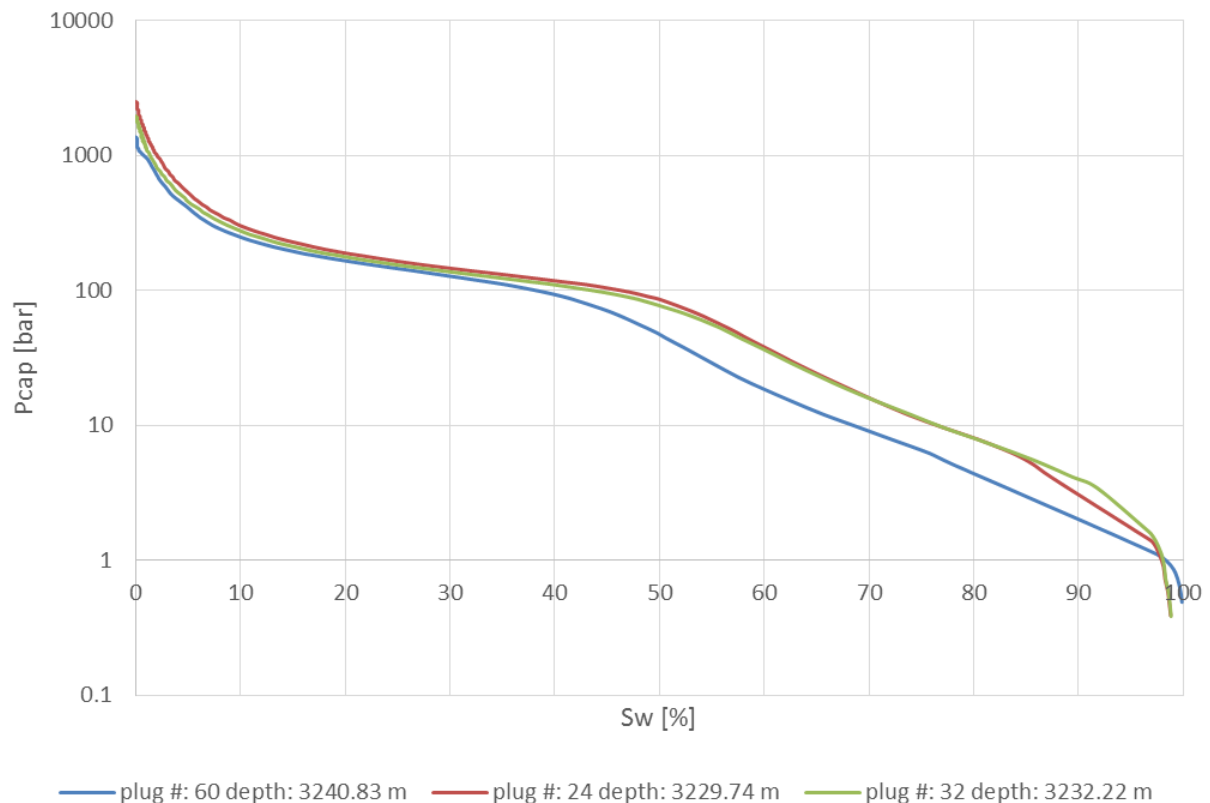
This is maybe caused also by the different pore size distribution of the reservoir rocks and has to be investigated.

The offset of the curves is caused by the difference in depth.

## WELL 6

Three different core plugs from depth starting at 3229.74 m down to 3240.83 m were analysed and afterwards plotted. The result is plotted in semi log plot to visualize the behaviour in a better way. The outcome of this measurement can be seen below in

Chart 3 Well 6



The curves of reservoir rock sample in well 6 are not showing the bimodal distribution like well 4 and 12 although there is a plateau indication relatively many micro pores of the same size. So still a large portion of the rock pore throats are made of micro porosity. The curve is simple showing, that the macro pores are more evenly distributed in this reservoir zone.

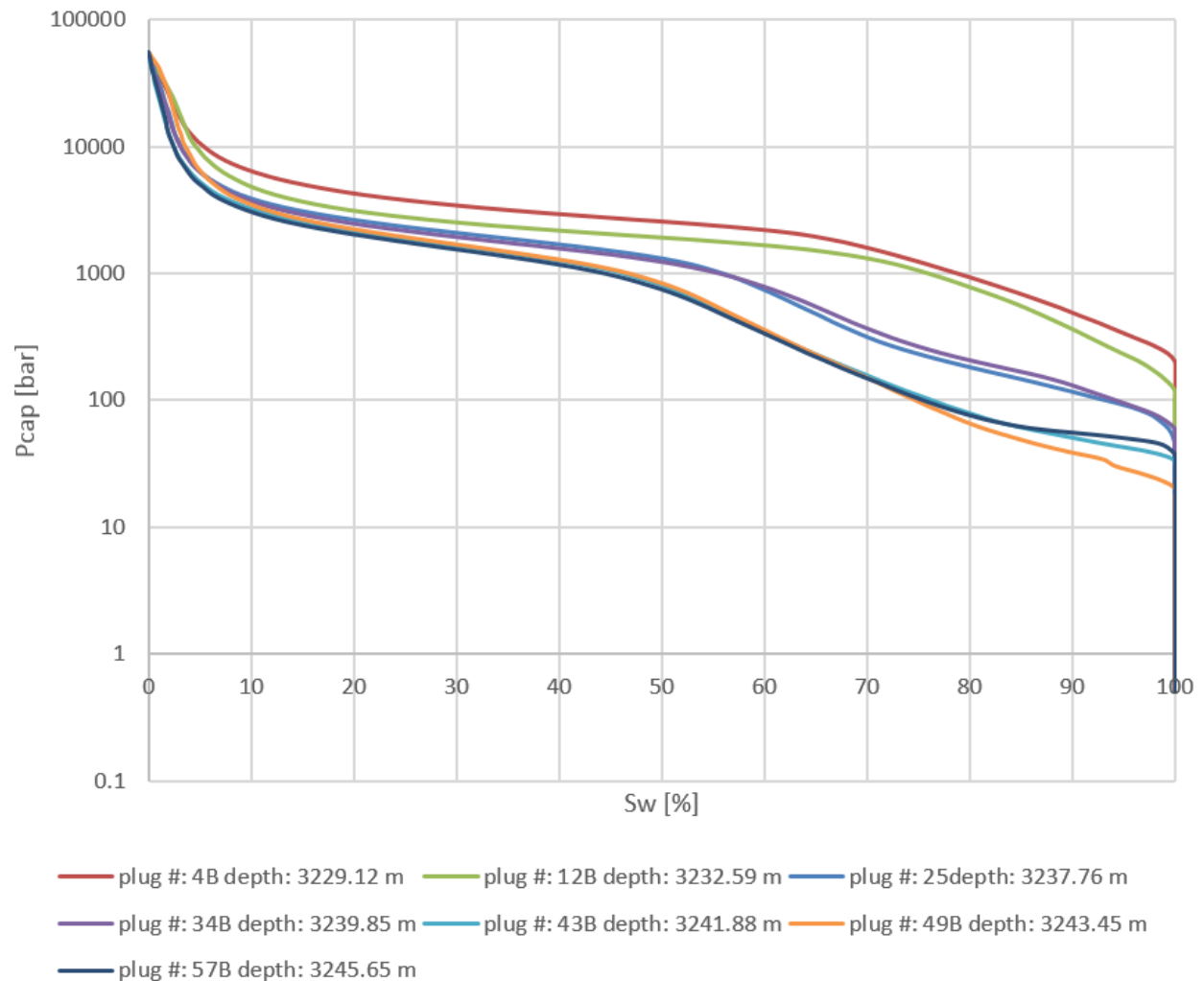
The rock consists of macro pores and micro pores. The micro pores can be seen in the area of high capillary pressure. High capillary pressure means that a high pressure is needed to enter these pores. The meaning of this outcome will be explained in the result section.

The offset of the curves is caused by the depth difference

## WELL 12

Seven different core plugs from depth starting at 3224.65m down to 3245.65m were analysed and afterwards plotted. The result is plotted in semi log plot to visualize the behaviour in a better way. The outcome of this measurement can be seen below in

Chart 4 Well 12



The curves show a bimodal behavior meaning that there are two distinct regions in the reservoir rock regarding the capillary pressure. This behavior is explained as follows. The rock consists of macro pores and micro pores. The meaning of this outcome will be explained in the result section. The offset of the curves is caused by the depth difference.

One can see that not all the wells shows clearly this bimodal distribution behaviour. Some samples of well 4 and 12 can be determined as bimodal but there are also samples without thus behaviour.

## 6 RESERVOIR MODEL

The creation of a complex reservoir model was not part of this thesis since it has been created already and provided by the company. The reservoir model was built in order to predict the gas production in the WELL South area. This process was successful for those wells having no production issues. But when it came to heavy water production, the matching process failed. Therefore an aquifer was added to the model. Partially information was taken from the model to create a simple generic one later on. The reason why the geological model was not used in this part of the project is simple that the model is already fed with some artificial data and this is it what should be avoided with the generic model.

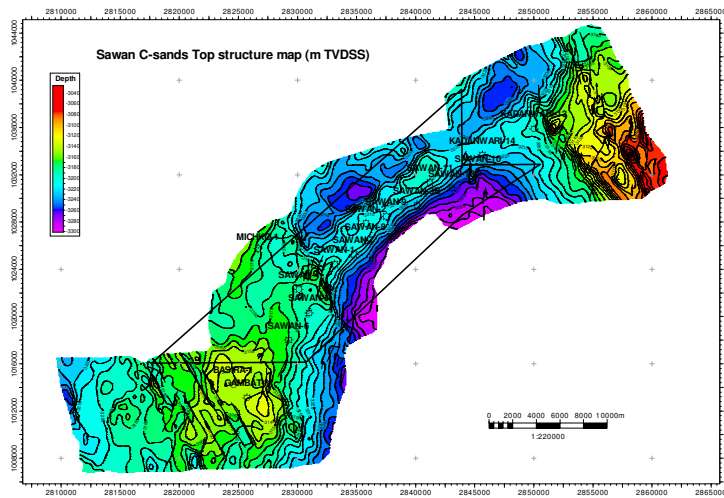


Figure 14C sands top structure map

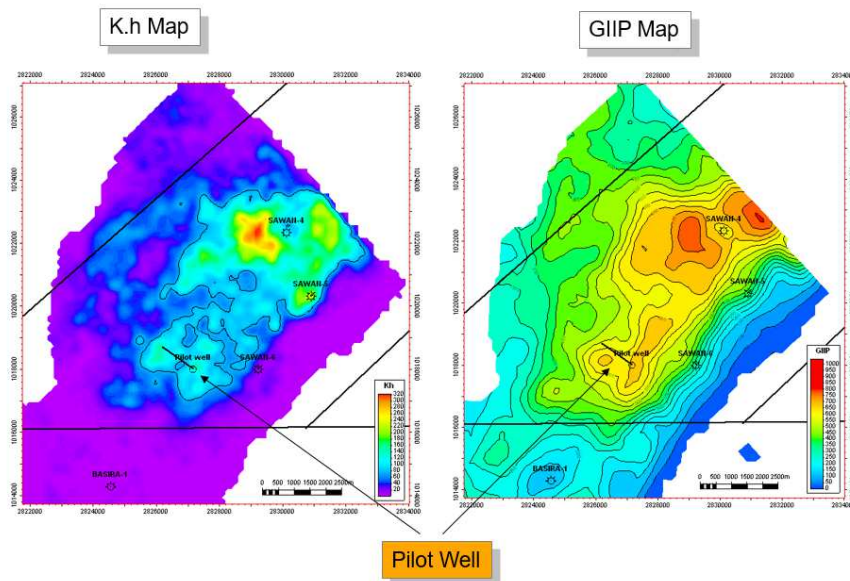


Figure 15 K.h and GIIP map [1]

## 7 GENERIC MODEL

A generic model was created in order to prove the fact, water is produced from inside the reservoir. The original theory of the company was that fracturing caused a connection to an underlying aquifer although geology proposed none below the reservoir. As mentioned above, a reservoir model was already created years ago. The high water rate was matched by introducing a Fetkovich aquifer. (This is one of several models determine water influx and other properties of the aquifer layer) The approach discussed in this thesis is not implementing any artificial reservoir objects. Goal is to clarify the water production according to special effects discussed already above. Important to note is that all the properties are taken from real reservoir data and can be found in the model input section.

### 7.1 Model Input

All the input parameters were taken from papers provided by the company in order to ensure a reliable model. Due to the fact that this model is a generic one, the complexity is kept low. This does not mean that the output is not useful, because goal is it to inspect the effect that causes water production. Furthermore it was not intended to match any rates, but to provide a certain relationship between production data and model output. A summarization including a detailed description can be found in the appendix. The following input section are used to determine the properties:

#### **Layer parameter:**

- This section contains information about the layer specification including depth, temperature, height, cementation factor, rock compressibility ...

#### **Fluid properties**

- All parameters somehow related to the fluids in the reservoir are listed here. Fluid parameters are important to specify, because they have a huge impact on production behaviour.

#### **Fracture properties:**

- The fracture properties were taken from post fracturing reports provided by the company. In order to ensure the proper model result this section was treated very carefully with respect to depth relations. A simulated fracture can be seen in the picture in the appendix. Simulation model assumes a rectangular fracture shape with an average value.

#### **Reservoir properties:**

- This section is to specify the reservoir properties itself. So here the porosity and permeability of the reservoir is defined.

#### **Gas composition:**

- The gas composition data was delivered from the laboratory where the gas was analysed. As expected, the gas is a very dry gas. Additionally to that a small amount of carbon dioxide was found within the probes.

## 7.2 Model Setup

The model setup is following the structure of the Builder Simulation tool from Computer Modelling Group (CMG) Ltd. and provides an insight in the structure of this tool. This tool is used in order to build easy reservoir models. It furthermore provides the ability to induce fractures and therefore this tool is sufficient in his respect.

### Reservoir

As mentioned already above, all the data are coming from real field data measurements. The grid dimensions were chosen in a way that the behaviour can be displayed reasonable. This means that the vertical extension is considerable low in comparison to the later extension since the reservoir height is very small compared to its horizontal dimensions.

The rock compressibility was measured in rock compressibility tests by the company and the reference pressure is by default 14.6923 psi (representing the surface pressure).

### Components

Here the selection of the system is made. In this specific case a gas- water model is chosen since there is no oil show in this reservoir. Different fluid data, meaning gas and water properties were entered in this section as well.

### Rock- Fluid

The relative permeability data are entered in this section. The relative permeability describes the ability of a fluid to flow in presence of another fluid. In a gas water system the relative permeability of gas and water is taken from special core measurements.

Another property that has to be defined in this section is the capillary pressure function. The capillary pressure function describes the saturation of a rock as a function of pressure.

The curve so describes the rock pore throat distribution. The reservoir rock is water wet- without any pressure difference of the wetting phase (water) and the non-wetting phase (gas) the rock is fully water saturated (A).

As the pressure difference increases, gas is forced to enter the pores. Since the pressure difference is low only the bigger pores are occupied by gas.

Situation (B) describes the beginning of the water drainage process (water is replaced by gas). Drainage means that the wetting phase is replace by a non- wetting phase. The pressure difference that causes the first replacement of the wetting phase is called capillary

entry pressure. Pores having a very low entry pressure are big pores in this regard. They are called macropores.

As the pressure difference increase further, more and more water is replaced by gas. This replacement depends on the pore throat sizes. The larger the pore throats are, the easier the replacement (lower pressure needed). For small pore throats a big pressure difference is needed in order to replace the wetting phase.

Situation (C) is indicating a zone of high entry pressure pores. This zone shows the presence of very small pore throats. Let's call them micropores. Having micro and macro pores in a system means that the reservoir is a dual porosity system. In this case the microporosity was formed by mineral growth around the grains as explained already before. Another possibility of dual porosity systems would be a fractured reservoir for example.

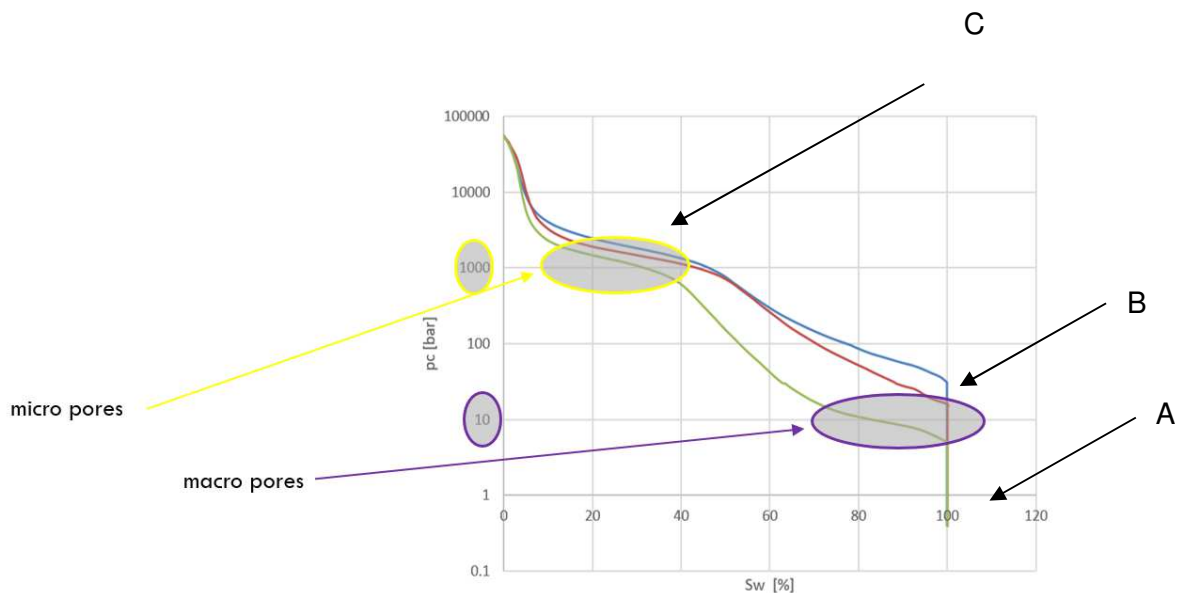


Figure 16 capillary pressure input curve

### Initial conditions

Setting initial conditions is mandatory for reservoir models. This ensures that the model is in equilibrium prior to simulation. This simulator setting is set to a situation that no flow is accruing with in the grid cells itself. Every grid block is in equilibrium as it is the real situation is the reservoir.

### Wells and recurrent

One well is placed in the middle of the reservoir, perforating the uppermost layers.

Since no gas can be produced without drilling a well into the reservoir also a well is included in the reservoir model. The model allows to define the position  $n$  of the well within the

reservoir. In this case the well is located in the middle of the reservoir, perforating the uppermost layers. This is representing the real field example. Perforation are set for all the three layers, meaning that the uppermost layers can be produced.

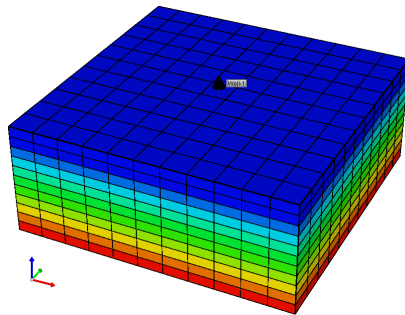


Figure 17 3D model

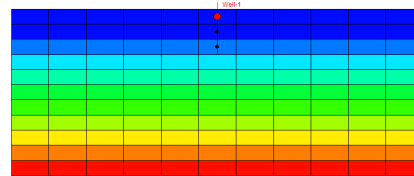


Figure 18 cross section slice

The production history of the wells in the field shows that the wells were fractured once in their production phase. At this point the issues with water production started. Therefore also fractures were initiated in the model. The data entered in this section are also coming from company data. A planar model was selected fracturing the three uppermost layers. The input data can be seen in the appendix.

Additional to that a local grid refinement is added to the model for the following reason. When a fracture is initiated in a grid block, the data entered for the fracture is taken as local property. Since grid block dimensions are very big compared to fracture width the whole grid block will get the fracture property. This property is influencing the whole grid and is not representative anymore. With grid refinement only a part of the grid block is assigned with the fracture properties including a more realistic scenario. For simplicity only horizontal fractures are set up and all the parameters were taken from the fracture evaluation papers. The fracture evaluation indicated horizontal fractures as well. Of course the geometry is more complex but since this is a generic model it is kept simple. The following figure shows the grid refinement according to the fracture. The color scale is showing the initial water saturation.

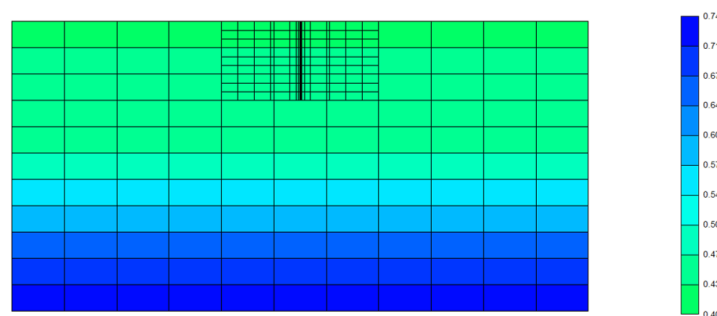


Figure 19 fracture grid refinement



## **7.3 Simulation Scenarios**

### **7.3.1 Normal production simulation**

This model concludes a normal production behaviour without any treatment. The model setup can be seen in the section model setup. The results are as following.

Important to note is that a high production rate was chosen in order to see the effect in reasonable time. This doesn't mean that the rate is not field related. It simple means that the production facilities are producing at their upper limit.

### **7.3.2 Including hydraulic fracturing**

This scenario is the most important since it either confirms the effect of micro pore feeding or not. The setup is the same as it was for the normal production scenario.

After one year of production, a hydraulic fracturing process was initiated like it was the case in the real field.

The production rate was kept at the same level than it was before the fracturing process. The input data for the fracture geometry is described in the model setup section.

### **7.3.3 Comparison normal production- hydraulic fracturing**

This part is to compare the output of both the normal production scenario and the one with hydraulic fracturing.

At this point one has to know that the aim was to make clear if there is a difference in water production (like in the field) or not. Therefore the focus is on water production with respect to gas production.

## 8 RESULTS

In this part of the thesis different Simulation scenarios were evaluated and the rates are plotted using the results graph and the results graph 3D tool from CMG. In order to make the effect visible different parameters were changed and compared to a base case. This allows to see whether there is a major influence in production behaviour according to a certain parameter change or not. At the end of the day this evaluation method helps to give a meaningful explanation about the sensitivity of this reservoir to an input parameter.

The primary task of the model was to confirm the effect of micro pore feeding effect or to state that this effect is not active in the field.

The scenarios were conducted in the following way:

A base case was created using the original input parameter. Afterwards a fracture stage was created one year after the start of production. From that point on the scenarios were split into different scenarios including parameter changes.

The following scenarios were evaluated with respect to Water gas ratio. Water gas ratio was chosen since the company has provided gas rate and the water gas ratio values after fracturing. Since no water production was given the model should confirm the water gas ratio (WGR).

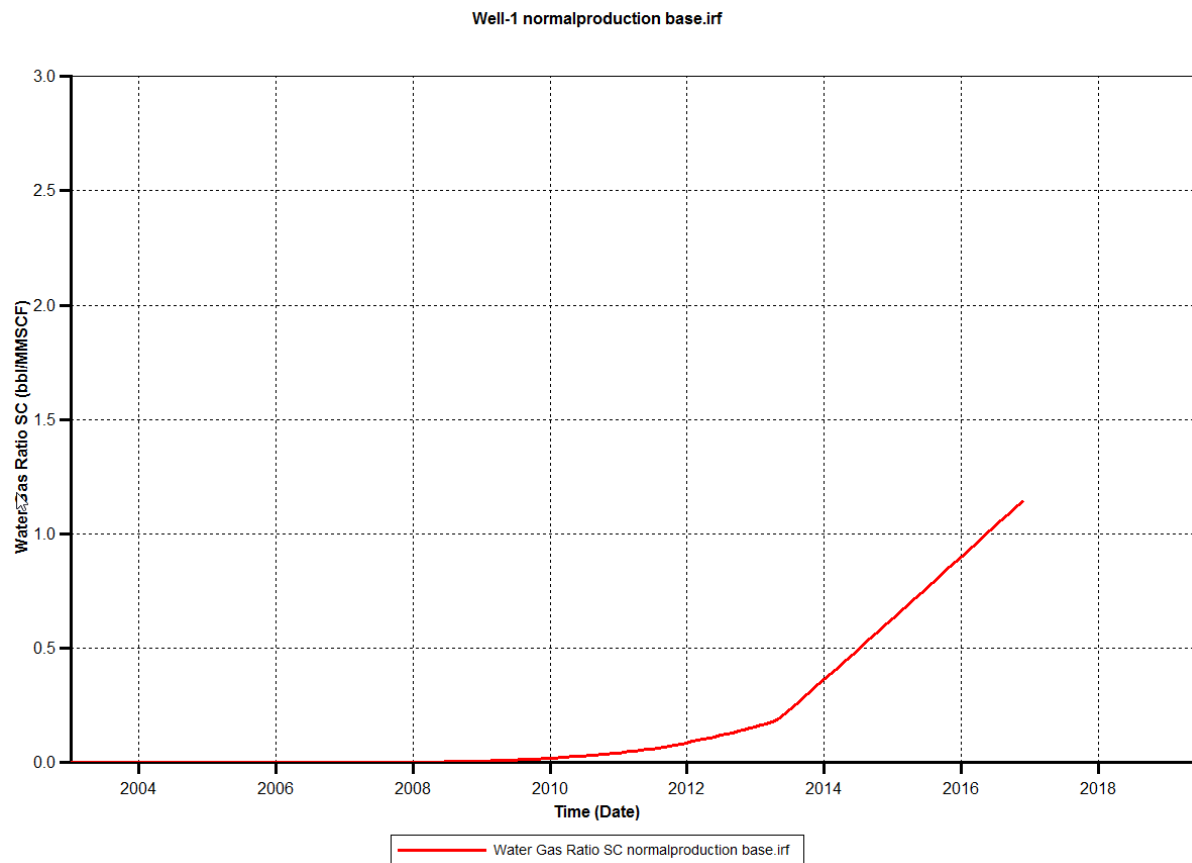
Table 4simulation scenarios

Parameter	scenario			
	Base case		Fractured scenario	
Capillary Pressure	Without fracturing	base case with fracture	Exclude special capillary pressure function	
Permeability			High permeability	Low permeability
Porosity			High porosity	Low porosity
Initial water saturation			High Swi	Low Swi

Table 5 scenario overview

## 8.1 Base case scenario

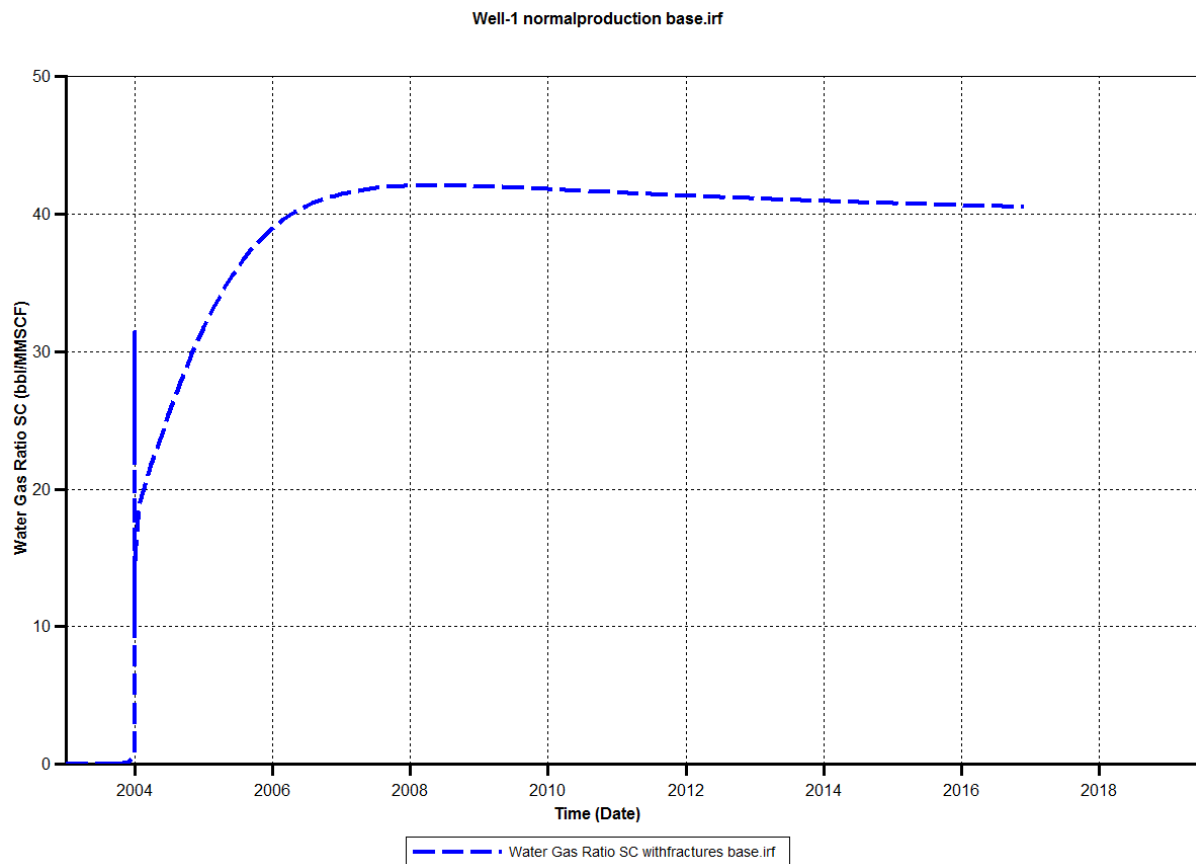
The base case scenario is assuming the given reservoir situation. No hydraulic stimulation treatment is considered at this point in time.



The base case scenario is showing the behaviour of the reservoir without any fracturing process. The water gas ratio of the not fractured case is indicating a very low ratio which means that very less water is produced from the reservoir. After a few years the water production increases caused by the effect that the gas is produced from the uppermost layers forcing the water from imbibing the layers and water is produced from the layers as well. In the beginning only gas is produced from this kind of reservoir according to the reservoir setting. The reservoir layers are showing a high water saturation but since water is the wetting phase gas is produced to a limit where also water is produced.

The increase in water gas ratio seems to be dramatic but in reality it is very low compared to the WGR of other reservoirs. So WGR of this scenario can be neglected.

## 8.2 Base case with fracture

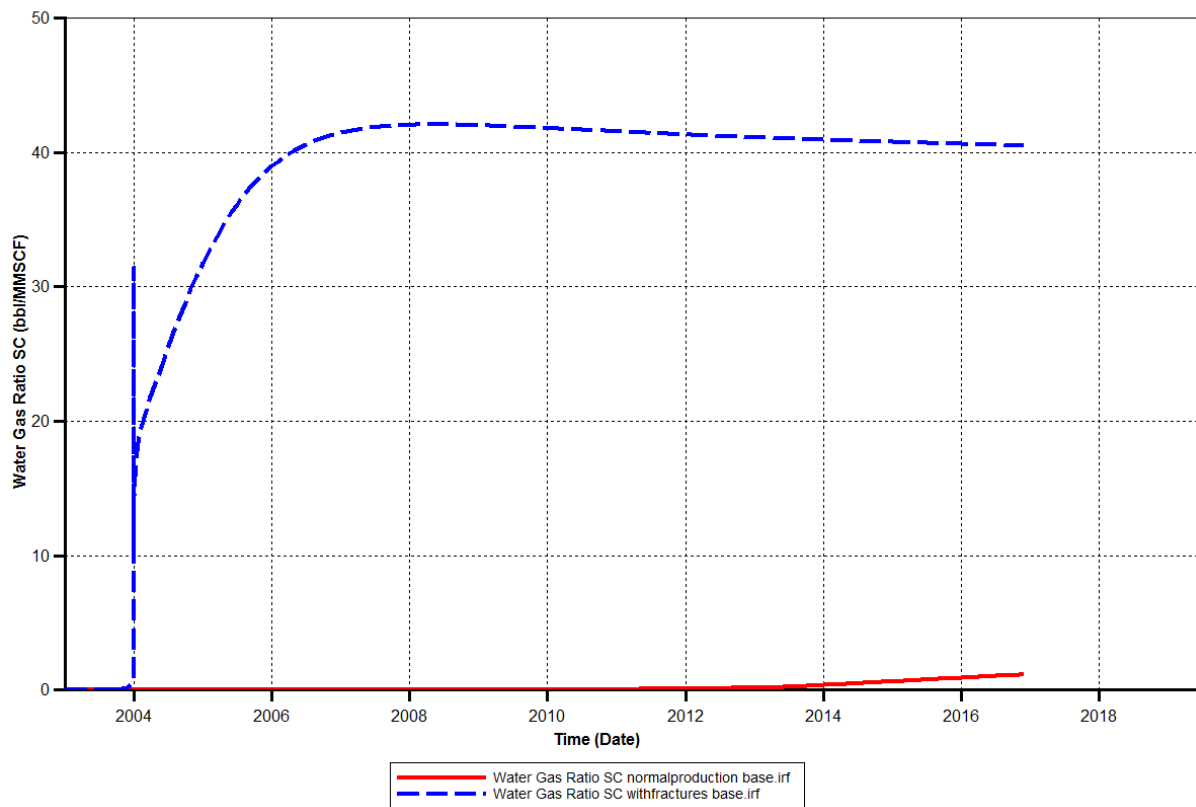


The WGR of this scenario is low for the first year where no production was considered. After fracturing the uppermost three layers the WGR increased by a factor of magnitude 40 compared to the original case. This increase is explained by the fracturing process. What is happening during this process? The effect is explained afterwards. It is important to show that the capillary pressure has a major influence on the production behaviour. This effect shows as well, that the capillary pressure influence plays a major role in producing water within this reservoir.

The increased water gas ratio shows the same behaviour than the company faced during production time in the field. The model so confirms the effect in this regard.

### 8.3 Comparison base case

This section compares the scenarios of normal production and the fractured case. Although production cannot be compared this scenario should consider the difference in production.



The comparison of the two different production scenarios shows that the difference in water gas ratio is huge.

One can see that after fracturing stage the water gas ratio increase dramatically in the scenario of hydraulically fracturing.

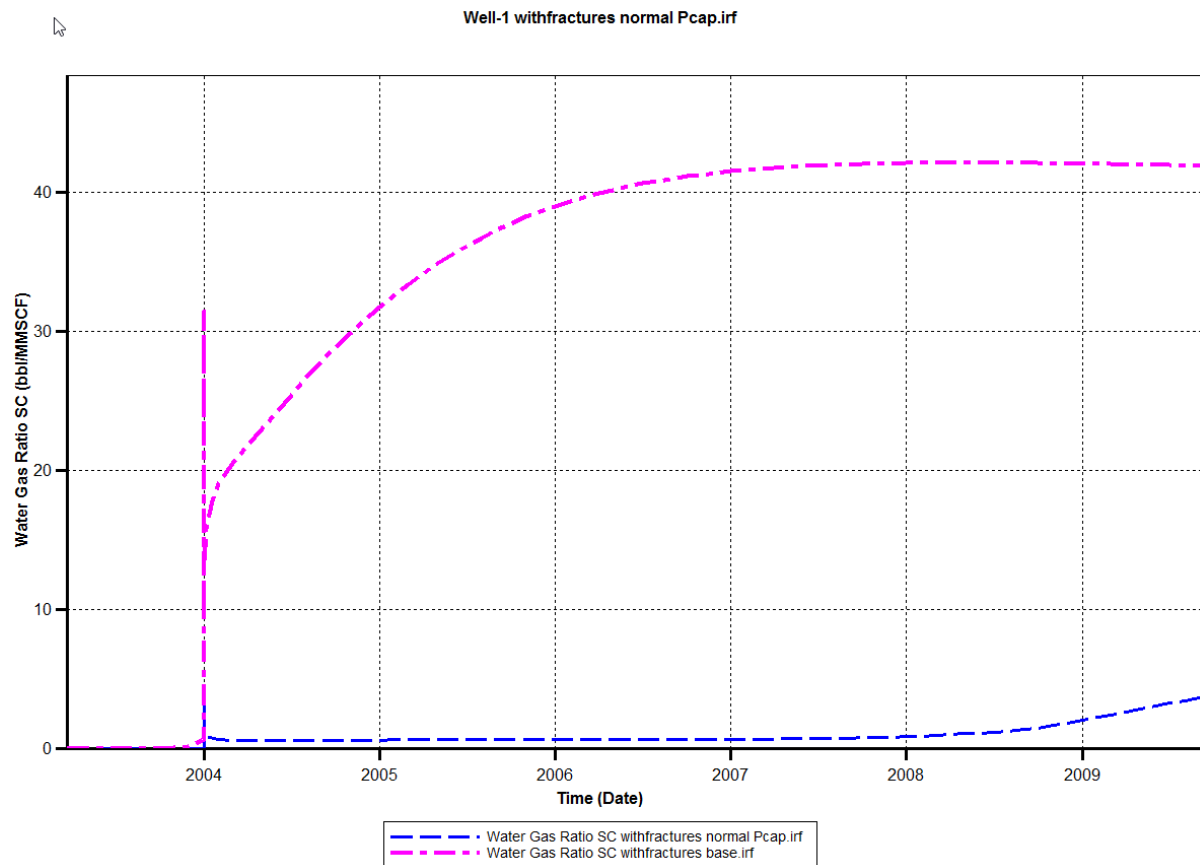
This behaviour is indicating that the fracturing process is affecting the gas production.

One can further see that the difference in water production differs very much from the production scenario without fracturing process. As a short notice here the gas ratio is increased due to fracturing but since this process is also increasing the water ratio to a higher amount, the WGR is increased and therefore the relative gas production is lower than before.

The water gas ratio is determined by the bbl of water produced as one MMSCF of gas is produced. The WGR ratio determines the economic of a well and since the water production is very high, wells producing at that high water rates are not economic at all.

## 8.4 Capillary pressure scenario

Since the curve from the plot on page 48 already confirms already the effect of the influence of capillary pressure, this plot is to state the effect in another way.

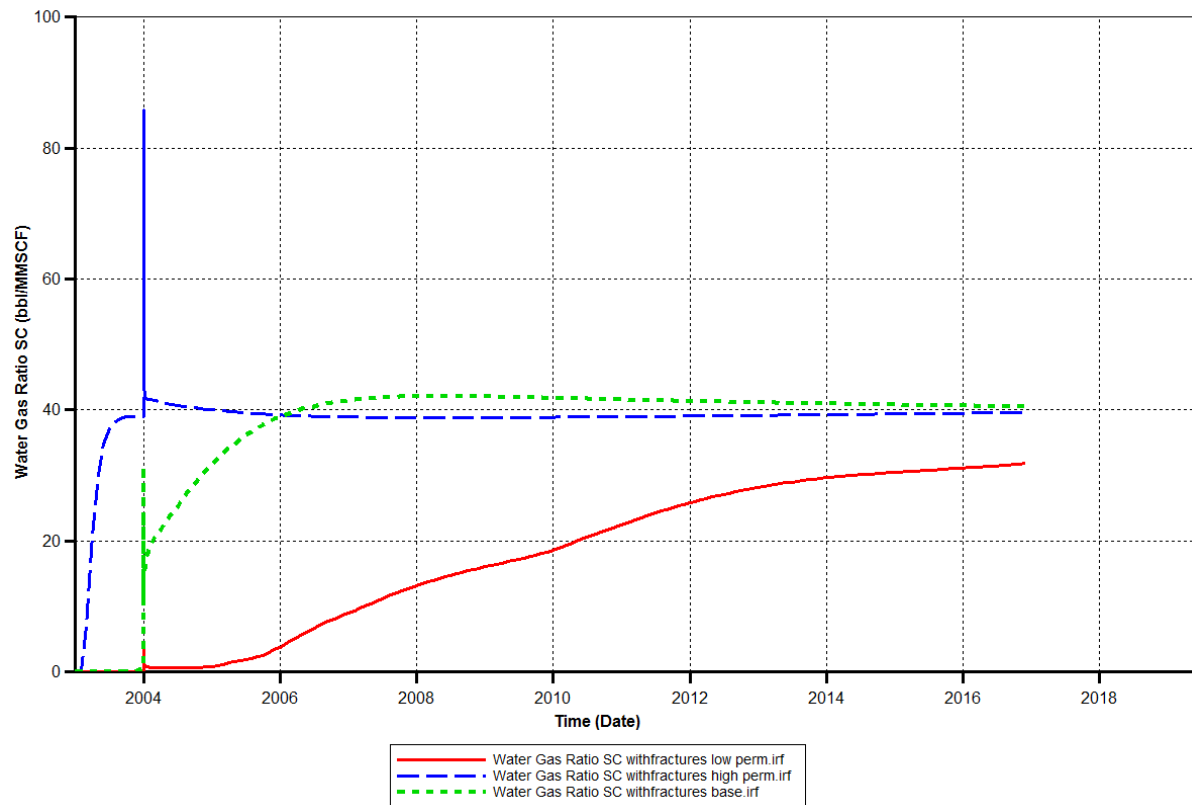


The blue curve is indicating the production behaviour of a well that is fractured after one year of production. One can see that the production behaviour with respect to water gas ratio is not changed after fracturing.

The purple line is showing the production behaviour including the special behaviour of the bimodal porosity model. Here the water gas ratio increased according to the capillary pressure function. So the effect can be seen in this scenario as well, showing that the prior shown scenario is proven right.

## 8.5 Permeability scenario

The permeability scenario is one way to show the influence of this parameter to the production behaviour.



Three different scenarios were evaluated in this section. One scenario is assuming low permeability and is showing that the water gas ratio is influenced indirectly by the fact that the water gas ratio is increased slower than in the original case.

The green line is indicating the original case showing the production behaviour as the company faced.

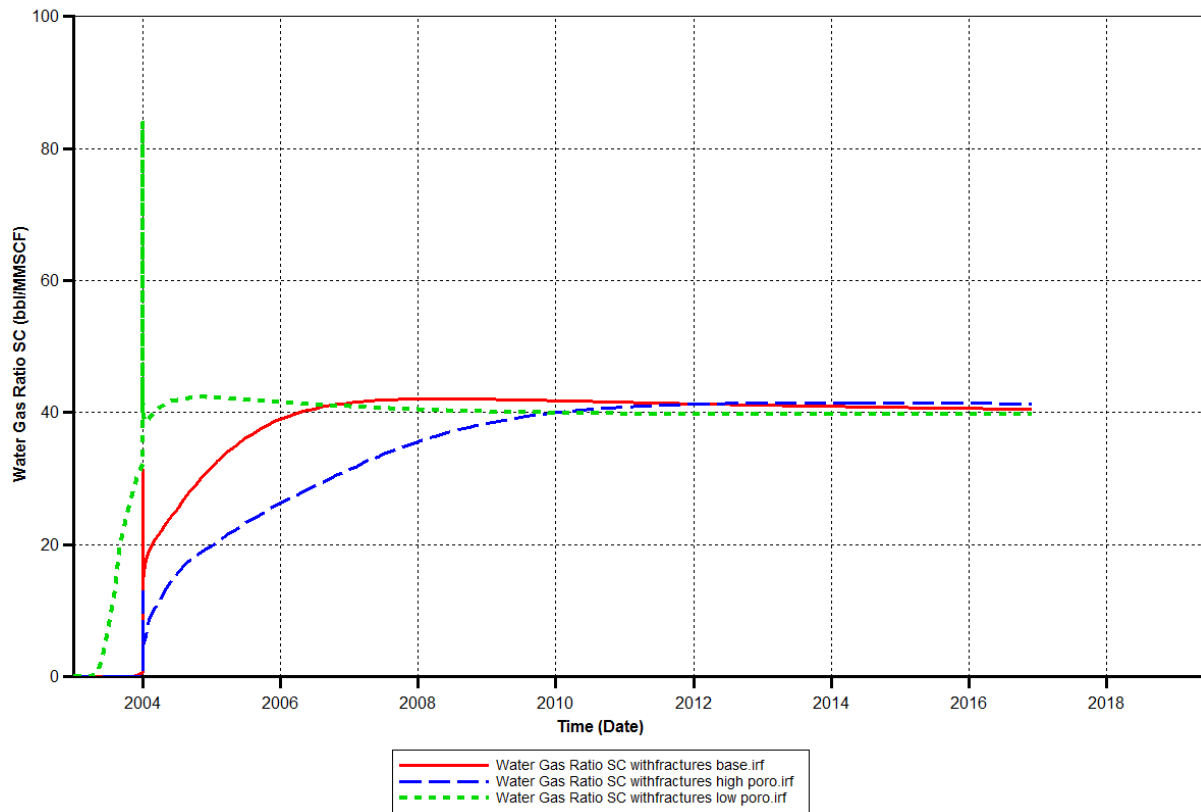
The blue line is indicating an increased permeability by the factor of ten. This means that all the grid cells are populated with a permeability ten times higher than the original one.

This scenario is delivering an artificial result since the permeability is increased dramatically while the capillary pressure is kept at a high level.

This scenario is very important since it shows the effect that high capillary pressures and high permeability's favours high water production.

## 8.6 Porosity scenario

The porosity scenario is an option to make sure how the porosity is influencing the production ratio- especially the WGR.



One can see that the porosity is not affecting the water gas ratio very much in late time production. The porosity is simply shifting the water gas along the time axis.

While low porosity is favouring water production already in the beginning prior to production, high porosity is causing a late response of the water to flow.

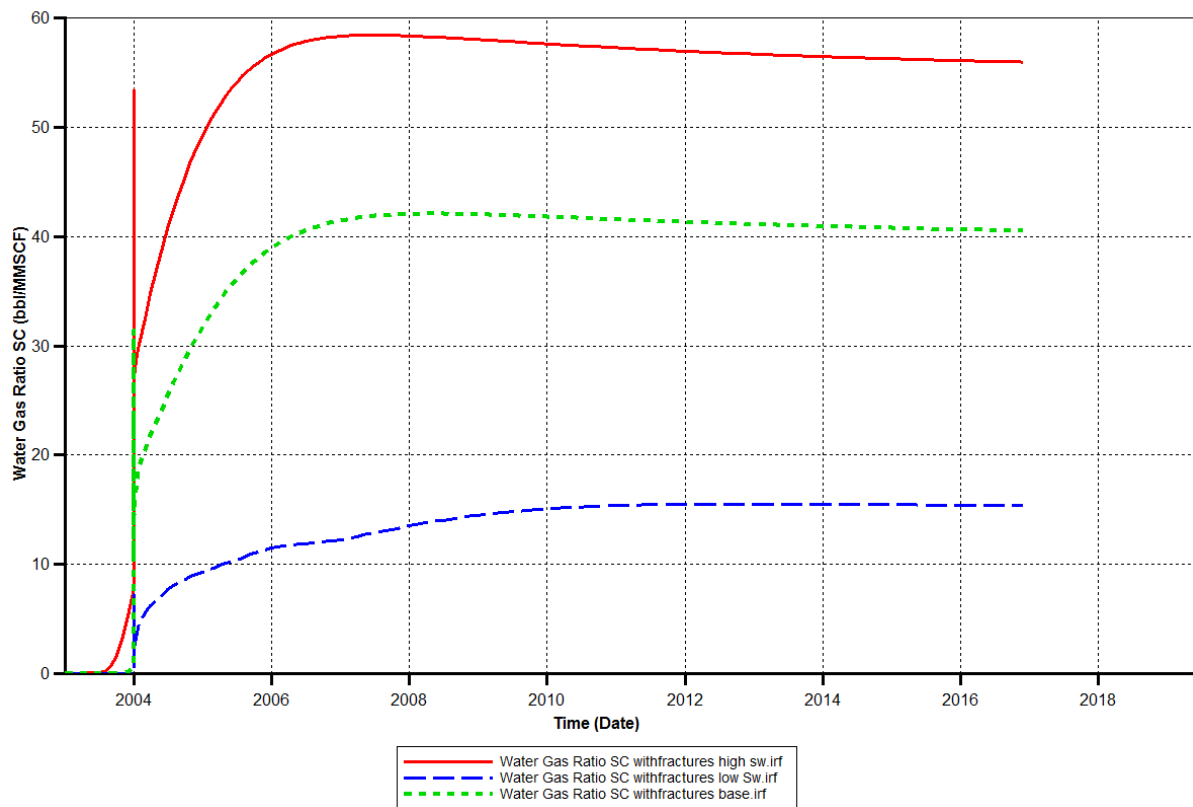
The effect of low porosities is exactly the opposite.

So one can see that the effect of porosity is normal relative to the water gas ratio and does not need to be considered too much.



## 8.7 Water saturation scenario

In order to ensure that the saturation is considered within these scenarios, the water saturation was changed to high and low values.



What can be seen in the upper figures is that the water saturation content is shifting the curve along the vertical axes.

The water gas ratio is dependent on the water saturation but the relation is showing a parallel behaviour of production.

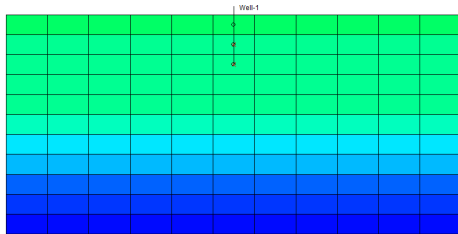
Water saturation is so to say influencing the water production but not having a dramatic influence on the water production.

As an outcome of this scenario one can see that the initial water saturation is influencing the WGR as well as the water production. The linear relationship between water saturation and WGR makes it easy to predict the water production rate for this scenario once the saturation is known.

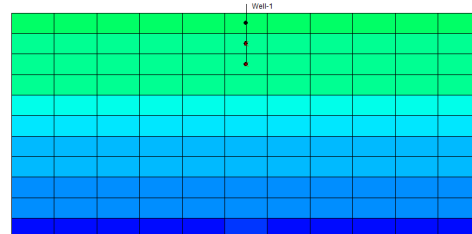
## 8.8 Grid block saturation changes

The following session of figures shows how the water saturation changes over time. Important to know is that the vertical permeability is very low. This means the horizontal permeability is already low but the vertical one is lower by a factor of ten again. So the gas flowing into the well is coming from the perforated layers only.

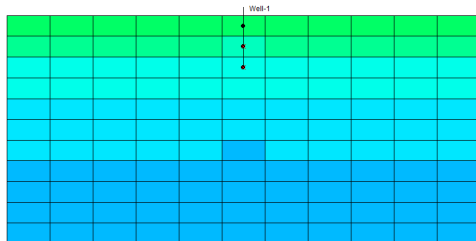
2003-01-01



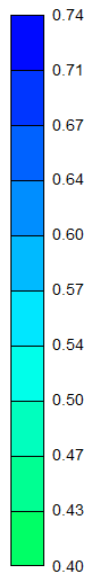
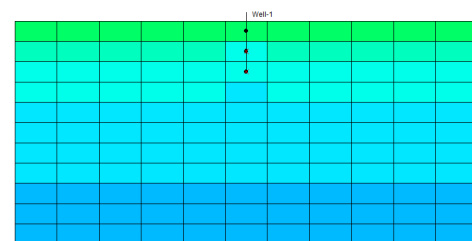
2003-04-01



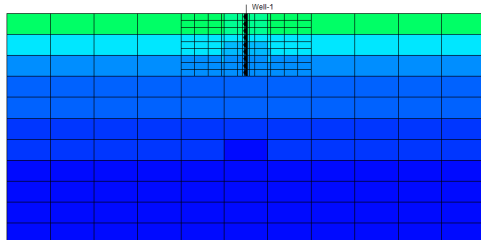
2003-09-01



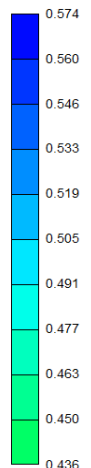
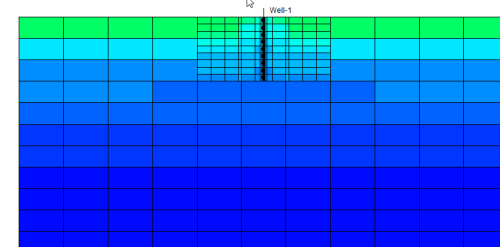
2003-11-01



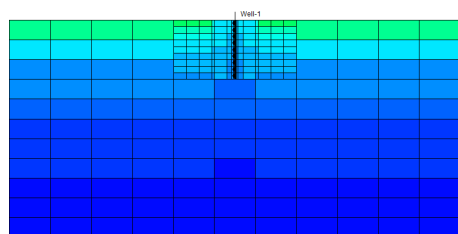
2004-01-01



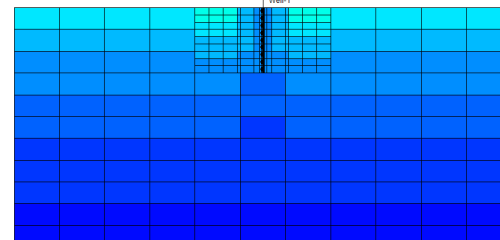
2004-01-12



2004-03-10



2004-06-24



What can be seen in the lower figures is that the overall gas saturation from the two uppermost layers is decreasing. So gas is produced from the layers, while in the near vicinity of the well the gas saturation is increasing. This shows that the gas is flowing into the well and accumulating at the well.

The explanation of the water influx after fracturing is the following.

The model shows that after fracturing water is flowing into the well and is produced. This water has to come from inside the reservoir layers since no aquifer is connected to the simulation model.

According to the proposed effect the model shows that this effect is acting in this reservoir.

Water is mobilized caused by hydraulic stimulation process and flows from the micro pores where it is located prior to fracturing, because of the wetting behaviour of the rock (water wet).

The fracturing process is changing the stress situation in the reservoir affecting the capillary pressure. The immobile water is mobilized and flowing. Once this effect has occurred, the model shows also that the mobilized water continues to flow until a point is reached where equilibrium is achieved again.

The reason, why this effect is not present in normal production, is that the pressure change is not that dramatically as it is during fracturing processes. But since the gas rate is not economical at all prior to fracturing, the company had no other option.

Model approves that fracturing is not a meaningful operation unless the prizes is that high that the removal of the inflowing water is still economical.

Another output of the model is that the fracture length respectively the vertical penetration depth plays a major role since the deeper reservoir layers are containing a lot more water that can be mobilized.

The different scenarios show how the ratio between water and gas rises (the higher amount of water with respect to gas).

Although the fracturing process is increasing the gas rate, at the end the increase in water is too high to achieve considerable gas rates.

Figure 20 pressure distribution

## 9 CONCLUSION/ INTERPRETATION

In low permeability zones in combination with low porosity and high water saturations the capillary pressure is very sensitive with respect to both, the permeability and the water saturation.

Important is the balance between capillary pressure and the formation pressure draw down. If the formation pressure draw down is high (hydraulic stimulation process) water is mobilized and flowing to the wellbore hindering the gas flow.

The first assumption of the company that an aquifer has been fractured is unfortunately the common approach, because this allows to easily match the rates without considering the real reservoir properties.

Although only little information was given with respect to the whole reservoir (heterogeneities, faults, etc.) it is most important to consider all the data available.

Including the capillary pressure function of the reservoir rocks can completely change the behaviour of the rock during simulation.

Adding artefacts to a simulation model should not be a common approach. Aquifers or similar objects can be added after one has ensured correct data input to match rates or pressures.

This thesis is an example of how easy a reservoir is interpreted in a wrong way by matching production data with an artificial model.

Furthermore this thesis wants to draw attention to the reliability of input data and the responsibility of the user to correctly use it.

The most important outcome of this paper is answering the statement from the introduction:

### WHAT IS THE SOURCE OF WATER?

This question can now easily be answered by checking the simulation results. The model, although it is only a generic one totally confirms the effect of micro pores feeding. This can be seen all the graphs and tables from the result section.

Sometimes not a complicated and artificial tool is the best solution to understand problems, but a simple model helps to understand complex reservoir behavior. The KISS (keep it super simple) principle is confirmed in this case.

*Wichtig ist,  
dass man nicht aufhört zu fragen.*

*The important thing is  
not to stop questioning.*

**A.Einstein** (\*14. März 1879 †18. April 1955)



## 10 REFERENCES

- [1] OMV, "data report" provided August 2016 [Online].
- [2] "Fekete," [Online]. Available:  
[http://fekete.com/SAN/TheoryAndEquations/HarmonyTheoryEquations/Content/images/Reference\\_Material/General\\_Concepts/Relative\\_Permeability/relative\\_permeability03.png](http://fekete.com/SAN/TheoryAndEquations/HarmonyTheoryEquations/Content/images/Reference_Material/General_Concepts/Relative_Permeability/relative_permeability03.png). [Accessed 02 08 2016].
- [3] "petrowiki.org," [Online]. Available:  
[http://petrowiki.org/Measurement\\_of\\_capillary\\_pressure\\_and\\_relative\\_permeability](http://petrowiki.org/Measurement_of_capillary_pressure_and_relative_permeability).  
[Accessed 11 October 2016].
- [4] W. Purcell, " Capillary Pressures—Their Measurement Using Mercury and the Calculation of Permeability Therefrom.," *J Pet Technol 1 (2): 39-48. SPE-949039-G*.  
<http://dx.doi.org/10.2118/949039-G> , 1949.
- [5] B. Swanson, "A simple correlation between permeabilities and mercury," *JPT*, pp. pp 2498 - 2504, 1981.
- [6] J. a. A. J. Walls, "Capillary pressure and permeability," *SPE/DOE 13879*, 1985.
- [7] T. O. Allen and A. P. Roberts, Production Operations, Well Completion, Workover, and Stimulation Volume 2, Tulsa, Oklahoma: OGCI,Inc.,PetroSkills,LLC., 2008.

- [8] W. Bierwerth, Tabellenbuch Chemietechnik, V. G. & C. K. Nourney, Ed., Haan-Gruiten: Verlag Europa-Lehrmittel, 2005.
- [9] T. J. Mason and J. P. Lorimer, Applied Sonochemistry, Weinheim: Wiley-VCH, 2002.
- [10] Edwin C. Moritz and Natalie Barron, "Wattenberg Field Unconventional Reservoir Case Study," in *SPE Middle East Unconventional Gas Conference*, Abu Dhabi, 2012.
- [11] S. Polczer, "Petroleum Economist," 15 02 2012. [Online]. Available: <http://www.petroleum-economist.com/Article/2979412/News-Analysis-Unconventional/Mind-the-oil-sands-price-gap.html>. [Accessed 20 02 2012].
- [12] K. a. W. C. Christoffersen, "Gas/Oil Capillary Pressure of Chalk at Elevated Pressures," *SPE Form Eval* 10 (3): 153-159. SPE-26673-PA. <http://dx.doi.org/10.2118/26673-PA>, 1995.
- [13] Z. a. R. D. Chen, "Measurement And Interpretation Of Centrifuge Capillary Pressure Curves-the Sca Survey Data," *The Log Analyst* 36 (5). SPWLA-1995-v36n5a2. , 1995.
- [14] G. a. B. E. Hassler, "Measurement of Capillary Pressures in Small Core Samples," *Trans. of AIME* 160 (1): 114-123. SPE-945114-G. <http://dx.doi.org/10.2118/945114-G>, 1945.



# APPENDICES

## Model Description

### Goals:

- Investigation of micro pore feeding effect
- Justification of proposed effect (micro pores feeding, capillary bound water)
- Estimation of amount of moveable/ producible water

### Model description:

- CMG Model
- Constant pressure boundaries
- Reservoir Properties Well 12
- 1 Producer Well
- Without/ with induced fractures
- Water saturation/ height function applied to different zones.

### Model sketch:

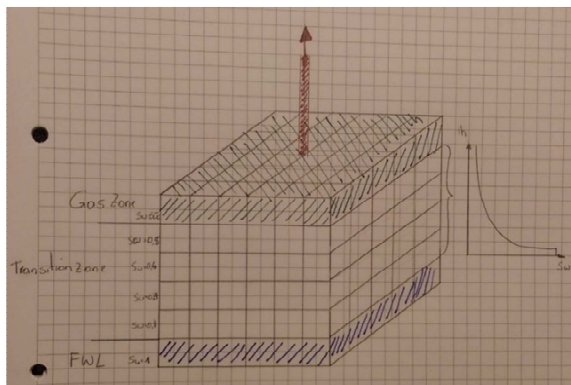


Figure 21 generic model sketch

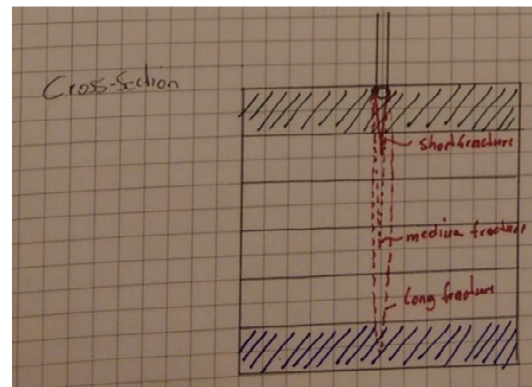


Figure 22 cross section n sketch

### Workflow:

- Generic model setup (simple flow model, constant pressure boundaries, reservoir properties from well Well 4)
- Simulation scenarios:
  - Without fractures
  - With short fractures
- Comparison with proposed effect

## Model Input

### Layer parameter:

This section contains information about the layer specification including depth, temperature, height, cementation factor, rock compressibility ...

Perforation interval:		3260- 3275m
Residual water saturation:	Swcon=	40%
Total system compressibility:	C <sub>t</sub> =	8.0118e <sup>-5</sup> psi <sup>-1</sup>
Temperature:	T=	346 °C
Cementation factor:	m=	2.03
Saturation exponent:	n=	1.76
Well radius:	rw=	0.25 ft

### Fluid properties

All parameters somehow related to the fluids in the reservoir are listed here. Fluid parameters are important to specify, because they have a huge impact on production behaviour.

Gas formation volume factor:	B <sub>g</sub> =	0.0045 ft <sup>3</sup> / scf
Water density:	ρ <sub>w</sub> =	55.441 lb/ ft <sup>3</sup>
Water viscosity	μ <sub>w</sub> =	0.1493 cp
Water formation volume factor	B <sub>w</sub> =	1.1053 RB/ STB
Z- factor:		1.0797
Gas gravity:		0.645
Water gas ratio:	WGR=	5 STB/ MMScf
Gas compressibility	C <sub>g</sub> =	1.3453 e <sup>-4</sup> psi <sup>-1</sup>
Water compressibility	C <sub>w</sub> =	4.4878 e <sup>-6</sup> psi <sup>-1</sup>
Contact angle:		130°
Interfacial tension:		485mN/m

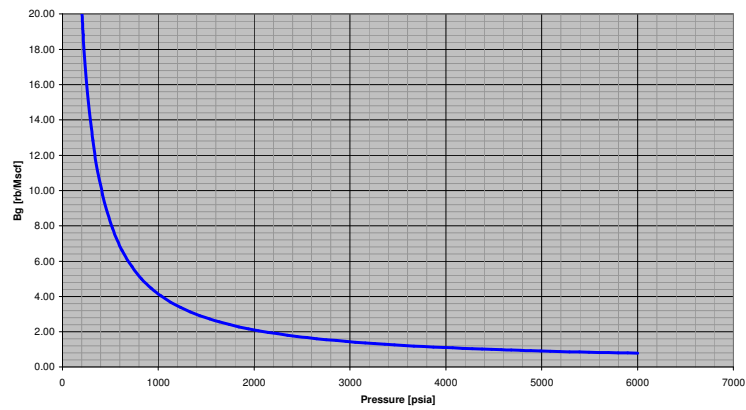


Figure 23 gas formation volume factor

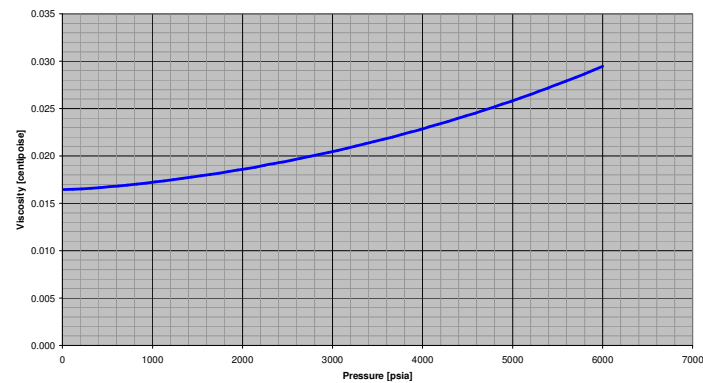


Figure 24 viscosity

### Fracture properties:

The fracture properties were taken from post fracturing reports provided by the company. In order to ensure the proper model result this section was treated very carefully with respect to depth relations. A simulated fracture can be seen below in the picture below the list.

Half length:		89m
Fracture height:		41m
Fracture top:		3243m
Fracture bottom:		3284m
Fracture width:		0.62 inch
Fracture conductivity:		4965.3 mD ft
Dimensionless conductivity:		19.32
Reservoir pressure:	$P_{res} =$	5350psi
Hydraulic head		5042psi
Surface pressure:		2057psi

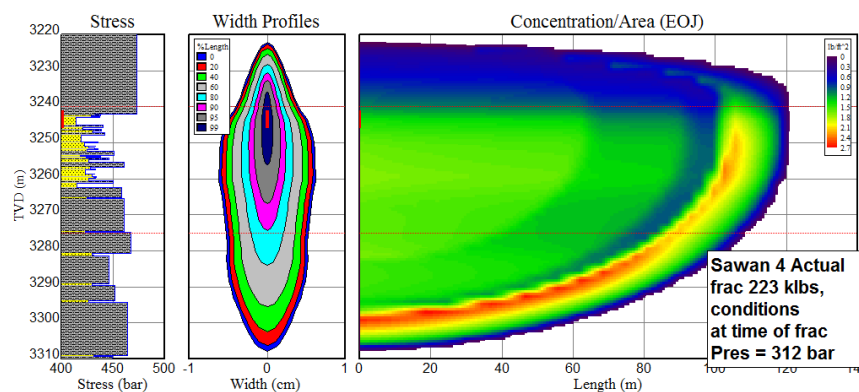


Figure 25 simulated fracture profile

**Reservoir properties:**

This section is to specify the reservoir properties itself. So here the porosity and permeability of the reservoir is defined.

Reservoir layer:		3227m- 3378m
Gross thickness:		23.8m
Net thickness:		23m
Average porosity:	$\Phi =$	15.2%
Average permeability:	$k =$	0.09mD

**Gas composition:**

The gas composition data was delivered from the laboratory where the gas was analysed. As expected, the gas is a very dry gas. Additionally to that a small amount of carbon dioxide was found within the probes.

<i>Components</i>	<b>Sawan-4</b> <i>Mole %</i>	<b>Sawan-6</b> <i>Mole %</i>
Methane	91.046536	90.948500
Ethane	0.343454	0.316200
Propane	0.016089	0.016000
Isobutane	0.002705	0.002200
n-Butane	0.002083	-
Neopentane	0.000745	-
Isopentane	0.000532	-
n-Pentane	0.000217	0.001700
C6	0.002570	0.000000
C6+	0.010585	0.000000
Carbon Dioxide	8.355290	8.473300
Nitrogen	0.220097	0.239600
Hydrogen Sulfide	0.001667	0.002500

Figure 26 gas composition

## Model Setup

- **Reservoir**

GRID:

Grid: Corner Point Grid

Blocks: 11\*11\*11

Block dimensions: 10m

Faults: 0

ARRAY PROPERTIES:

Porosity, Permeability, saturation etc. from data above

ROCK COMPRESSIBILITY:

CPOR: 4.11E-6 1/psi (pressure dependence of formation)

PRPOR 14.6923 psi (reference pressure)

- **Components**

MODEL:

Gas Water

PVT REGION

#	Description	Option	Default	Value
1	Reservoir temperature (T...			325 F
2	DENSITIES			
3	Oil density (DENSITY O...	Stock tank oil de...		
4	Gas density/gravity (DE...	Gas gravity (Air=1)		0.645
5	Water phase density (D...			57.2069 lb/ft3
6	Undersaturated Co (CO)			
7	Vo pressure dependence...		0 cp/psi	
8	Water properties			
9	Formation Volume Fact...			1.09841
10	Compressibility (CW)			4.58212e-006 1/psi
11	Reference pressure for ...			14.696 psi
12	Viscosity (VWI)		1 cp	0.185269 cp
13	Pressure dependence ...		0 cp/psi	0.0 cp/psi
14	Solution gas ratio max. inc...	Not Used		

Figure 27 PVT data

- **Rock- Fluid**

ROCK FLUID TYPES

Rock type 1

	Sw	krw
1	0.4	0
2	0.4375	7.32422e-005
3	0.475	0.000585938
4	0.5125	0.00197754
5	0.55	0.0046875
6	0.5875	0.00915527
7	0.625	0.0158203
8	0.6625	0.0251221
9	0.7	0.0375
10	0.7375	0.0533936
11	0.775	0.0732422
12	0.8125	0.0974854
13	0.85	0.126562
14	0.8875	0.160913
15	0.925	0.200977
16	0.9625	0.247192
17	1	0.3

Figure 28 relative permeability input

The curves of both, the relative permeability of gas and the relative permeability of water can be seen in the following figures below.

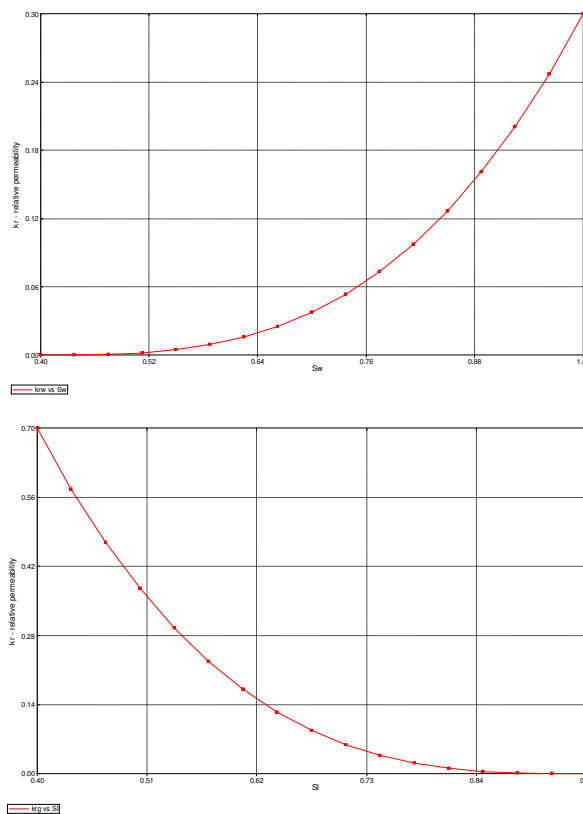


Figure 29 relative permeability output

- Initial conditions

Figure 30 initial conditions setting

- Wells and recurrent

#	User Block Address	Connect to	Form facto...	Status	Ref. Layer	WI (md*ft)	Length (ft)	Block Top...	Block Bottom (ft)
1	6 6 1	Surface	1	Open	<input checked="" type="radio"/>	0.171	10.0	0.0	10.0
2	6 6 2	1	1	Open	<input type="radio"/>	0.171	10.0	10.0	20.0
* 3	6 6 3	2	1	Open	<input type="radio"/>	0.171	10.0	20.0	30.0

Figure 31 well perforations

Figure 32 fracture specification

#	User Block Address	Connect to	Form facto...	Status	Ref. Layer	WI (md*ft)	Length (ft)	Block Top...	Block Bottom (ft)
1	661/331	Surface	1	Open	<input checked="" type="radio"/>	1284.228	10.0	0.0	10.0
2	662/331	1	1	Open	<input type="radio"/>	1284.228	10.0	10.0	20.0
* 3	663/331	2	1	Open	<input type="radio"/>	1284.228	10.0	20.0	30.0

Figure 33 auto created fracture design

shows the block addresses for the hydraulic fracturing process. A local grid refinement is included in this process

## Detailed Core Interpretation

### SAWAN 4 Porosity and Permeability data

SAMPLE NUMBER	LT	RT	DEPTH (LEP) (m)	DEPTH (Karachi) (m)	POROSITY (%)	PERMEABILITY Kh (Md)	GRAIN DENSITY (g/cc)
Core #1							
1	1A	B1	3234.30	3234.30	11.51	0.11	2.83
2	1A	C1	3234.60	3234.60	14.54	0.18	2.78
3	1A	B1	3234.90	3234.90	12.62	0.12	2.84
4	1A	B1	3235.23	3235.23	11.33	0.13	2.82
5	1A	B1	3235.53	3235.53	11.56	0.11	2.83
6	1A	B1	3235.83	3235.83	12.02	0.12	2.80
7	1A	B1	3236.09	3236.13	11.96	0.19	2.86
8	1A	B0	3236.42	3236.43	11.45	0.07	3.03
9	1A	A0	3236.70	3236.73	6.53	0.05	2.87
10	1A	B1	3236.99	3237.03	13.13	0.15	2.82
11	1A	B0	3237.29	3237.33	11.32	0.09	2.83
12	1A	C1	3237.58	3237.63	15.78	0.17	2.80
13	2C	B1	3237.89	3237.93	13.26	0.39	2.70
14				3238.19	NPP	NPP	NPP
15	3B	C1	3238.45	3238.49	18.47	0.4	2.74
16	2Ca	C1	3238.77	3238.80	15.48	0.16	2.74
17	2Ca	C2	3239.07	3239.13	18.68	1.45	2.72
18	2Ca	C1	3239.36	3239.43	15.48	0.91	2.73
19	2Cc	A0	3239.66	3239.73	6.25	0.05	2.72
20	2Ca	C1	3240.00	3240.06	16.68	0.25	2.71
21	3Ba	C1	3240.30	3240.36	17.65	0.79	2.72
22	2Ca	C1	3240.60	3240.66	17.89	0.84	2.71
23	3Ba	C1	3240.90	3240.97	15.68	0.45	2.72
24	3Ba	C1	3241.20	3241.27	18.21	0.63	2.73
25	3Ba	C2	3241.50	3241.57	19.38	1.15	2.71
26	2Ca	C1	3241.81	3241.87	16.42	0.4	2.73
27	3Ba	D3	3242.11	3242.17	21.13	18.66	2.72
28	3Ba	D2	3242.41	3242.47	21.60	3.59	2.72
29	2Ca	C2	3242.71	3242.77	20.07	1.85	2.71
30	2Cc	B1	3243.03	3243.07	12.52	0.29	2.70
31	3B	C2	3243.33	3243.37	20.61	4.69	2.70
32	3Ba	C2	3243.62	3243.67	19.25	1.83	2.70
33	3Ba	C1	3243.92	3243.97	15.50	0.84	2.70
34	3Ba	C1	3244.22	3244.27	15.70	0.38	2.73
35	3Ba	C2	3244.51	3244.57	16.96	1.43	2.72
36	2Cc	B1	3244.81	3244.87	12.00	0.47	2.71
37	3Ba	C1	3245.13	3245.17	18.65	0.97	2.73
38	3Ba	C1	3245.44	3245.47	19.36	0.80	2.71
39	3Ba	C1	3245.72	3245.77	14.99	0.30	2.70
40	2Ca	C1	3246.03	3246.07	16.05	0.26	2.74
41	3Ba	C2	3246.31	3246.35	18.41	2.73	2.70
42	3Ba	C1	3246.60	3246.65	18.71	0.88	2.72
43	3Ba	C1	3246.90	3246.95	18.52	0.52	2.73
44	3Ba	C1	3247.21	3247.25	15.52	0.62	2.71
45	3Ba	C1	3247.51	3247.55	18.55	0.46	2.73
46	3Ba	C1	3247.81	3247.85	15.92	0.21	2.74
47	3Ba	C1	3248.12	3248.15	17.65	0.42	2.72



48	3Ba	C1	3248.41	3248.45	18.39	0.92	2.72
49	3Ba	C2	3248.71	3248.75	18.86	1.30	2.70
50	2Ca	C1	3249.02	3249.05	15.76	0.69	2.71
51	2Ca	B2	3249.34	3249.37	13.85	1.66	2.81
52	3Ba	C2	3249.64	3249.67	17.61	3.12	2.69
53	3Ba	C2	3249.93	3249.97	19.39	1.81	2.71
54	2Ca	C1	3250.24	3250.27	15.19	0.52	2.72
55	2Ca	B0	3250.53	3250.57	11.32	0.07	2.74
56	3Ba	D2	3250.82	3250.87	21.09	1.96	2.71
57				3251.17			
58	3Ba	C2	3251.44	3251.47	19.31	2.68	2.71
59	3Ba	C2	3251.74	3251.77	14.88	1.72	2.65
60	3Ba	C1	3252.03	3252.07	16.83	0.82	2.71
61	3Ba	C2	3252.34	3252.37	19.23	1.58	2.72
62	3Ba	C2	3252.64	3252.67	19.26	2.26	2.72
63	3Ba	D2	3252.92	3252.97	21.31	2.42	2.71
64	3Bc	B1	3253.29	3253.3	8.75	0.89	2.68
65	3Bc	A1	3253.56	3253.6	6.90	0.85	2.70
66	3B	C2	3253.86	3253.9	18.69	6.23	2.68
67	3B	D2	3254.17	3254.2	21.84	5.11	2.69
68	3B	C2	3254.48	3254.5	19.74	9.05	2.73
69	3B	C2	3254.78	3254.8	14.36	1.55	2.67
70	3Bc	B1	3255.04	3255.08	12.21	0.63	2.71
71	2Ca	C0	3255.34	3255.38	14.51	0.07	2.72
72	2Ca	B0	3255.64	3255.68	12.26	0.05	2.74
73	2C	B2	3257.99	3256.04	12.70	1.55	2.69
74	2C	B1	3256.29	3256.34	13.90	0.54	2.70
75	3Bc	B0	3256.65	3256.69	7.91	0.06	2.70
76	3Ba	C2	3256.94	3256.98	15.62	1.19	2.72
77	3Bc	A0	3257.37	3257.4	6.54	0.09	2.70
<b>Core #2</b>							
78	3Ba	C2	3261.30	3261.3	18.17	4.66	2.69
79	2Ca	C2	3261.60	3261.60	18.90	2.94	2.71
80	2Ca	C1	3261.90	3261.90	14.59	0.25	2.72
81	3B	D3	3262.20	3262.20	23.01	117.84	2.66
82	3Bc	B1	3262.52	3262.52	7.19	0.51	2.67
83	2C	C2	3262.83	3262.84	18.32	4.48	2.68
84	3B	D3	3263.12	3263.14	24.29	79.68	2.68
85	3Ba	C2	3263.41	3263.44	17.61	8.14	2.66
86	3Ba	D3	3263.72	3263.74	21.18	23.86	2.68
87	2Ca	C1	3264.03	3264.04	16.90	0.55	2.71
88	2Ca	C2	3264.32	3264.34	16.92	2.80	2.70
89	3Bc	A0	3264.62	3264.64	4.86	0.03	2.70
90	2Ca	C1	3264.92	3264.94	14.69	0.99	2.68
91	2Ca	C1	3265.22	3265.24	15.10	0.42	2.70
92	2Ca	C2	3265.52	3265.54	16.48	1.66	2.68
93	2Ca	B1	3265.81	3265.84	11.09	0.25	2.77
94	3Ba	C2	3266.11	3266.14	19.63	4.41	2.68
95	3Ba	B1	3266.42	3266.44	10.29	0.60	2.79
96	3Ba	C1	3266.71	3266.74	16.28	0.66	2.70
97	2Ca	C1	3267.06	3267.08	14.57	0.17	2.69
98	2Ca	C1	3267.36	3267.38	16.72	0.30	2.69
99	2Cc	B0	3267.66	3267.68	7.64	0.05	2.68
100	2Ca	B0	3268.01	3268.03	12.00	0.06	2.73
101	3Bc	B0	3268.31	3268.33	9.38	0.07	2.67

102	2Ca	C2	3268.60	3268.63	17.79	2.06	2.68
103	3Ba	C2	3268.91	3268.93	18.65	1.51	2.69
104	2Ca	C1	3269.21	3269.23	15.16	0.18	2.67
105	3Ba	C2	3269.51	3269.53	16.98	1.26	2.67
106	3Bc	B0	3269.80	3269.83	7.04	0.04	2.67
107	3Ba	C1	3270.09	3270.13	15.58	0.77	2.67
108	2Ca	C1	3270.40	3270.42	14.60	0.63	2.66
109	2Ca	C1	3270.74	3270.74	17.71	0.99	2.67
110	3Ba	B0	3271.04	3271.04	12.85	0.07	2.72
111	3Ba	C1	3271.41	3271.42	15.87	0.95	2.68
<b>Core #3</b>							
112	2A	A0		3288.30	5.28	0.01	2.72
113	2A	A0		3288.60	6.40	0.01	2.73
114	2A	A0		3288.86	5.62	0.01	2.70
115	2A	A0		3289.14	4.11	>0.01	2.76
116	2A	A0		3289.50	4.31	>0.01	2.73
117	2A	A0		3289.80	5.69	0.01	2.75
118	2A	A0		3290.10	6.37	>0.01	2.71
119	2A	A0		3290.40	6.46	0.01	2.71
120	2A	A0		3290.73	5.09	>0.01	2.77
121	2A	A0		3291.03	3.73	>0.01	2.70
122	2A	A0		3291.33	3.52	>0.01	2.72
123	2A	A0		3291.65	4.43	0.02	2.74
124	2A	A0		3291.95	4.68	0.01	2.67
125	2A	A0		3292.25	7.00	>0.01	2.73
126	2A	A0		3292.55	6.71	0.01	2.71
127	2A	A0		3292.85	5.05	0.01	2.74
128	2A	A0		3293.15	6.04	>0.01	2.75
129	2A	A0		3293.45	6.93	0.01	2.71
130	2A	A0		3293.75	6.26	0.01	2.72
131	3Ac	A0		3294.09	1.93	0.03	2.68
132	2A	A0		3294.39	6.04	0.02	2.71
133	2A	A0		3294.66	5.59	0.01	2.72
134	2A	A0		3294.96	6.71	---	2.72
135	2A	B0		3295.26	7.25	---	2.72
136	2A	B0		3295.54	7.81	---	2.71
137	2A	A0		3295.84	6.59	---	2.70
138	2A	B0		3296.14	7.63	---	2.70
139	2A	A0		3296.44	5.88	---	2.72
140	2A	A0		3296.74	6.93	---	2.70
141	2A	B0		3297.04	8.04	---	2.71

**PLATE 4**

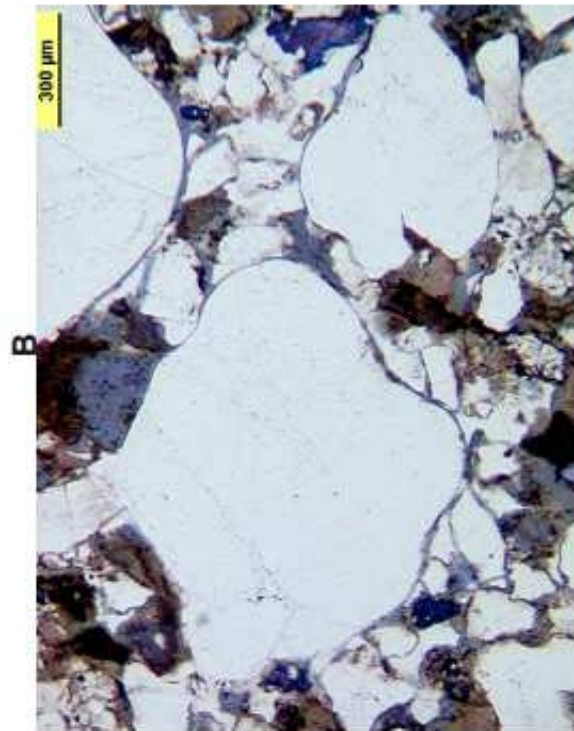
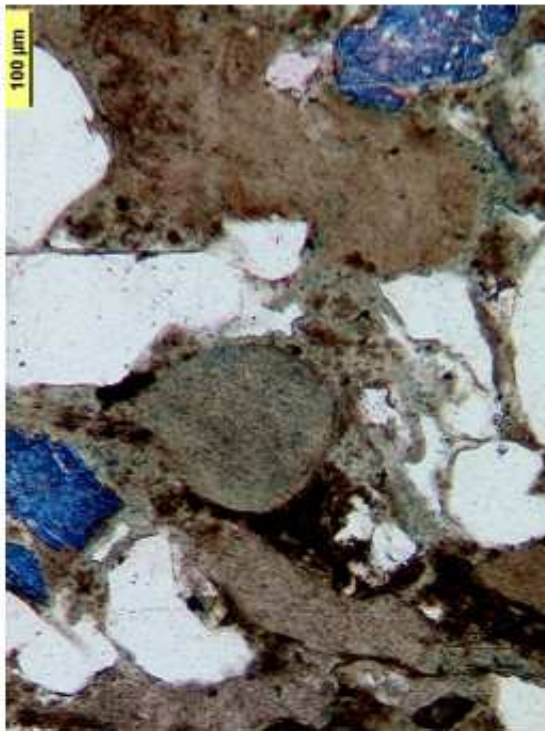
- A. **Sawan 4, core #1 (3235.83 m)**  
Por=12.02%, Perm=0.12 md  
Lithotype: 1A  
Thin-section overview of medium-grained, chamosite-rich sandstone with irregularly dispersed coarse-grained quartz grains.
- B. **Sawan 4, core #1 (3235.83 m)**  
Por=12.02%, Perm=0.12 md  
Lithotype: 1A  
Detail of A. Visible are partially squeezed chamosite grains and detrital quartz grains cemented by iron chlorite cement, iron-rich calcite- and quartz cement.
- C. **Sawan 4, core #1 (3237.58 m)**  
Por=15.78%, Perm=0.17 md  
Lithotype: 1A  
Thin-section overview of medium-grained, partially quartz-cemented chamosite-rich sandstone with irregularly dispersed coarse-grained quartz grains.
- D. **Sawan 4, core #1 (3237.58 m)**  
Por=15.78%, Perm=0.17 md  
Lithotype: 1A  
Thin-section overview. Visible are irregularly dispersed coarse grains of detrital quartz, embedded in a matrix of finer grains (quartz, chamosite and volcanic rock fragments) cemented by iron chlorite and quartz cement.



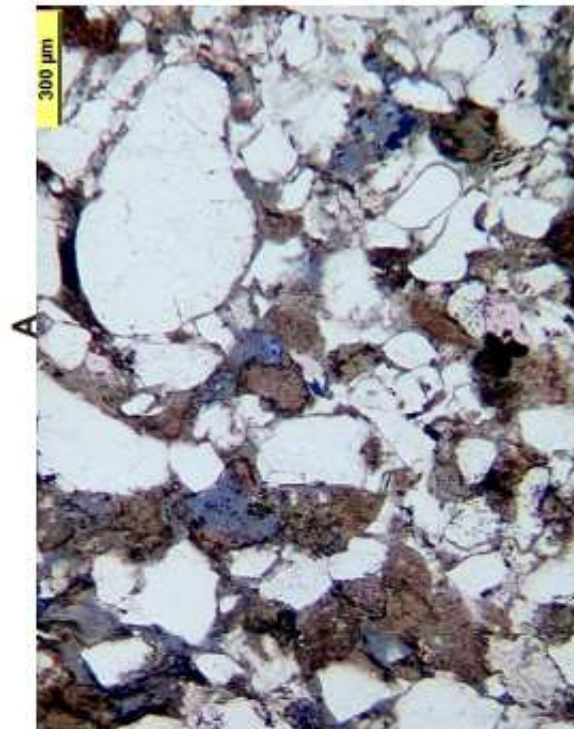
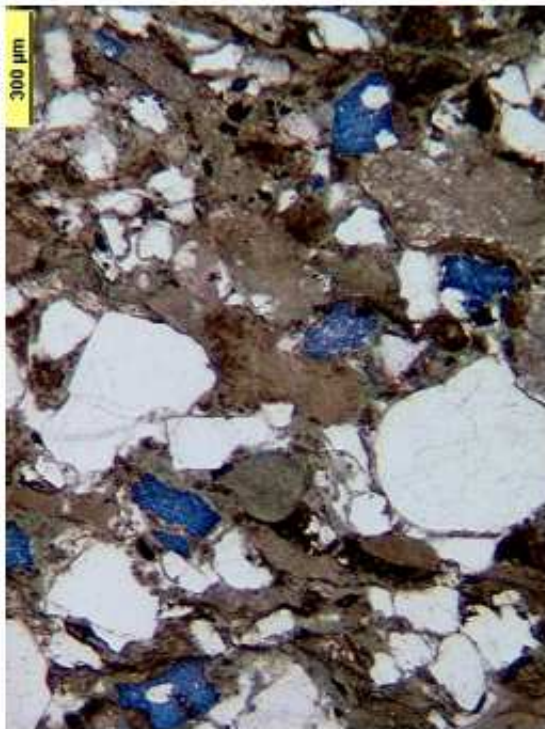


PLATE 4

TEC-LEP  
GEO20020033  
SAWAN 4



D



C

**PLATE 5**

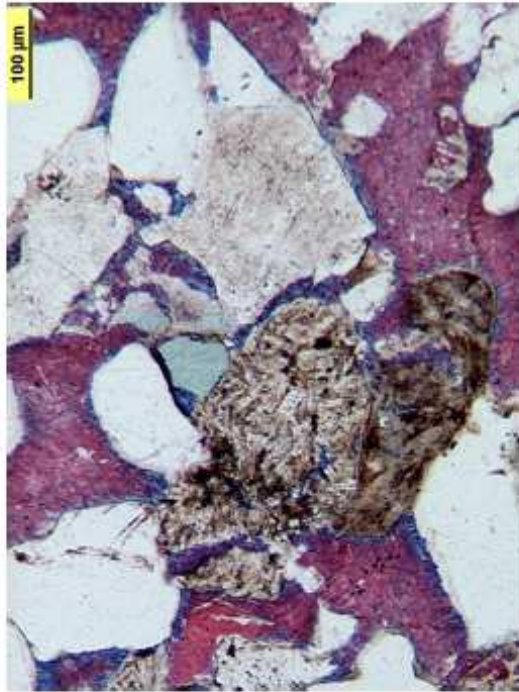
- A. **Sawan 4, core #2 (3264.62 m)**  
Por=4.86%, Perm=0.03 md  
Lithotype: 3Bc  
Thin-section overview of strongly calcite-cemented lithic arenite rich in volcanic rock fragments.
- B. **Sawan 4, core #2 (3264.62 m)**  
Por=4.86%, Perm=0.03 md  
Lithotype: 3Bc  
Detail of A. Visible are partly strongly altered volcanic rock fragments, quartz and few glauconite grains cemented by iron-rich calcite. Calcite replaces partially the framework grains.
- C. **Sawan 4, core #2 (3244.81 m)**  
Por=12%, Perm=0.47 md  
Lithotype: 2Cc  
Thin-section overview of strongly calcite-cemented lithic arenite rich in volcanic rock fragments. Note the presence of some particle dissolution porosity (porosity is stained light blue).
- D. **Sawan 4, core #2 (3244.81 m)**  
Por=12%, Perm=0.47 md  
Lithotype: 2Cc  
Visible grains are volcanic rock fragments, quartz and chamosite grains cemented by iron-rich calcite and chlorite. Note the presence of an isolated intergranular pore.



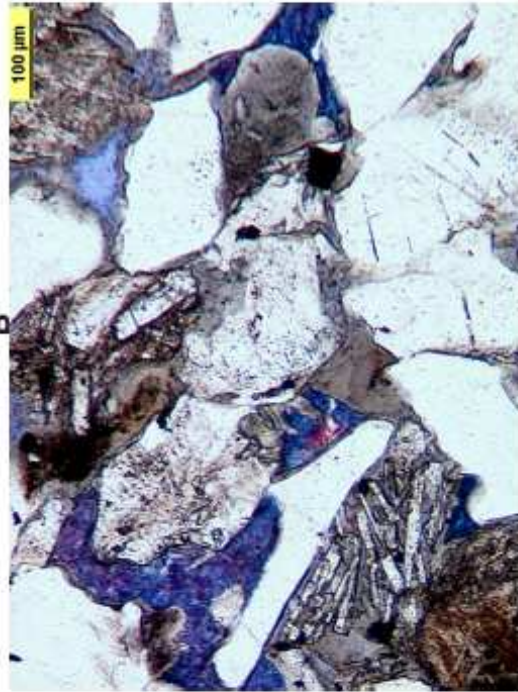


PLATE 5

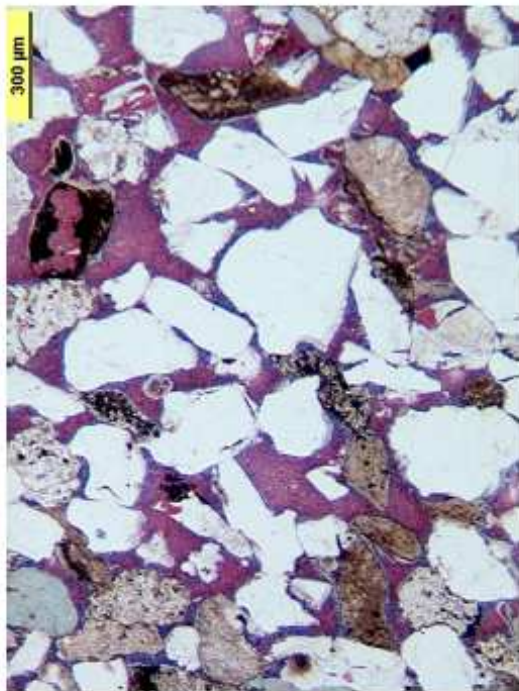
TEC-LEP  
GEO20020033  
SAWAN 4



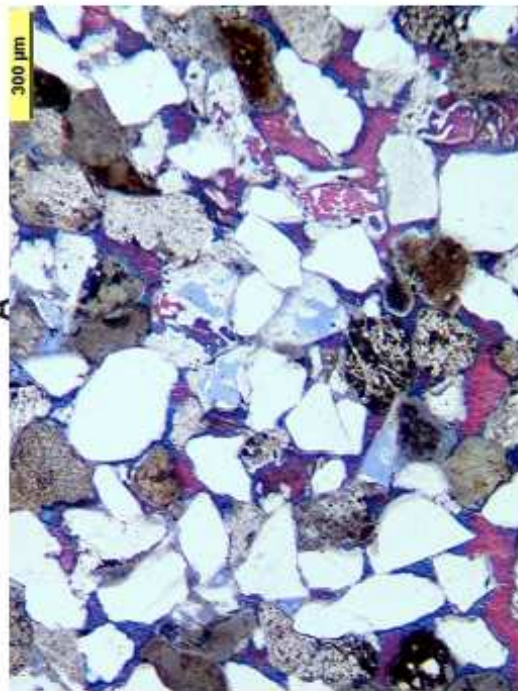
B



D



A



C

**PLATE 6**

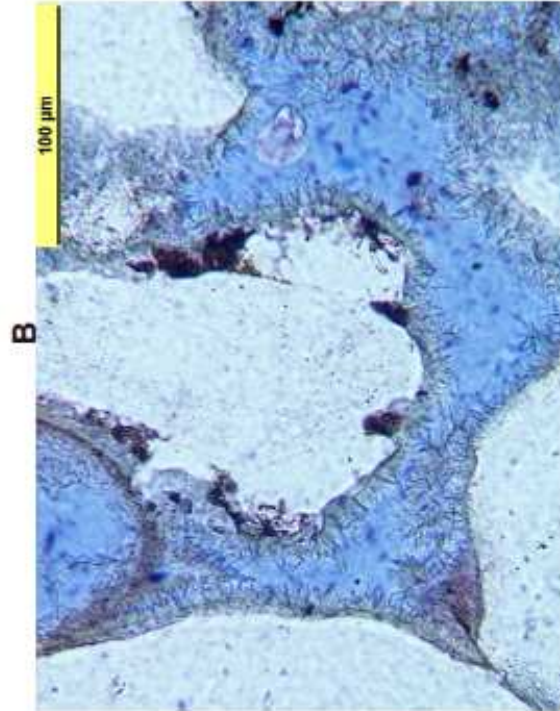
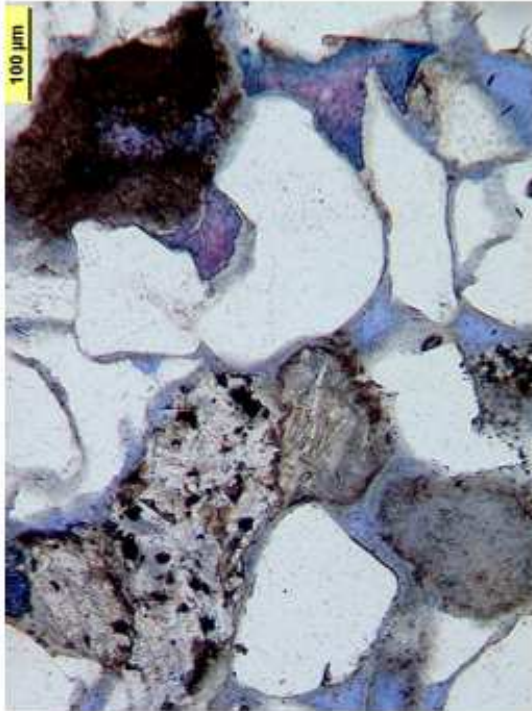
- A. **Sawan 4, core #1 (3239.36 m)**  
Por=15.48%, Perm=0.91 md  
Lithotype: 2Ca  
Thin-section overview of medium-grained, calcite-and iron chlorite-cemented sublithic to lithic arenite.
- B. **Sawan 4, core #1 (3239.36 m)**  
Por=15.48%, Perm=0.91 md  
Lithotype: 2Ca  
Detail of medium-grained, iron chlorite-cemented and partially iron- calcite and quartz-cemented sublithic to lithic arenite. Note the partially altered volcanic rock fragments.
- C. **Sawan 4, core #1 (3239.36 m)**  
Por=15.48%, Perm=0.91 md  
Lithotype: 2Ca  
Intergranular pore space and pore throats are strongly reduced by pore-lining and pore-filling chlorite cement. Note the numerous small intercrystalline pores between the chlorite crystals (forming microporosity).
- D. **Sawan 4, core #1 (3239.36 m)**  
Por=15.48%, Perm=0.91 md  
Lithotype: 2Ca  
Intergranular pores with pore-lining iron-chlorite cement.





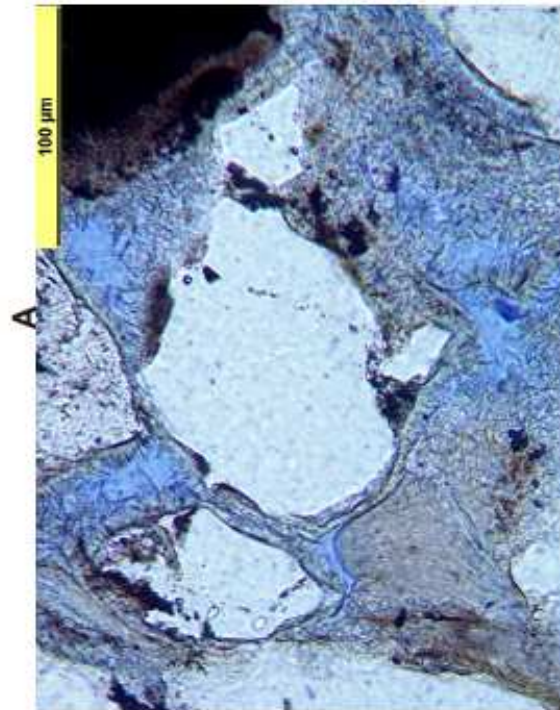
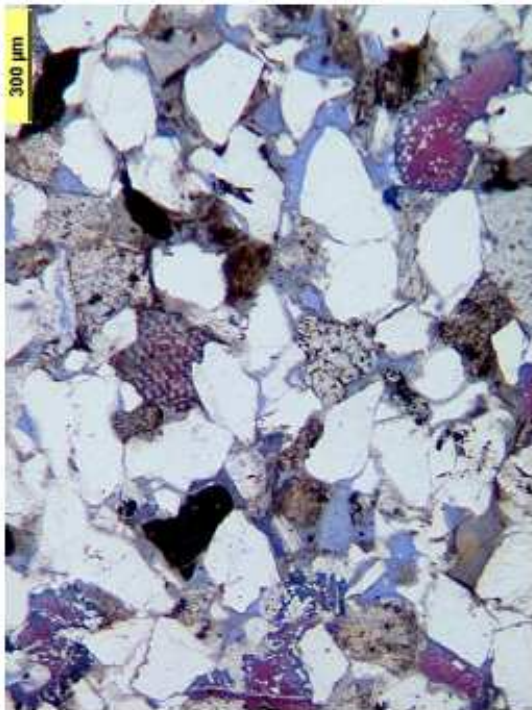
PLATE 6

TEC-LEP  
GEO20020033  
SAWAN 4



B

D



A

C



**PLATE 7**

- A. **Sawan 4, core #1 (3239.36 m)** **SEM-microphotograph**  
Por=15.48%, Perm=0.91 md  
Lithotype: 2Ca  
SEM overview of mainly iron chlorite-cemented, medium-grained arenite.  
Intergranular pore space and pore throats are strongly reduced by pore-lining chlorite cement.
- B. **Sawan 4, core #1 (3239.36 m)** **SEM-microphotograph**  
Por=15.48%, Perm=0.91 md  
Lithotype: 2Ca  
Detail of A. Isolated pore, lined and partly filled with microporous chlorite cement.
- C. **Sawan 4, core #1 (3239.36 m)** **SEM-microphotograph**  
Por=15.48%, Perm=0.91 md  
Lithotype: 2Ca  
Detail of A. Isolated secondary dissolution porosity (dissolved volcanic rock fragment).
- D. **Sawan 4, core #1 (3239.36 m)** **SEM-microphotograph**  
Por=15.48%, Perm=0.91 md  
Lithotype: 2Ca  
Detail of A. Detail of microporous chlorite cement together with small siderite rhombohedrons.



PLATE 7

TEC-LEP  
GEO20020033  
SAWAN 4

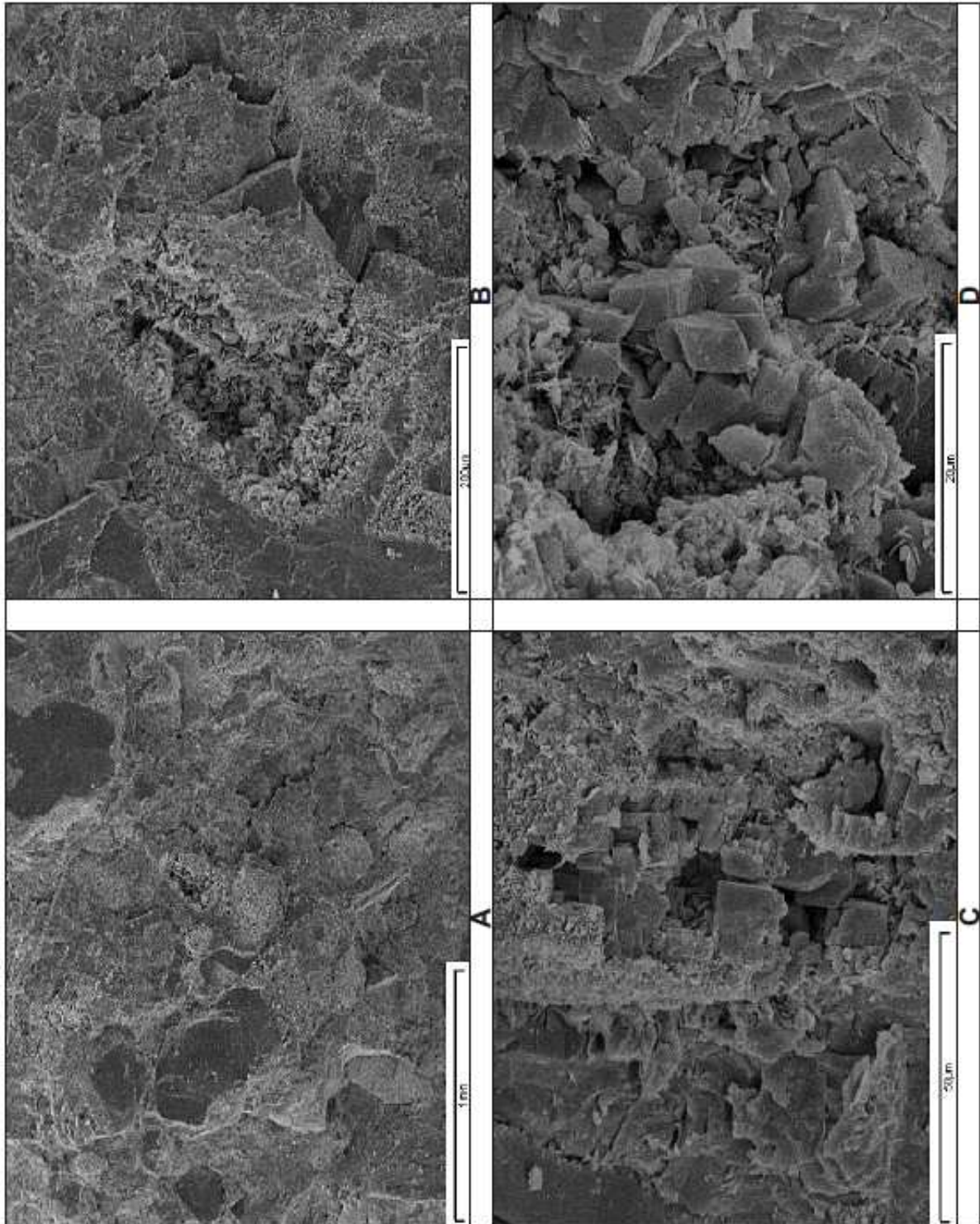


PHOTO	LITHOLOGY	SEDIMENTARY STRUCTURES	PHOTO		LITHOLOGY	SEDIMENTARY STRUCTURES	PHOTO		LITHOLOGY	SEDIMENTARY STRUCTURES	LITHOLOGY	SEDIMENTARY STRUCTURES	
			UV	NORMAL			UV	NORMAL					UV
3261.0 m	CLAY SILT FINE MEDIUM COARSE GRANULE PEBBLE	indistinct laminae CHON low angle common scattered coarse sand grains BT CHON	3261.60 m	CLAY SILT FINE MEDIUM COARSE GRANULE PEBBLE	occasional scattered coarse sand grains BT CHON low angle CHON CHON BT	3262.60 m	CLAY SILT FINE MEDIUM COARSE GRANULE PEBBLE	3263.60 m	CLAY SILT FINE MEDIUM COARSE GRANULE PEBBLE	BT small CCL small CCL indistinct CHON low angle low angle OPH trough cross OPH BT CHON occasional scattered coarse sand grains	3 Bc 2 C 3 B 3 Ba 3 B 2 C 3 B 3 Ba 2 Ca	occasional scattered coarse sand grains	
DEPTH BOTTOM	BOX	DEPTH BOTTOM	BOX	DEPTH BOTTOM	BOX	DEPTH BOTTOM	BOX	DEPTH BOTTOM	BOX	DEPTH BOTTOM	BOX	DEPTH BOTTOM	BOX
3261.0 m	11		3261.60 m	10		3262.60 m	9	3263.60 m	9				

PHOTO	LITHOLOGY	SEDIMENTARY STRUCTURES	PHOTO		LITHOLOGY	SEDIMENTARY STRUCTURES	PHOTO		LITHOLOGY	SEDIMENTARY STRUCTURES
			UV	NORMAL			UV	NORMAL		
DEPTH TOP 3263.60 m	CLAY SILT FINE MEDIUM COARSE GRANULE REBBLE	occasional scattered coarse sand and grains			CLAY SILT FINE MEDIUM COARSE GRANULE REBBLE	OPH CHON BT tangential foresets CHON BT CHON BT CHON BT set boundary CHON			CLAY SILT FINE MEDIUM COARSE GRANULE REBBLE	BT OPH CHON BT low angle low angle trough cross BT CHON PY low angle CHON BT
DEPTH BOTTOM 3264.60 m	CLAY SILT FINE MEDIUM COARSE GRANULE REBBLE				CLAY SILT FINE MEDIUM COARSE GRANULE REBBLE	small CCL's large CCL small OPH CHON CHON CCL tangential foresets occasional scattered coarse sand grains OPH high angle BT CHON			CLAY SILT FINE MEDIUM COARSE GRANULE REBBLE	2 Ca 3 Ba 2 Ca 3 Ba 2 Ca 3 Ba 2 Ca
DEPTH TOP 3264.60 m	CLAY SILT FINE MEDIUM COARSE GRANULE REBBLE				CLAY SILT FINE MEDIUM COARSE GRANULE REBBLE				CLAY SILT FINE MEDIUM COARSE GRANULE REBBLE	2 Ca 3 Ba 2 Ca 3 Ba 2 Ca
DEPTH BOTTOM 3265.60 m	CLAY SILT FINE MEDIUM COARSE GRANULE REBBLE				CLAY SILT FINE MEDIUM COARSE GRANULE REBBLE				CLAY SILT FINE MEDIUM COARSE GRANULE REBBLE	2 Ca 3 Ba 2 Ca 3 Ba 2 Ca
DEPTH TOP 3265.60 m	CLAY SILT FINE MEDIUM COARSE GRANULE REBBLE				CLAY SILT FINE MEDIUM COARSE GRANULE REBBLE				CLAY SILT FINE MEDIUM COARSE GRANULE REBBLE	2 Ca 3 Ba 2 Ca 3 Ba 2 Ca
DEPTH BOTTOM 3266.60 m	CLAY SILT FINE MEDIUM COARSE GRANULE REBBLE				CLAY SILT FINE MEDIUM COARSE GRANULE REBBLE				CLAY SILT FINE MEDIUM COARSE GRANULE REBBLE	2 Ca 3 Ba 2 Ca 3 Ba 2 Ca

DEPTH BOTTOM  
3263.60 m

BOX 8

DEPTH BOTTOM  
3264.60 m

BOX 7

DEPTH BOTTOM  
3265.60 m













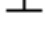


BOX 6







## Legend for geologic core description

	ripple bedding
	cross bedding
	stylolite
	lenticular bedding
	parallel lamination
	vertical and horizontal burrows
	wavy bedding
	herringbone cross-bedding
	fossil fragments undetermined
BT	bioturbation
CHON	<i>Chondrites</i> sp.
HEL	<i>Helminthopsis</i> sp.
MAC	<i>Macaronichnus</i> sp.
OPH	<i>Ophiomorpha</i> sp.
PAL	<i>Palaeophycus</i> sp.
PLAN	<i>Planolites</i> sp.
PY	pyrite
TEICH	<i>Teichichnus</i> sp.
TER	<i>Terebellina</i> sp.
 ,CCL	clay clasts
	carbonized plant debris
	calcite cementation
	common scattered coarse sand grains (to granules)
	occasional scattered coarse sand grains (to granules)
	disturbed core material (rubble)

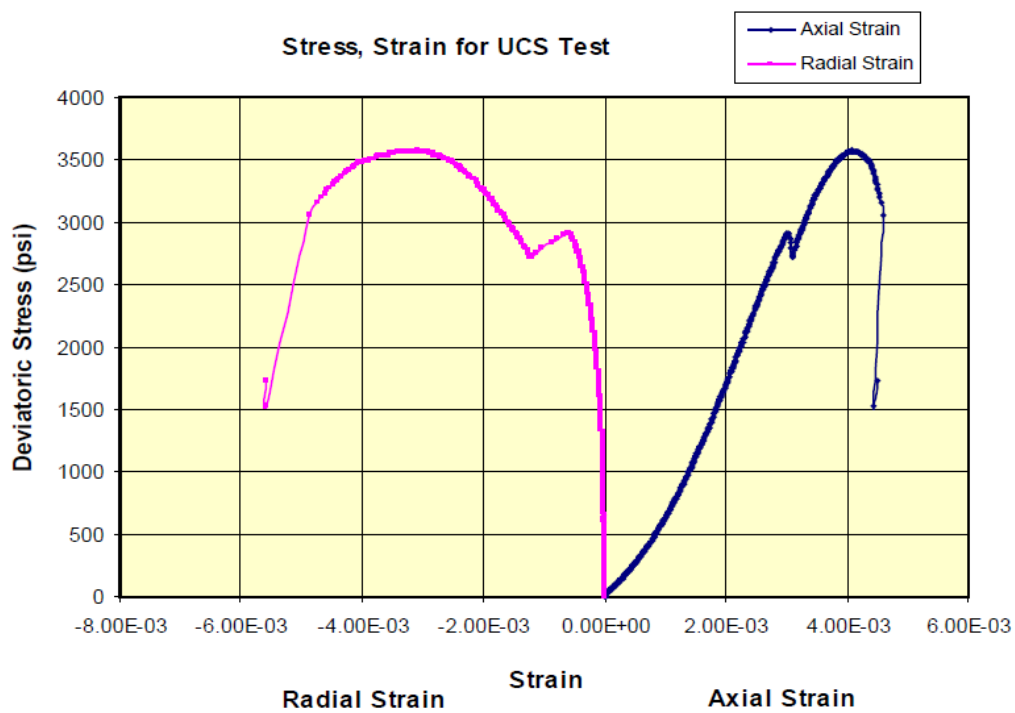
## Geo Mechanical Core Testing Results

### Uniaxial Compressive Strength

Sample Number	Depth (m)	Well	Confining Pressure (psi)	Compressive Strength (psi)	Young's Modulus (10 <sup>6</sup> psi)	Poisson's Ratio
6	3241.35	Sawan South-4	0	4480	1.63	0.18
15	3261.70	Sawan South-4	0	3572	1.26	0.22
21	3231.59	Sawan South-6	0	2196	0.56	0.20
29	3242.83	Sawan South-6	0	6892	2.32	0.24
36	3243.78	Sawan South-12	0	3529	1.29	0.23
42	3252.78	Sawan South-12	0	5332	1.83	0.24

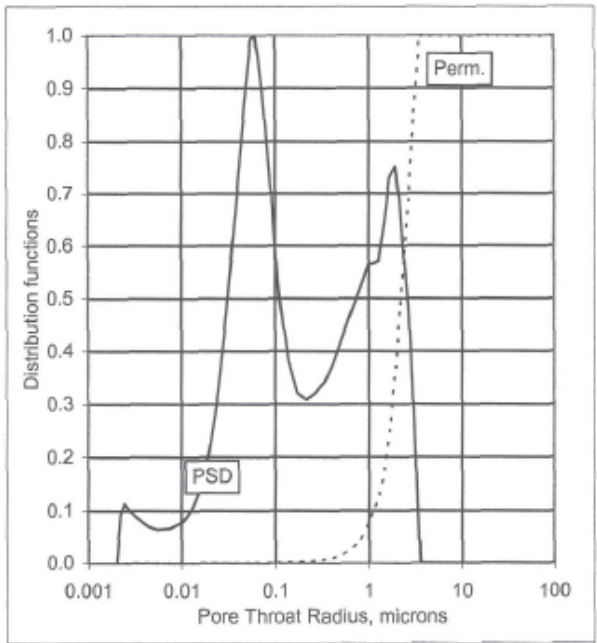
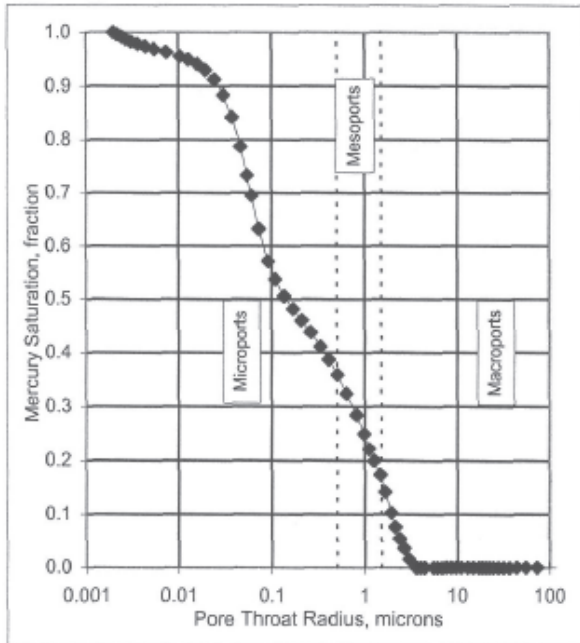
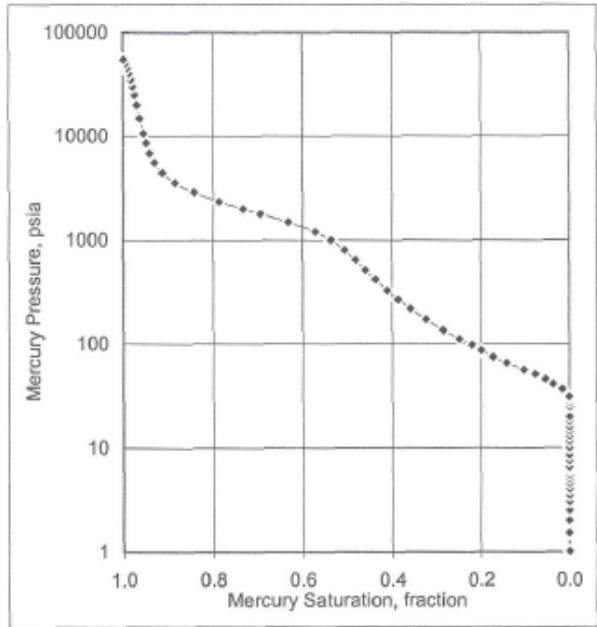
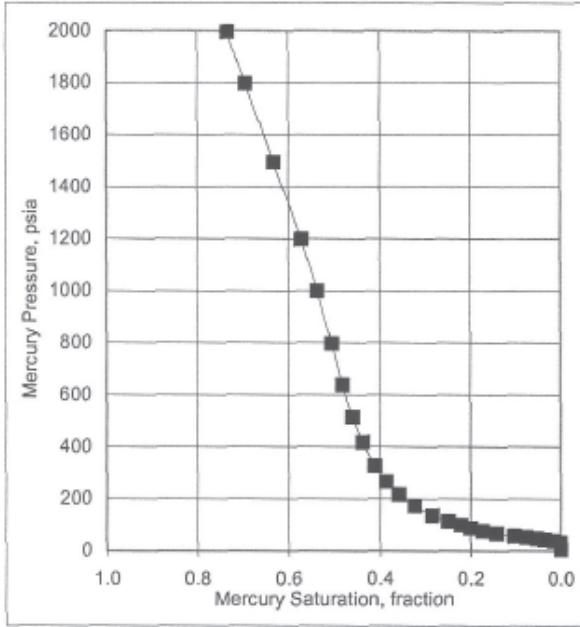
### Triaxial Static Young's Modulus, Poisson's Ratio and Compressive Strength

Sample Number	Well Name	Depth (m)	Confining Pressure (psi)	Bulk Density (g/cm <sup>3</sup> )	UCS (psi)	Young's Modulus (10 <sup>6</sup> psi)	Poisson's Ratio
6	Sawan South-4	3241.35	0	2.37	4480	1.63	0.18
15	Sawan South-4	3261.70	0	2.35	3572	1.26	0.22
21	Sawan South-6	3231.59	0	2.29	2196	0.56	0.20
29	Sawan South-6	3242.83	0	2.53	6892	2.32	0.24
36	Sawan South-12	3243.78	0	2.31	3529	1.29	0.23
42	Sawan South-12	3252.78	0	2.35	5332	1.83	0.24



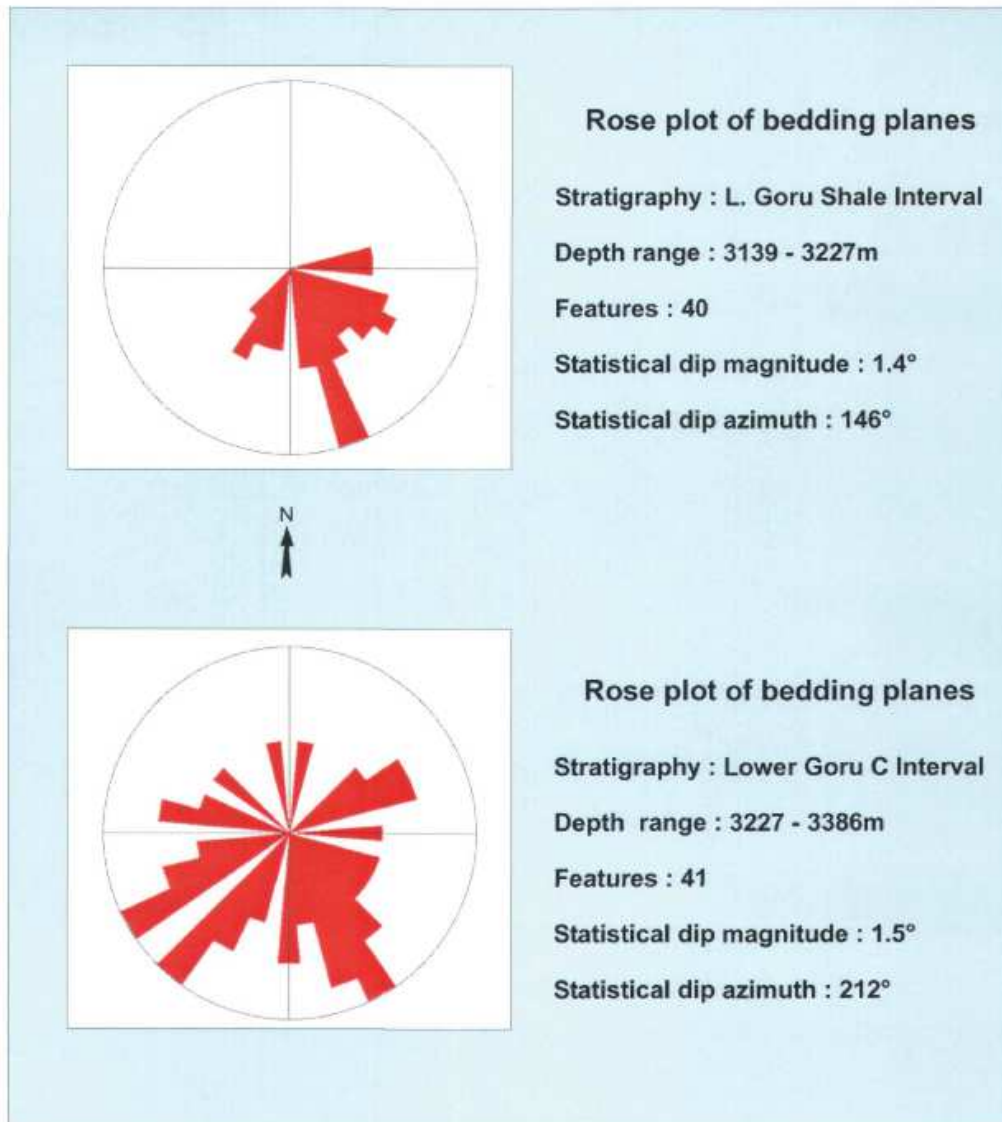


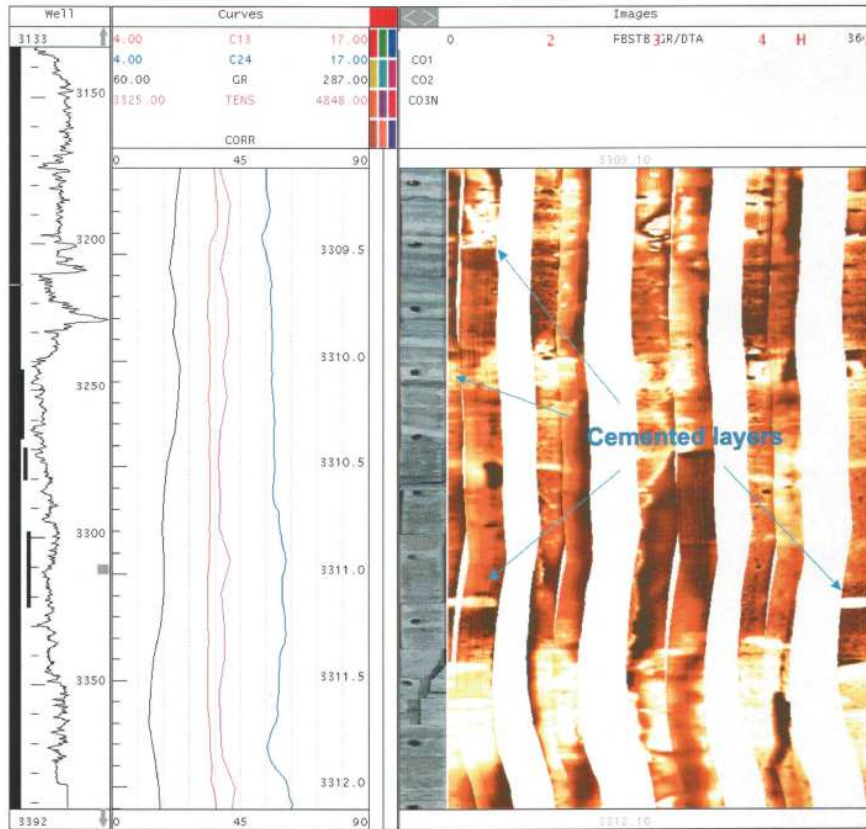
### Special Core Analysis Results



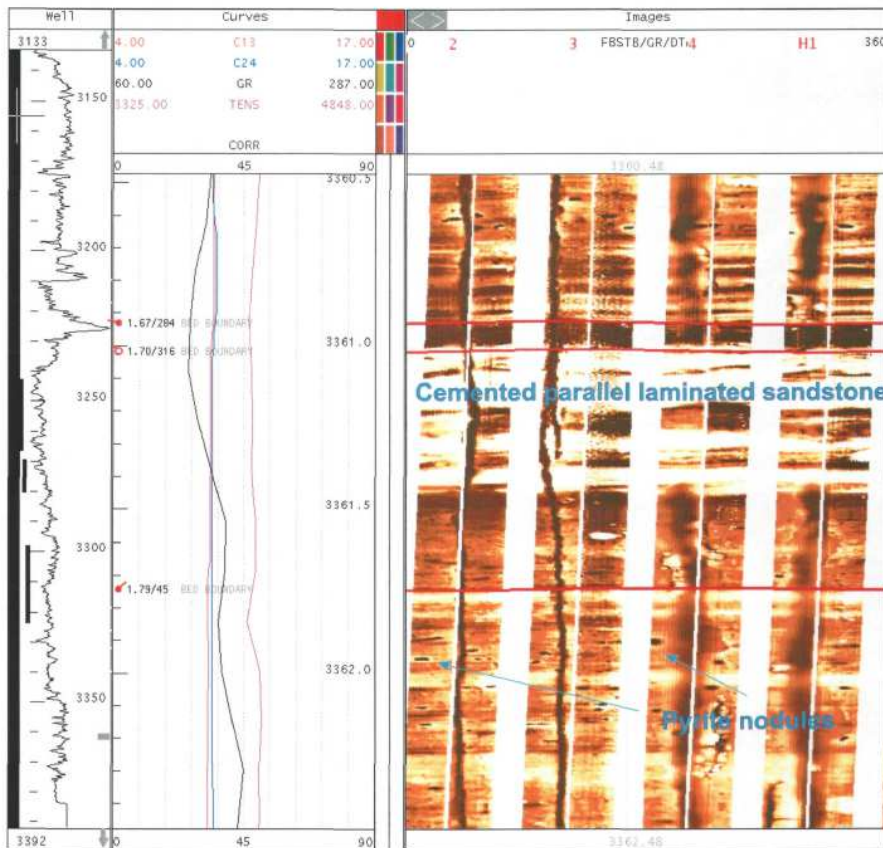
## Formation Imaging Result

### Structural dip





Lower Goru C Interval 3309.1-3312.1m

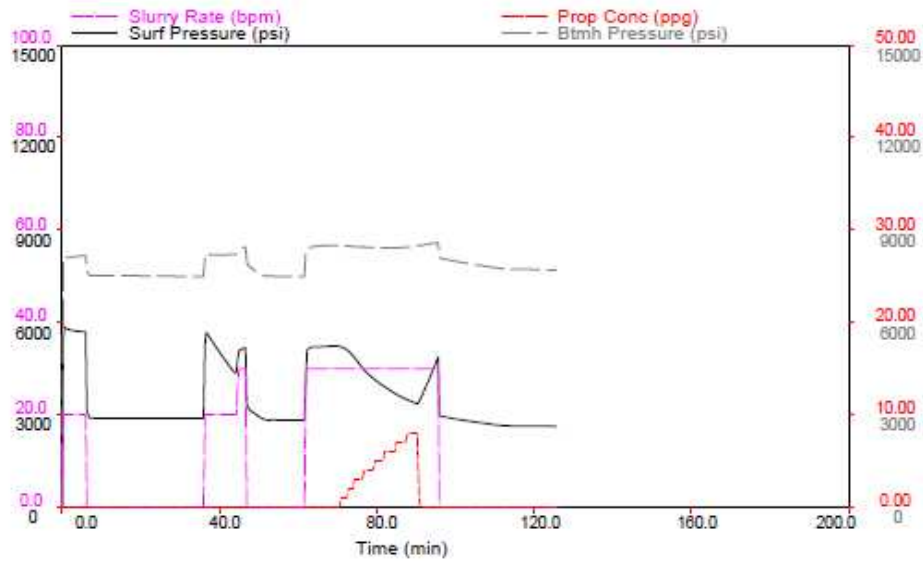


Lower Goru C Interval 3360.5-3362.5m

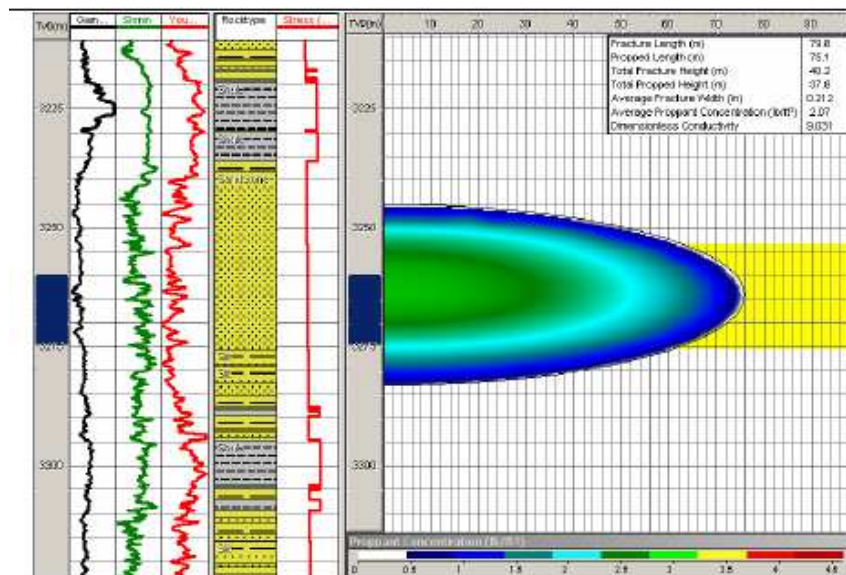
# Fracture Treatment Sensitivity Analysis

Treatment size 100klb (interval 3260m- 3275m)

Treatment design



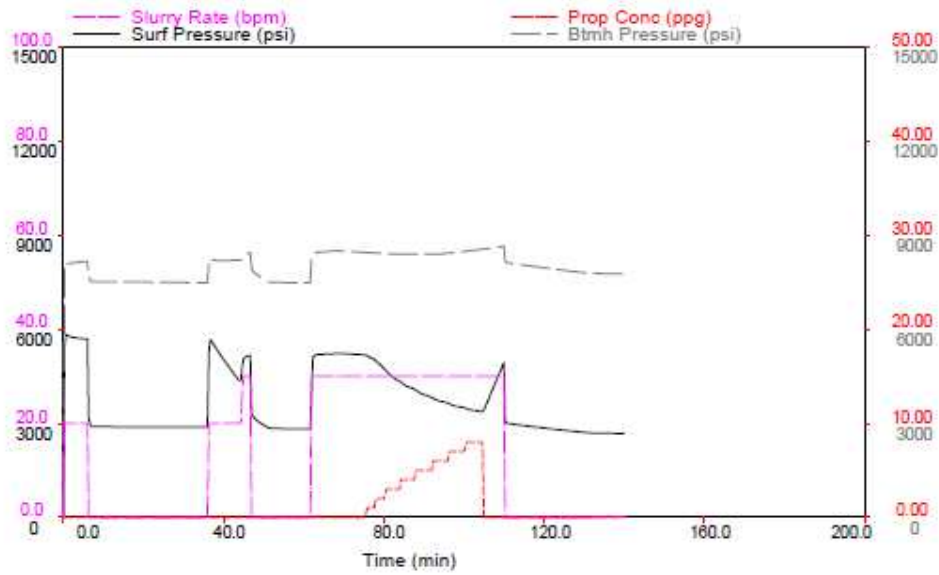
Fracture geometry



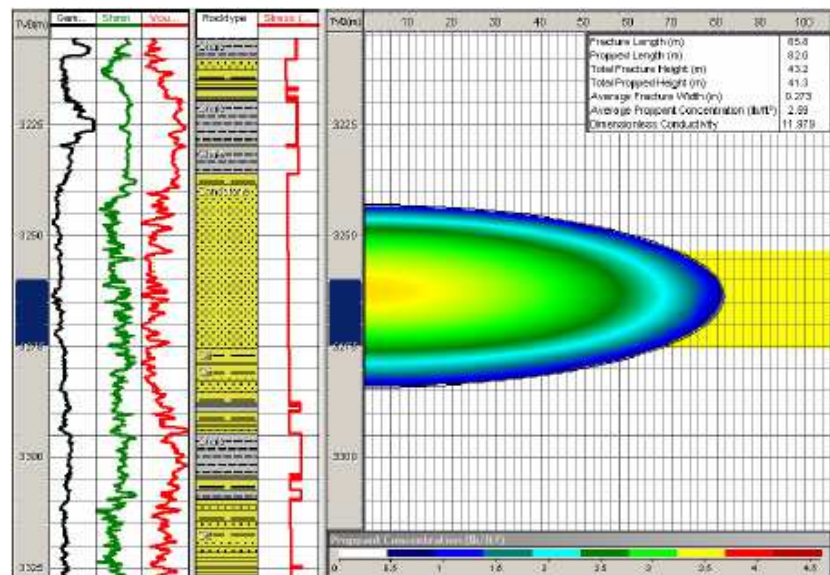


Treatment size 150klb (interval 3260m- 3275m)

Treatment design

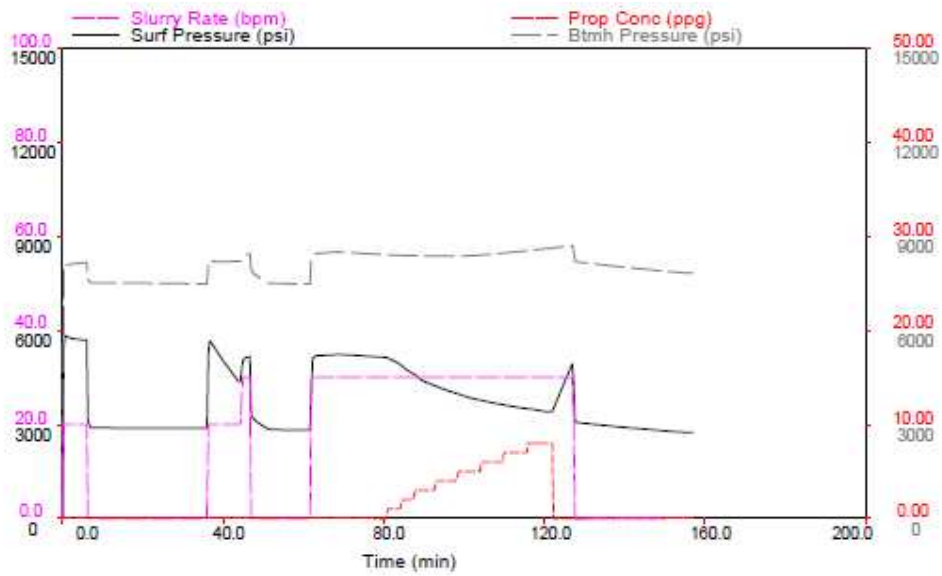


Fracture geometry

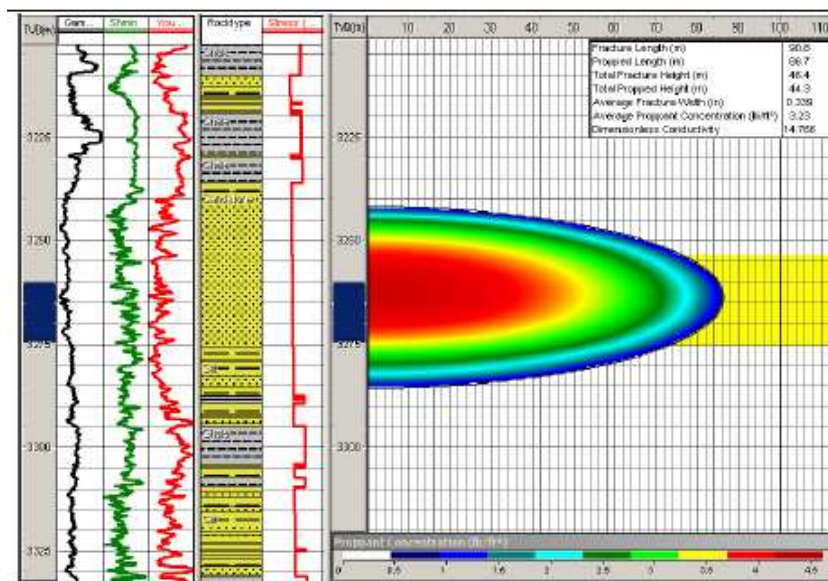


Treatment size 210klb (interval 3260m- 3275m)

Treatment design

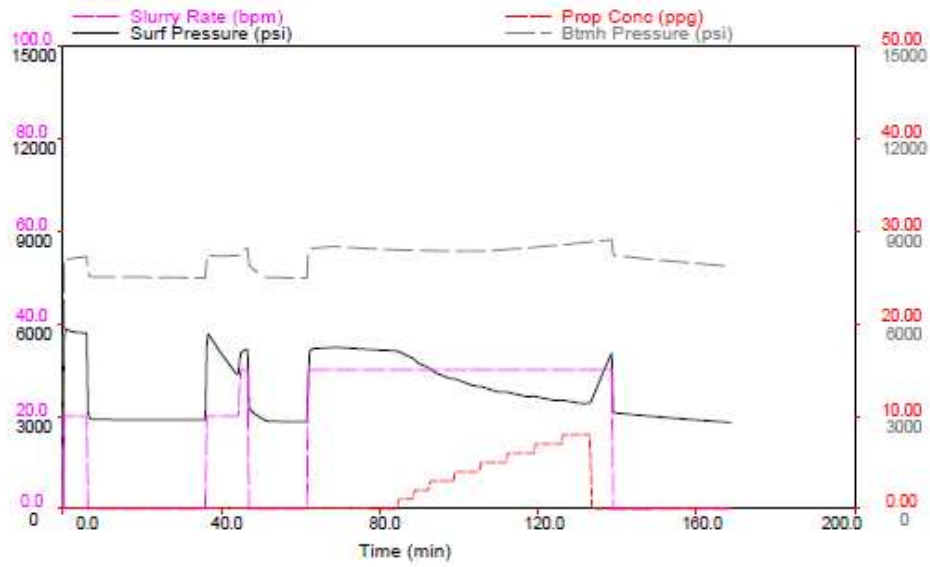


Fracture geometry

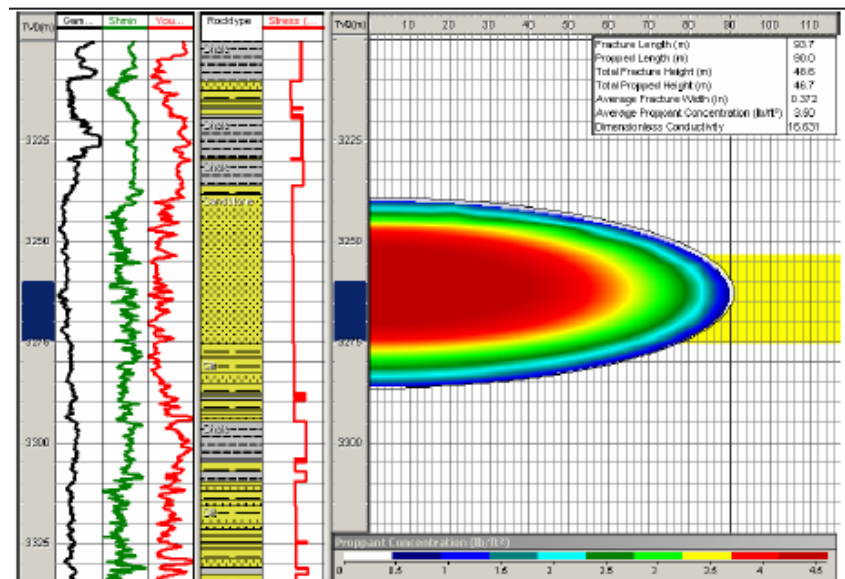


Treatment size 250klb (interval 3260m- 3275m)

Treatment design

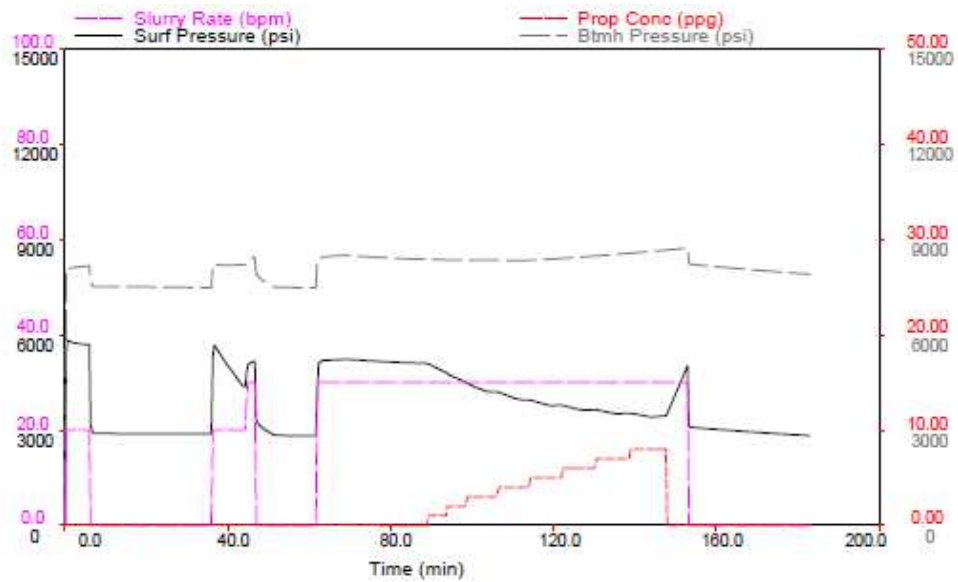


Fracture geometry

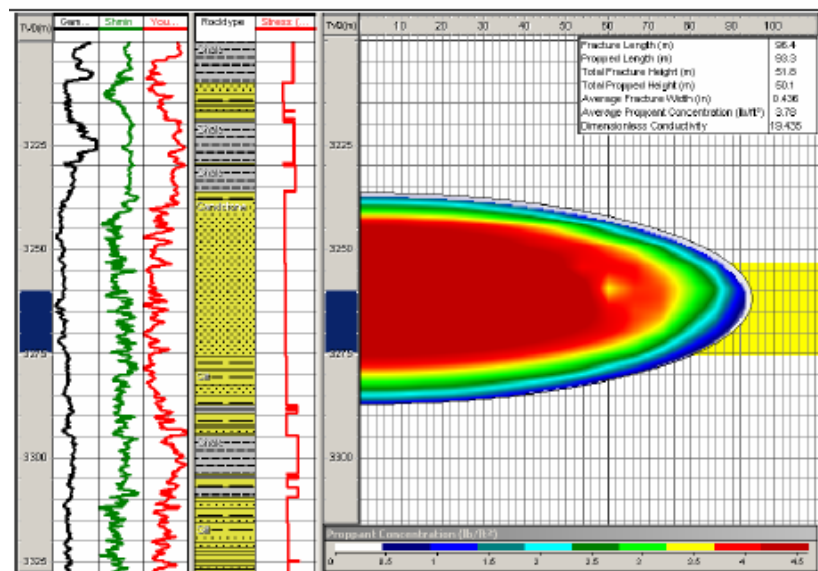


Treatment size 300klb (interval 3260m- 3275m)

Treatment design



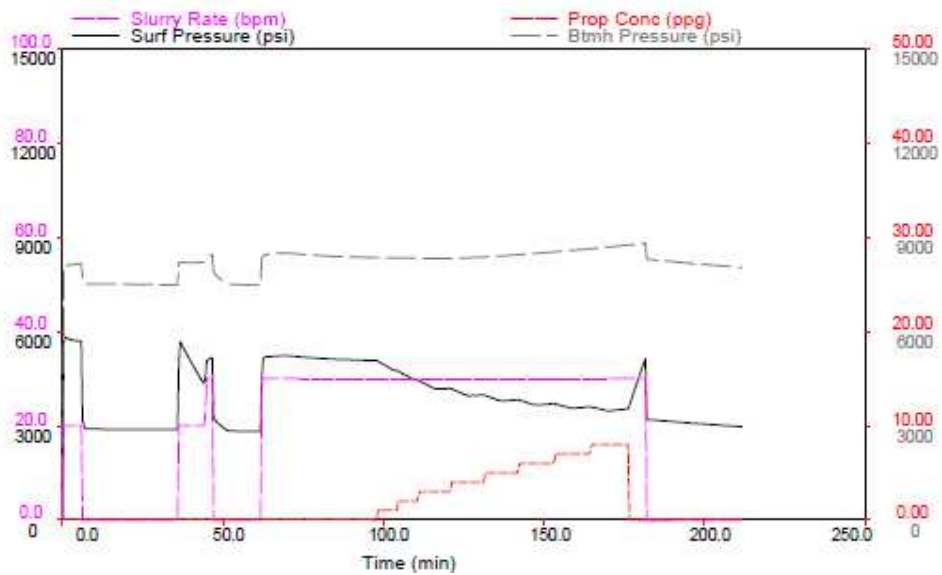
Fracture geometry





Treatment size 400klb (interval 3260m- 3275m)

Treatment design



Fracture geometry

